ADVANCEMENT OF EROSION TESTING, MODELING, AND DESIGN OF CONCRETE PAVEMENT SUBBASE LAYERS

A Dissertation

by

YOUN SU JUNG

Submitted to the Office of Graduate Studies of
Texas A&M University
in partial fulfillment of the requirements for the degree of

DOCTOR OF PHILOSOPHY

August 2010

Major Subject: Civil Engineering

ADVANCEMENT OF EROSION TESTING, MODELING, AND DESIGN OF CONCRETE PAVEMENT SUBBASE LAYERS

A Dissertation

by

YOUN SU JUNG

Submitted to the Office of Graduate Studies of
Texas A&M University
in partial fulfillment of the requirements for the degree of

DOCTOR OF PHILOSOPHY

Approved by:

Chair of Committee,	Dan Zollinger
Committee Members,	Robert Lytton
	Zachary Grasley
	Mohammed Haque
Head of Department,	John Niedzwecki

August 2010

Major Subject: Civil Engineering

ABSTRACT

Advancement of Erosion Testing, Modeling, and Design of
Concrete Pavement Subbase Layers. (August 2010)
Youn Su Jung, B.S., Pusan National University;
M.S., Pusan National University;
M.E., Texas A&M University
Chair of Advisory Committee: Dr. Dan G. Zollinger

Concrete pavement systems have great capacity to provide long service lives; however, if the subbase layer is improperly designed or mismanaged, service life would be diminished significantly since the subbase layer performs many important roles in a concrete pavement system. The erosion of material beneath a concrete slab is an important performance-related factor that if applied to the selection of base materials can enhance the overall design process for concrete pavement systems. However, erosion of the subbase has not been included explicitly in analysis and design procedures since there is not a well accepted laboratory test and related erosion model suitable for design.

Previous erosion test methods and erosion models are evaluated in terms of their utility to characterize subbase materials for erosion resistance. With this information, a new test configuration was devised that uses a Hamburg wheel-tracking device for evaluating erodibility with respect to the degree of stabilization and base type. Test devices, procedures, and results are explained and summarized for application in mechanistic design processes. A proposed erosion model is calibrated by comparing erosion to lab test results and LTPP field performance data. Subbase design guidelines are provided with a decision flowchart and a design assistant spread sheet for the economical and sustainable design of concrete pavement subbase layers by considering many design factors that affect the performance of the subbase.

DEDICATION

To my parents

ACKNOWLEDGMENTS

The author wishes to express great appreciation to his advisor, Dr. Dan G. Zollinger, for his guidance and continuous encouragement during the course of this work. Special thanks are extended to Dr. Robert Lytton, Dr. Zachary Grasley, and Dr. Mohammed Haque for their useful suggestions and for serving as advisory committee members. The author would also like to thank Dr. Andrew Wimsatt for his obliging advice and support. Finally, this research was conducted in cooperation with Federal Highway Administration and the Texas Department of Transportation. The author is grateful for their supports.

NOMENCLATURE

AASHTO	American Association of State Highway and Transportation Officials
AASHO	American Association of State Highway Officials
AC	Asphalt concrete
ACP	Asphaltic concrete pavement
ADT	Average daily traffic
ADTT	Average daily truck traffic
ASB	Asphalt stabilized base
ASTM	American Society of Testing Materials
CoTE	Coefficient of thermal expansion
COPES	Concrete Pavement Evaluation System
CPCD	Concrete pavement contraction design
CRC	Continuously reinforced concrete
CRCP	Continuously reinforced concrete pavement
CSB	Cement stabilized base
CTB	Cement treated base
DC	Dielectric constant
DCP	Dynamic cone penetrometer
EER	Equivalent erosion ratios
ESAL	Equivalent single axle load
FDR	Full depth repair
FWD	Falling weight deflectometer
GPR	Ground penetration radar
HWTD	Hamburg wheel-tracking device
JC	Jointed concrete
JPCP	Jointed plain concrete pavement
JRCP	Jointed reinforced concrete pavement
LDF	Lane distribution factors

LS	Loss of support
LTE	Load transfer efficiency
LTPP	Long-term pavement performance
LTS	Lime treated subgrade
LVDT	Linear Variable Differential Transducer
MEPDG	Mechanistic-Empirical Pavement Design Guide
NCHRP	National Cooperative Highway Research Program
NDT	Nondestructive testing
PCA	Portland Cement Association
PCC	Portland cement concrete
PIARC	Permanent International Association of Road Congresses
RAP	Reclaimed asphalt pavement
RaTT	Rapid tri-axial test
RC	Recycled concrete
SCI	Surface curvature index
TxDOT	Texas Department of Transportation
UCCS	Unconfined compressive strength

TABLE OF CONTENTS

Page

Page

CHAPTER

Page

CHAPTER

LIST OF FIGURES

Page

Page

Page

Page

LIST OF TABLES

Page

Page

CHAPTER I

STATEMENT OF THE PROBLEM

BACKGROUND

The need for the use of a subbase (or base) under rigid pavements was well recognized to prevent severe erosion and pumping of subgrade induced by frequent heavy truck traffic. A subbase layer performs many important roles in a concrete pavement system such as providing:

- a stable construction platform,
- uniform and consist support,
- erosion resistance,
- drainage,
- increased slab support, and
- a gradual transition with depth in layer moduli.

During construction, a subbase needs to provide a stable platform and over the service-life uniform slab support. The importance of uniform support cannot be overstated in the performance of long-lasting concrete pavement systems; good performing concrete pavements can co-exist with a wide range of support strength, but variation from the slab center to the edge or corner area or differences in support between segments due to erosion or for any reason cannot be tolerated to any great extent, which is why erosion is a key factor in performance.

Erosion creates a nonuniform support condition that often leads to faulting in jointed concrete (JC) pavements and punchout-related distress in continuously reinforced concrete (CRC) pavements. Erosion potential is greatest where upward curling and

---

This dissertation follows the style and format of the *Transportation Research Record.*

warping along edge and corner areas separate the slab from the subbase enabling the slab to behave under load independently for the supporting layer enabling the "pumping" of water that may be trapped between the slab and the subbase under an applied wheel load back and forth along the slab/subbase interface.

Unfortunately, most subbases are not sufficiently erosive resistant or permeable to allow for an acceptable means of removal of water to avoid erosion damage. Subbase layers certainly can add structural capacity to a concrete pavement but only to the degree that interlayer bond can be employed to contribute to the inherent load spreading capability of the slab. Consequently, increasing slab support is not always accomplished depending upon the type of subbase material used.

Another more important feature is the provision of a gradual change in layer stiffness from the bottom of the slab to the top of the subgrade layer. Abrupt changes in this regard can lead to undesirable load-induced shear stress concentrations along the corners and pavement edges, increasing the potential of poor support conditions developing over time and loading cycles. Stiff subbases, unless fully bonded to the slab, also tend to magnify the environmentally induced load stresses in the slab and shorten fatigue life of the pavement system. Proper material, design, construction, and maintenance are essential to achieve long-term performance in a cost effective and reliable manner.

RESEARCH SIGNIFICANCE AND SCOPE

Subbase erosion is a key to understanding the process of major distresses in concrete pavement such as faulting and punchout. Review of the literature revealed that some studies addressed laboratory testing protocols along with test results regarding erosion resistance of asphalt cement and portland cement stabilized materials. However, subbase erosion has not been included explicitly in design related analysis and accordingly, design procedures have suffered due to the lack of an acceptable laboratory test procedure and related erosion design model.

In this regard, the primary objectives of this research were developing a simple but effective laboratory test method to evaluate erodibility of a subbase material and validating a mechanistic erosion model using the associated laboratory test results and field data. Consequently, subbase design guidelines addressing erosion and other related factors are provided as a result of this research.

STRUCTURE OF DISSERTATION

This dissertation consists of six chapters, each with specific objectives. Chapter I provides background information, research objectives, the scope of this research, and the overall structure of the dissertation. In following paragraphs, a brief description of each of the chapter is provided, highlighting the main ideas presented.

Previous test methods and erosion models as to their utility in characterizing subbase materials in terms of erosion resistance are briefly reviewed in Chapter II. Moreover, most popular past and current subbase design methods pertaining to erosion are thoroughly reviewed.

Field investigation results for subbase erosion study are discussed in Chapter III. The objectives of the field investigation were to identify the factors associated with the erosion process. Sample sections were identified and investigated using a number of techniques including visual survey, nondestructive testing (NDT) using falling weight deflectometer (FWD), and the ground penetrating radar (GPR) as well as dynamic cone penetrometer (DCP) and coring.

A new test procedure to evaluate the sustainability of a subbase layer and a mechanistic-empirical model are proposed and developed in Chapter IV. This test procedure evaluates subbase erosion under the contact of a concrete layer which qualifies a subbase material under dry and wet erosion conditions relative to the magnitude of the shear stress associated with the erosive action. Test devices, procedures, and results are explained and summarized for application in a mechanistic-empirical design processes. A mechanistic-empirical model for subbase erosion is developed and calibrated using the results from the Hamburg wheel-tracking device (HWTD) and long-term pavement

performance (LTPP) data. The prediction results match well with test data and observed field faulting and punchout data trends.

The subbase design guidelines are provided in Chapter V to achieve economical and sustainable concrete pavement subbase layer design relative to many factors that affect the performance of the subbase. A decision flowchart formats the guidance for a decision maker to efficiently select a subbse material and design a concrete pavement subbase by categorizing the decision process into three areas of consideration or criteria: materials, design, and sustainability.

Finally, a summary of the major findings along with an overview of the research are summarized in Chapter VI. In addition, recommendations for future research are provided.

In the appendices, detailed erosion test procedure using the HWTD is explained in Appendix A. Appendix B provides a design example along with inputs/outputs of design guide sheet and step by step check list for design considerations.

CHAPTER II

LITERATURE REVIEW

EROSION MECHANISM

The shear stress or water under pressure due to the effect of a moving load along the interface between concrete slab and subbase layer plays a major role in the erosion process. As the stiffness of the joint or crack decreases, the interfacial shear stress under the applied loading increases generating fines along the slab-subbase interface, which are susceptible to dislocation and transport under pressurized water movement via pumping through joints or cracks to the pavement surface. Consequently, the effects of pumping can grow a void under the slab eventually leading to a loss of joint stiffness and a mirage of associated distress types; this sequence is also accelerated by mutual effects.

Figure 2-1 shows conceptually the action of pumping at the corner of a concrete slab (*1*). The water induced shear stresses on the subbase are developed based on the slab movement simulated by a stiff plate rotating about an axis. The initial edge gap, H, can be attributed to curling and warping of the concrete pavement separating the slab from the subbase allowing a passing wheel load to pressurize any water permeating the interfacial area. In this manner, water pressure increases with vehicle speed.

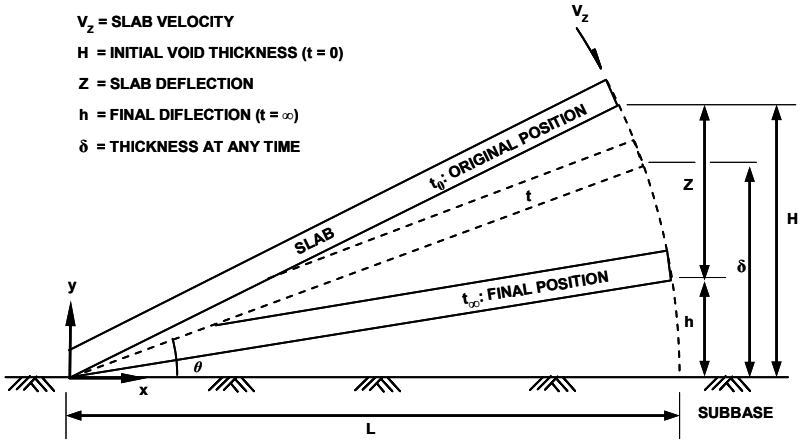

Figure 2-1 Slab Configuration of Erosion Modeling by Pumping (*1*).

Phu and Ray conducted an extensive investigation into the erosion for various material type and stabilization levels and identified water velocity with respect to three void thickness zones in which water behaves differently according to theoretical, laboratory, and in-situ observations. Water behaves as a viscous fluid in the void less than 20 mils (0.5 mm) while it behaves as an ideal fluid in the void larger than 40 mils (1 mm) in thickness. Water velocity was calculated by different equations for each condition and the interpolated water velocity was applied for transition zone voids between 20 and 40 mils (0.5 mm and 1 mm). Maximum shear stresses in Figure 2-2 were obtained from ideal fluid conditions which drop with an increase of void thickness, but increases with vehicle speed (*2*). Since the slab is not deflected at a constant velocity, the resistance of water reduces slab speed and shear stress with void thicknesses less than 40 mils (1mm). On the other hand, fluid pressures drop significantly when the void thickness exceeds 40 mils (1 mm), but that pressure increases with vehicle speed.

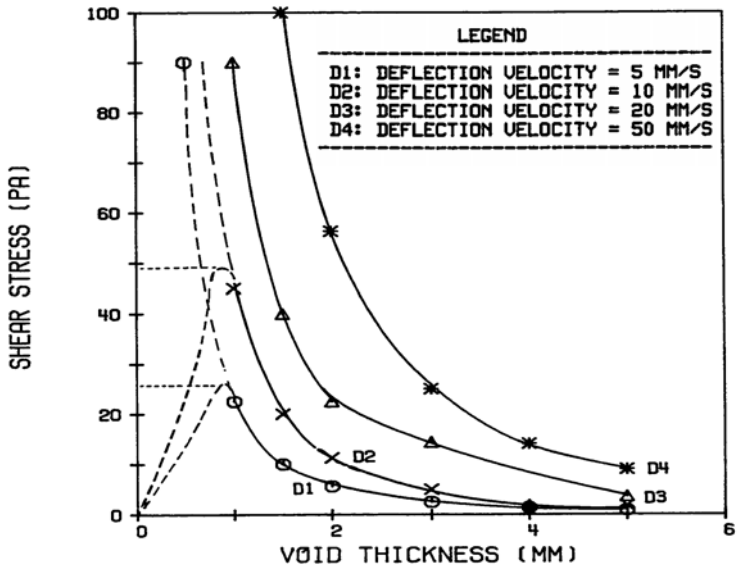

Figure 2-2 Effect of Void Size and Velocity of Slab Deflection on the Shear Stress (*2*).

PREVIOUS LABORATORY TEST METHODS FOR EROSION

Many erosion tests were developed in the 1970s and 1980s using various testing devices but none of those tests have been selected as a standardized form of testing. Some of the more prominent test methods are described below relative to their utility to characterize subbase and subgrade materials for erosion resistance.

Rotational Shear Device and Jetting Device

Figure 2-3 shows the testing devices developed by Van Wijk (*1*) to measure erosion using pressurized water. The concept is based on surface erosion occurring when water-induced shear stress is higher than the shear strength of test material. Two different devices are used depending upon the cohesive nature of the tested material. Stabilized (cohesive) materials are tested using a rotational shear device, while unstabilized (non-cohesive) materials are tested using a jetting device. Both methods consider only hydraulically induced shear in the erosion process. Weight loss is determined as a result of the test but it could be overestimated by the loss of aggregate-sized particles, which may not take place in under field conditions.

Rotational Shear Device

Stabilized test samples are eroded by application of hydraulic shear stress using various rotating water velocity around specimen and measured the weight of eroded materials to determine the critical shear stress defined as the shear stress at which erosion of the particles abruptly accelerates. The critical shear stress of each material is recommended as an index of erosion resistance.

Jetting Device

The jetting device test equipment ejects pressurized water at an angle of approximately 20 degrees to the upper surface of unstabilized samples generating weight loss over time. Critical shear stress determinations on the surface are calculated based on the assumption

of the stress being placed over a uniform area even though the surface area and the distribution of pressure changes with time.

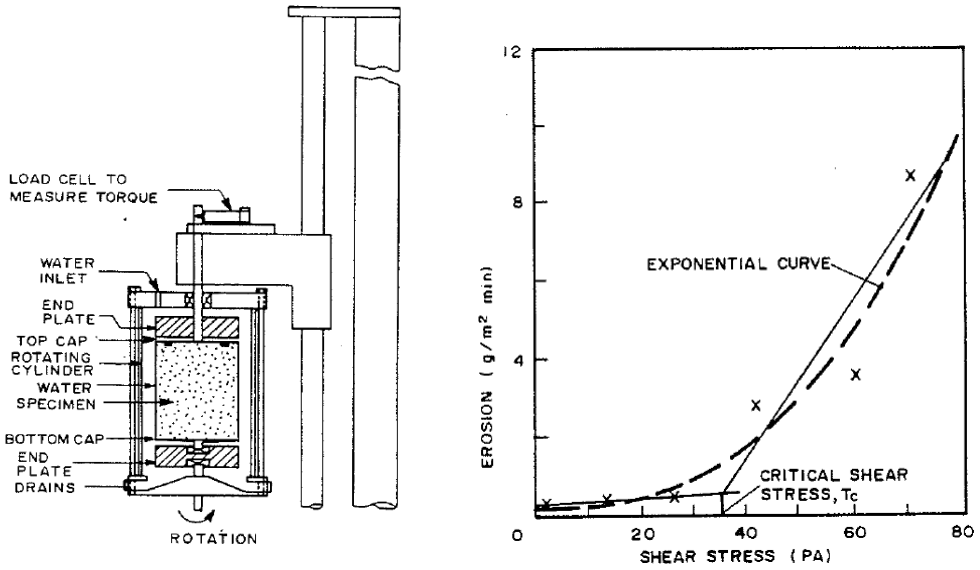

Rotational Shear Device

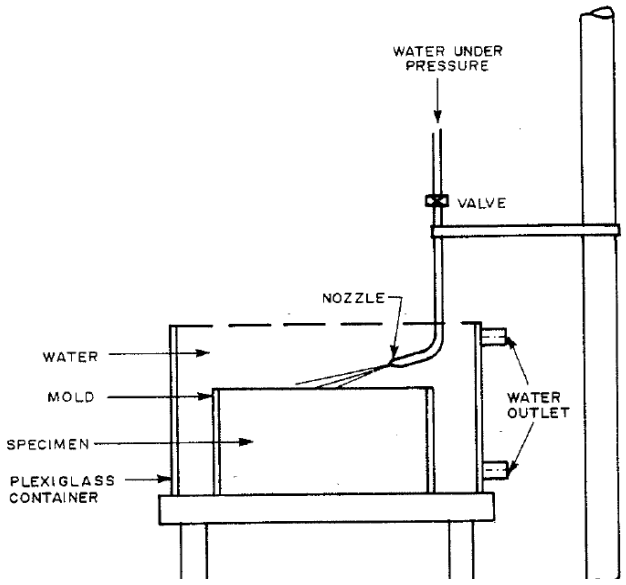

Jetting Device

Figure 2-3 Rotational Shear Device and Jetting Device (*1*).

Brush Test Device

Figure 2-4 shows details of the brush test used by French researchers, Phu and Ray (*2*), allowing various material types to be subjected to abrasion due to the brushing action. The major drawback is the length of the test time involved (6 weeks for wet-dry durability brush tests). Although a common issue with all erosion tests, base materials consisting of large-sized aggregates that loosen and dislodge during testing exaggerate weight loss data.

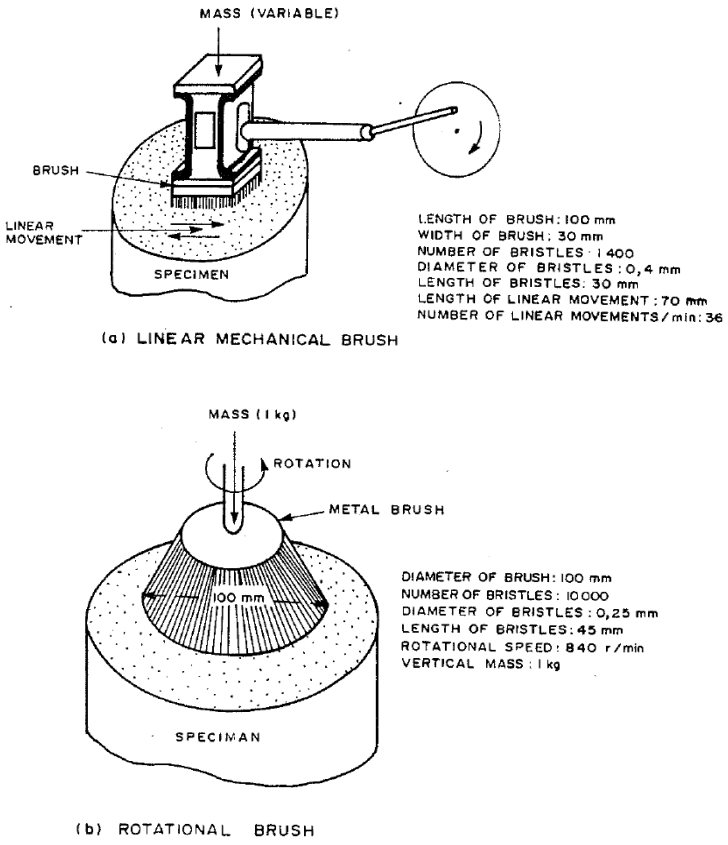

Figure 2-4 Brush Test Devices (*2*).

According to rotational brush test, an erosion index, IE is defined as the ratio of the weight loss to that of a granular material stabilized with 3.5 percent cement (reference material) where 26 g/min is regarded as one unit of IE. Lower IE means better erosion resistance.

A chart and table of various material types was suggested as a design guide for erosion in Figure 2-5. IE of 0.2 to 0.4 is recommended for heavy traffic on undowelled rigid pavements while IE of 0.4 to 1.0 for dowelled rigid pavements. Critical cement content determined from IE criteria is recommended to be increased at least 0.5 percent to compensate for defection in material composition, workmanship, and curing.

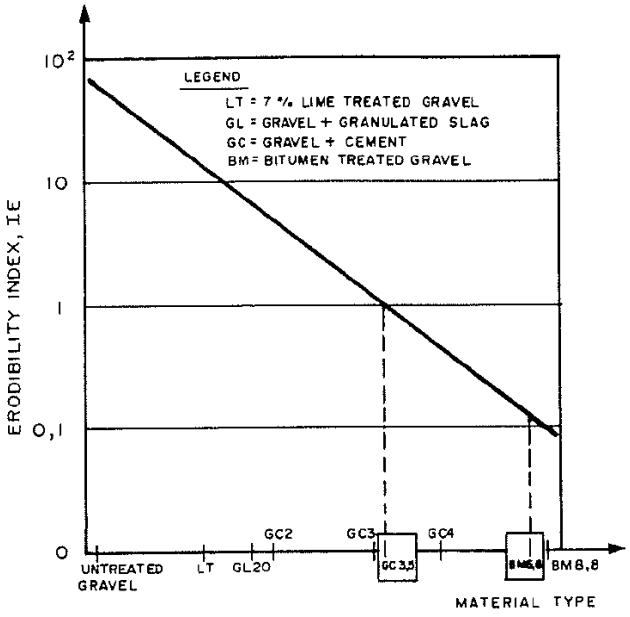

TABLE: DETAIL OF MATERIALS

MATERIALS		STABILIZER (%)	AVERAGE EROBIBILITY (g/min)	EROBIBILITY INDEX, IE
BITUMEN TREATED GRAVEL	BM 2,2	2,2	57	2,19
	BM 4,4	4,4	10	0,38
	BM 6,6	6,6	6	0,23
	BM 8,8	8,8	3	0,10
GRAVEL + CEMENT	GC 2,2	2,0	132	5,00
	GC 3	3,0	30	1,15
	GC 3,5	3,5	26	,00
	GC 4	4,0	12	0,46
	GC 6	6,0	10	0,38
	GC 9	9,0	8	0,30
GRAVEL + GRANULATED SLAG	GL 20/40	20	168	6,46
	GL 40/60	20	193	7,42
LIME TREATED GRAVEL	LT	7	350	13,50
UNTREATED GRAVEL	GNT		1 231	47,00

Figure 2-5 Proposed Erodibility Index (*2*).

Rolling Wheel Erosion Test Device

Figure 2-6 and Figure 2-7 show an empirical test procedure for erosion proposed by de Beer (*3*). Wheel movement over a friction pad serves as the source of erosion of the test sample. Fines are produced on the surface of the test sample by direct contact between the friction pad (neoprene membrane) and the test sample; submerging the test sample during testing allows water to wash out generated fines similar as would take place under pumping action. The erosion index is the measure of erosion and defined as the average depth of erosion after 5000 wheel load applications. The test method evaluates the erodibility based on the depth of erosion rather than the weight loss of the sample.

This test attempts to simulate field conditions since it addresses mechanical abrasive and hydraulic erosion together. However, pumping action caused by the flexible membrane in this test may not be similar to the pumping action that occurs under a rigid pavement; nether is the applied shear stress under this method easily determinable. The voiding of the subbase material due to erosion would be difficult to represent in this test configuration. The other factor that could affect the erodibility of this test is the surface condition of the sample. When preparing the test sample, the testing surface is cut by a saw blade. Accordingly, this sample preparation could generate surface damage causing artificially high weight loss.

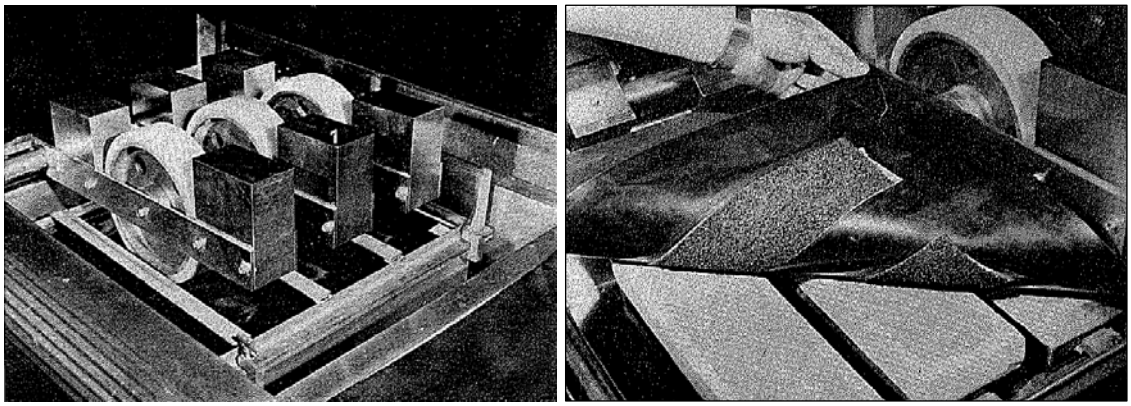

Figure 2-6 Rolling Wheel Erosion Test Device (*3*).

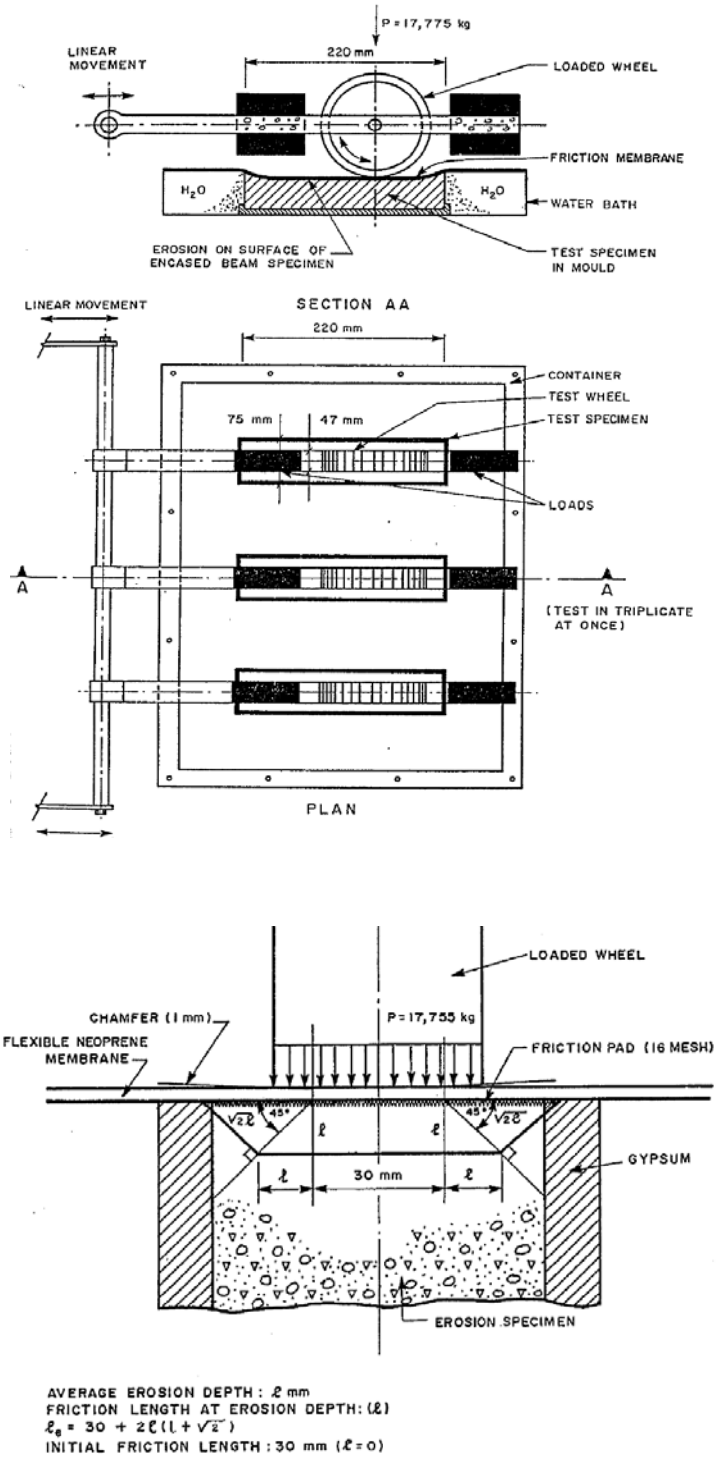

Figure 2-7 Schematic Diagram of the Rolling Wheel Erosion Test Device (*3*).

Other Erosion Related Tests

Erosion tests were developed not only for the study of pavement sub-layers but also for the research of river scour and erosion of earth dams. Some of recent erosion related tests were briefly reviewed; however, emphasis will be focused on pavement subbase erodibility test rather than the various durability test methods.

Erosion Function Apparatus

Briaud et al. (*4*) developed the erosion function apparatus, EFA to measure the erosion rate in cohesive soils; it is a method to predict the scour depth versus time curve around a cylindrical bridge pier standing in the way of a constant velocity flow and founded in a uniform cohesive soil (Figure 2-8). The scour rate versus shear stress curve is used to quantify the scour rate of a soil as a function of the flow velocity in a stream. A straight line DE shows scour rate of incohesive soils such as sand while S shape curve OABC represents the scour rate of cohesive soils such as clay. Erosion trend of cohesive soil in scour test is similar with the one of stabilized subbase material under pavement.

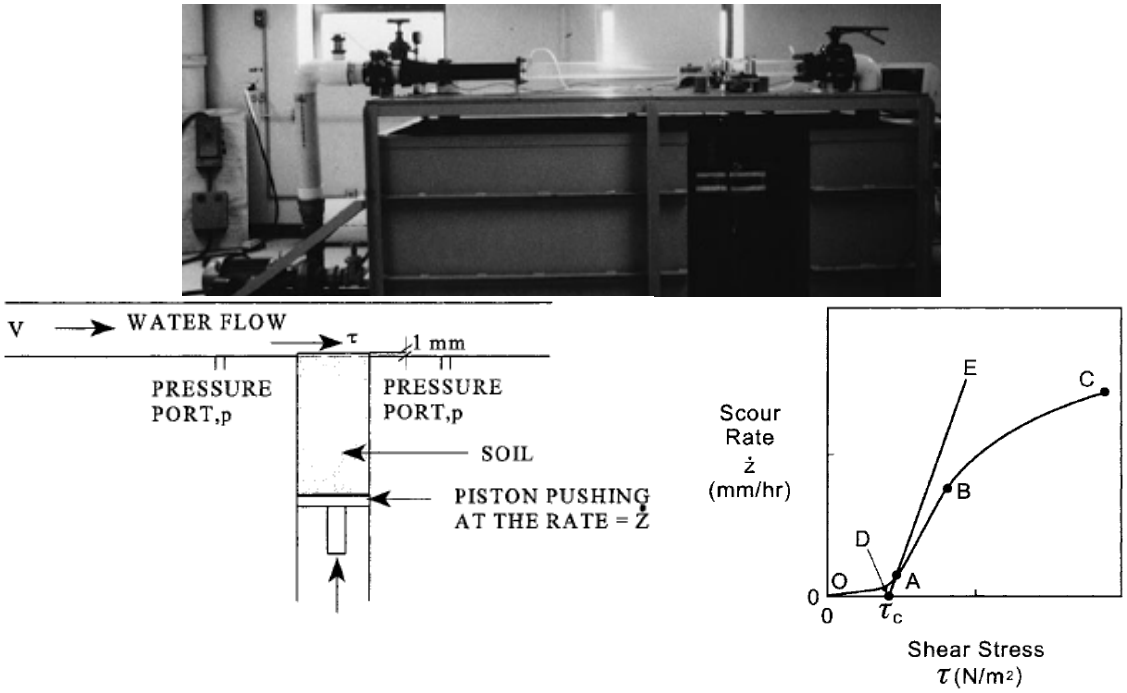

Figure 2-8 Concepts of EFA and Scour Rate versus Shear Stress Curve (*4*).

Hole Erosion Test

Figure 2-9 shows a schematic diagram of the hole erosion test designed by Wan and Fell (*5*). The soil specimen is compacted inside a standard mold used for the standard compaction test. A 6 mm-diameter hole is drilled along the longitudinal axis of the soil sample to simulate a concentrated leak. Hydraulic shear stress along the pre-formed hole generates erosion and an erosion rate index derived from the test results was defined for each soil sample. Specimen compacted to a lower dry density eroded more rapidly and expected to develop large diameter pipe result collapse of dam along with more erosion as shown in Figure 2-10.

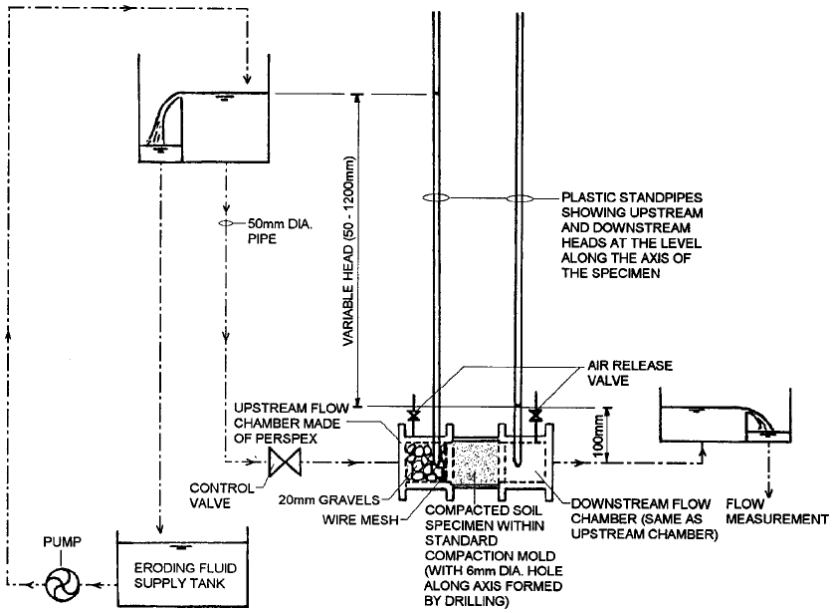

Figure 2-9 Schematic Diagram of Hole Erosion Test Assembly (*5*).

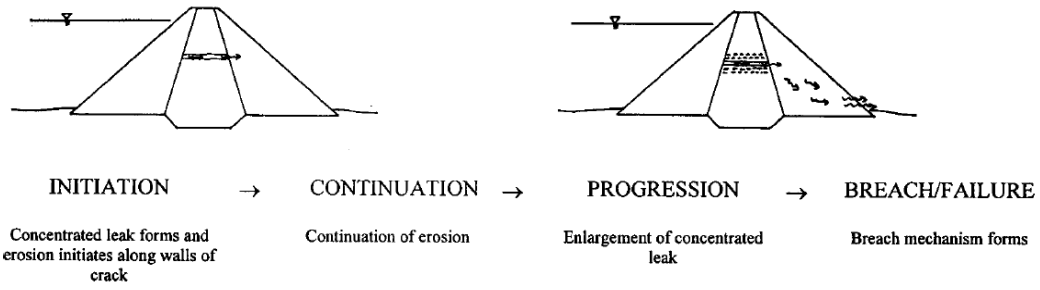

Figure 2-10 Model for Development of Failure by Piping in Embankment (*5*).

PREVIOUS EROSION MODELS

The presence of water, the erodibility of a subbase material, the rate of water ejection, the amount of deflection, and the number of load are factors that influence erosion but apparently current design procedures scarcely address these factors. Below are models listed in the literature to address the erosion mechanism.

Model by Rauhut

In the model by Rauhut (*6*), the level of pumping damage was empirically related, based on nonlinear regression analysis of the Concrete Pavement Evaluation System (COPES) database, to many comprehensive factors such as precipitation, drainage, subbase type (stabilized or not), subgrade soil type and strength, load transfer, slab thickness, freezing index, Thornthwaite moisture index, and single axle load (ESAL). Equation 2-1 is separated for jointed plain concrete pavement (JPCP) in Equations 2-2 and 2-3, and jointed reinforced concrete pavement (JRCP) in Equations 2-4 and 2-5.

$$g = \left(\frac{ESAL}{\rho} \right)^{\beta} \quad \textbf{(2-1)}$$

JPCP

$$\ln\rho = 1.39 \cdot DRAIN + 4.13 \quad \textbf{(2-2)}$$

$$\beta = \frac{0.772(D - 2.3)^{1.61}}{PPTN} + 0.0157 \cdot JLTS \cdot D + 0.104 \cdot STAB + 0.17 \cdot DRAIN + 0.137 \cdot SOILTYP - 0.247 \quad \textbf{(2-3)}$$

JRCP

$$\ln\rho = 1.028 \cdot STAB + 0.0004966 \cdot D^{3.47} - 0.01248 \cdot FRINDEX + 1.667 \cdot CBR + 5.476 \quad \textbf{(2-4)}$$

$$\beta = -0.01363 \cdot DMOIST + 0.02527 \cdot D - 0.423 \quad \textbf{(2-5)}$$

where: g = amount of distress as a fraction of a pumping level of 3 (severe)
ESAL = equivalent 80 kN (18,000 lb) single axle loads
DRAIN = 0; no underdrains, 1; underdrains

PPTN = average annual precipitation (cm)
JLTS = 0; undoweled, 1; doweled
STAB = 0; unstabilized subbase, 1; stabilized subbase
SOILTYP = 0; granular foundation soil, 1; coarse foundation soil
DMOIST = Thornthwaite moisture index
FRINDEX = freezing index
CBR = California bearing ratio of foundation soil
D = slab thickness (in)

Model by Markow

An empirical model (Equation 2-6) by Markow (*7*) based on the American Association of State Highway Officials (AASHO) road test data relating slab thickness to ESAL and subbase drainage conditions. The model is simple but does not consider many important factors. The pumping index indicates the potential of erosion that increases with cumulative number of ESAL and diminishing drainage conditions but decreases quickly with an increase in slab thickness. Drainage adjustment factor is considered based on subbase permeability.

$$P_i = m \cdot \sum ESAL \cdot f_d$$
$$\log m = 1.07 - 0.34D \qquad \textbf{(2-6)}$$

where: P_i = pumping index
$ESAL$ = equivalent 80 kN (18,000 lb) single axle loads
D = slab thickness (in)
f_d = drainage adjustment factor
= 0.2 for good drainage (k =10,000 ft/day)
= 0.6 for fair drainage (k = 100 ft/day)
= 1.0 for poor drainage (k = 0.1 ft/day)
k = subbase permeability

Model by Larralde

Another empirical model was developed by Larralde (*8*) based on the AASHO road test data relating erosion to the amounts of deformation energy imposed by the application of load. The deformation energy was computed using finite element modeling; a pumping index is normalized to eliminate the effect of slab length and reinforcement. The model in Equation 2-7 is empirical in nature and consequently does not consider many important factors related to erosion.

$$NPI = \exp\left[-2.884 + 1.652 \cdot \log\left(\frac{\sum ESAL \cdot DE}{10{,}000}\right)\right] \quad \textbf{(2-7)}$$

where: NPI = normalized pumping index of volume of pumped material (in^3)

$ESAL$ = equivalent 80 kN (18,000 lb) single axle loads

DE = deformation energy per one application of ESAL

$= \log(DE) = 3.5754 - 0.3323\,D$

D = slab thickness (in)

Model by Van Wijk

Equations 2-8 and 2-9 by Van Wijk (*1*) included factors derived from field data using Rauhut model to make improvement over the Larralde model to predict the volume of eroded material as a function of the deformation energy produced by traffic. The effect of many factors on pumping such as subbase and subgrade type, drainage, load transfer, and climate condition are considered in this model. Since this model is empirical in nature, its application is limited to the variable ranges included in the database.

$$P = 36.67 \cdot NPI \quad \textbf{(2-8)}$$

$$NPI = F \cdot \exp\left[-2.884 + 1.652 \cdot \log\left(\frac{\sum ESAL \cdot DE}{10{,}000}\right)\right] \quad \textbf{(2-9)}$$

where: P = volume of pumped material (ft^3/mile)

NPI = normalized pumping index (in^3)

DE = deformation energy per application (in-lb)

$\log(DE) = 3.5754 - 0.3323\,D$

D = slab thickness (in)

F = f_{JPCP} if nonreinforced portland cement concrete (PCC),

f_{JRCP} if reinforced PCC

$f_{JPCP} = f_{sbl}\, f_d\, f_{lt}\, f_{prec}\, f_{sg}$

f_{sbl} = subbase adjustment factor: 1; unstabilized

$0.65+0.18 \log(\Sigma ESAL)$; stabilized

f_d = drainage adjustment factor: 1; poor drainage

$0.91+0.12 \log(\Sigma ESAL)-0.03D$; fair drainage

$0.68+0.15 \log(\Sigma ESAL)-0.04D$; good drainage

0.01; excellent drainage

f_{lt} = load transfer adequacy adjustment factor: 1; with dowel

$1.17-0.68 \log(\Sigma ESAL)-0.078D$; without dowel

f_{prec} = rainfall adjustment factor:

$0.89+0.26 \log(\Sigma ESAL)-0.07D$; dry climates

$0.96+0.06 \log(\Sigma ESAL)+0.02D$; wet climates

f_{sg} = subgrade adjustment factor: 1; granular subgrades

$0.57+0.21 \log(\Sigma ESAL)$; coarse subgrade

$f_{JRCP} = f_{sb2}\, f_e$

f_{sb2} = subbase adjustment factor: 1; unstabilized

$0.91-0.02 \log(\Sigma ESAL)$; stabilized

f_e = adjustment for climate:

$0.011+0.003 \log(\Sigma ESAL)-0.001D$; dry, warm climates

$1.44-0.03 \log(\Sigma ESAL)-0.06D$; wet, warm climates

$1.04-0.32 \log(\Sigma ESAL)-0.08D$; dry, cold climates

$0.54-0.85 \log(\Sigma ESAL)-0.19D$; wet, cold climates

PCA Model

Equations 2-10 and 2-11 were developed by PCA (*9*) based on the results of the AASHO Road Test for allowable load repetitions and erosion damage. Erosion is related to pavement deflection (at the slab corner) due to axle loading. Since the erosion criterion was developed primarily from the results of the AASHO Road Test using a specific type of subbase (that was incidentally highly erodible), the application of the model is limited to a single subbase type. Nonetheless, even today this procedure represents a significant advancement in the mechanistic analysis of pavement support condition in design.

$$\log N = 14.524 - 6.777(C_1 P - 9.0)^{0.103} \quad \textbf{(2-10)}$$

$$\text{Percent erosion damage} = 100\sum_{i=1}^{m} \frac{C_2 n_i}{N_i} \quad \textbf{(2-11)}$$

where: N = allowable number of load repetitions based on a pressure of a PSI of 3.0

C_1 = adjustment factor (1 for untreated subbase, 0.9 for stabilized subbase)

P = rate of work or power = $268.7\frac{p^2}{hk^{0.73}}$

p = pressure on the foundation under the slab corner in psi, $p = kw$

k = modulus of subgrade reaction, psi/in.

w = corner deflection, in.

h = thickness of slab, in.

m = total number of load groups

C_2 = 0.06 for pavement without concrete shoulder,
0.94 for pavements with tied concrete shoulder

n_i = predicted number of repetitions for *i*th load group

N_i = allowable number of repetitions for *i*th load group

Model by Jeong and Zollinger

A mechanistic model (Equation 2-12) was developed by Jeong and Zollinger (*10*) using the water-induced shear stresses model proposed by Van Wijk (*1*). Key factors such as vehicle load and speed, load transfer, number of applications, and climatic conditions are included in the model prediction of erosion. Erosion potential increases with higher initial edge gap and liftoff distance due to the effect of upward curling along slab corners and edges inducing shear stress on the base layer by pumping of trapped water.

The magnitude of shear stress depends on the dynamic viscosity of water governed by water temperature and the speed of slab deflection. Higher slab deflection velocity and lower viscosity of water result in more erosion of the base while higher load transfer reduces the erosion rate as depicted in the performance equation. The accuracy of the model should be calibrated using performance data such as that may be available in the LTPP database. This model can be advanced through improved consideration of abrasive frictional stress between concrete and subbase layer.

$$v = v_0 e^{-\left(\frac{\rho}{N_i}\right)^a} \qquad \textbf{(2-12)}$$

where: v_0 = ultimate erosion depth (L)

N = number of axle loads per load group

ρ = calibration coefficient based on local performance

a = $a'\alpha_f$

a' = environmental calibration coefficient

α_f = inverse of the rate of void development

$$= \left[\frac{\partial v_i}{\partial t}\right]^{-1} = \left[\frac{Log^{-1}(a_m\tau + b_m)}{\gamma_b}\right]^{-1} = \left[\frac{\beta}{\gamma_b}\right]^{-1}$$

τ = shear stress = $\frac{\eta B}{\delta_{void}}\left(1 - \frac{LTE}{100}\right)$

η = dynamic viscosity of water ($FL^{-2}t$)

$= \left\{2056.82 + 10.56T - 284.93\sqrt{T} - 265.02e^{-T}\right\}10^{-6}$

T = water temperature (°C)

$B = V_{z_i} \sin\theta + 6V_{z_i}\left[\frac{\sin\theta}{2} + \frac{\cos^2\theta}{\sin\theta}\right]$ (L/t)

δ_{void} = void space below slab for water movement

LTE_i = joint or crack load transfer efficiency (LTE)

θ = slab angle = $\tan^{-1}\left[\frac{z_o}{s}\right]$

z_o = edge gap (L) = $\frac{(1+\nu)}{H}\Delta\varepsilon_{tot}\ell^2$

$V_{z_i} = \frac{\delta_{\text{int}}}{s \diagup V_i}$

$\delta_{\text{int}} = \frac{P_i}{8k\ell}\left\{1 + \left[0.3665\log\left(\frac{a_L}{\ell}\right) - 0.2174\left(\frac{a_L}{\ell}\right)^2\right]\right\}$

a_L = loaded radius (L)

P_i = axle load (F)

s = slab liftoff distance (L)

$= \sqrt{2}\ell(\gamma - 1)$

$\gamma = \sqrt{\frac{z_o}{w_o}}$

$w_o = \frac{\rho H}{k}$

CURRENT DESIGN GUIDELINE FOR BASE/SUBBASE

The design guides published by Texas Department of Transportation (TxDOT), American Association of State Highway and Transportation Officials (AASHTO), National Cooperative Highway Research Program (NCHRP) 1-37 A: Mechanistic-Empirical Pavement Design Guide (MEPDG), and Portland Cement Association (PCA) are reviewed relative to design of the subbase based on material type and the erosion mechanism.

TxDOT Pavement Design Guide

TxDOT's pavement design guide (*11*) published October 2006 approved the 1993 AASHTO *Guide for Design of Pavement Structures* for rigid pavement design. This design guide suggests using one of two types of base layer combinations and a k-value of 300 psi/in. in the rigid pavement design procedure:

- 4 in. of asphaltic concrete pavement (ACP) or asphalt stabilized base (ASB) or
- a minimum 1 in. asphalt concrete bond breaker over 6 in. of a cement stabilized base.

TxDOT aims to prevent pumping by using non-erosive stabilized bases in accordance with Table 2-1, which shows the strength requirements for the three classes of cement treated base:

> *Bases that are properly designed and constructed using TxDOT specifications and test methods should provide adequate long-term support. Where long-term moisture susceptibility of ACP is a concern, using a plan note to increase the target laboratory density (and thus total asphalt content) may be beneficial. To ensure long-term strength and stability of cement stabilized layers, sufficient cement must be used in the mixture. Item 276, Cement Treatment (Plant-Mixed) currently designates three classes of cement-treated flexible base, based on 7-day*

unconfined compressive strength. Classes L and M are intended for use with flexible pavements. Class N, which has a minimum strength as shown on the plans, is intended for use with rigid pavements. There are several approaches to selecting an appropriate strength (and thus indirectly cement content):

- *successful long-term experience with similar materials,*
- *laboratory testing using 100 percent of the retained strength of a conditioned specimen to determine if the design cement content and strength are acceptable,*
- *laboratory testing using the tube suction test to determine if the design cement content and strength are acceptable.*

A bond breaker should always be used between concrete pavement and cement-stabilized base.

Table 2-1 Strength Requirements (*12*).

Class	7-Day Unconfined Compressive Strength, Min. psi
L	300
M	175
N	As shown on the plans

To achieve economical design, the guide needs to develop various subbase type and thickness guidelines over different treated subgrades (i.e., can possibly use 2 in. ACP if 8 in. lime treated subgrade (LTS) has adequate stiffness and durability). Table 2-2 is a partial listing of typical design moduli by material type for new materials in the TxDOT design guide.

Table 2-2 Recommended Material Design Modulus Values (*11*).

Material Type	2004 Specification	Design Modulus	Poisson's Ratio
Asphalt Treatment (Base)	Item 292	250-400 ksi	0.35
Emulsified Asphalt Treatment (Base)	Item 314, various OTU special specs	50-100 ksi	0.35
Flexible Base	Item 247	If historic data not available, modulus should be from 3-5 times the subgrade modulus or use FPS default. Typical range 40-70 ksi.	0.35
Lime Stabilized Base	Item 260, 263	60-75 ksi	0.30 – 0.35
Cement Stabilized Base	Item 275, 276	80-150 ksi	0.25-0.30
Fly Ash or Lime Fly Ash Stabilized Base	Item 265	60-75 ksi	0.30
Lime or Cement Stabilized Subgrade	Item 260, 275	30-45 ksi	0.30
Emulsified Asphalt Treatment (Subgrade)	Item 314, various OTU special specs	15-25 ksi	0.35
Subgrade	(Existing)	Priority should be to use the project-specific back-calculated subgrade modulus. Defaults by county are available in the FPS design program. Typical range is 8-20ksi.	0.40-0.45

1993 AASHTO Design Guide

The AASHTO design guide (*13*) suggests the sub-layer material property of concrete pavement is the composite modulus subgrade reaction determined from Figure 2-11. The composite modulus of subgrade reaction is estimated based on a subbase thickness and subbase elastic modulus with a road soil resilient modulus. However, this method is criticized by Huang (*14*) as follow:

> *The chart was developed by using the same method as for a homogeneous half-space, except that the 30-in. plate is applied on a two-layer system. Therefore, the k values obtained from the chart are too large and do not represent what actually occurs in the field.*

The 1993 design guide also considers potential loss of support (LS) due to foundation erosion by effectively reducing the modulus of subgrade reaction in the design procedure relative to four different contact conditions (i.e., with LS = 0, 1, 2, and 3). The best case is LS = 0, where the slab and foundation are assumed to be in full contact, while the worst case is LS= 3, where an area of slab is assumed not to be in contact with the subgrade, thus warranting reduced values of k-value over the non-contact area.

In Table 2-3, the possible ranges of LS factors for different types of subbase materials are provided to adjust the effective modulus of subgrade reaction as shown in Figure 2-12. The subjective nature of determining the LS value is based on the wide range of possibilities for each material type inherently reduces the sensitivity of the design process to the erosion mechanism leading to inconsistency and limiting applicability of the design procedure.

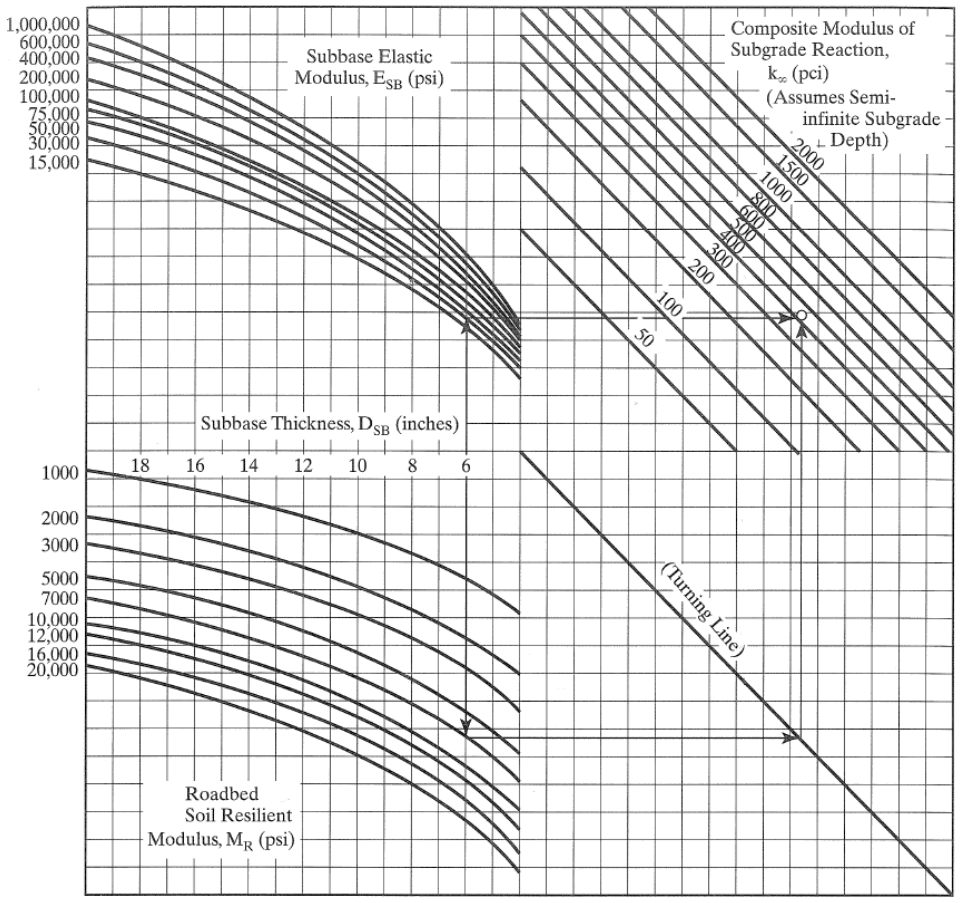

Figure 2-11 Chart for Estimating Modulus of Subgrade Reaction (*13*).

Table 2-3 Typical Ranges of LS Factors for Various Types of Materials (*13*).

Type of Material	Loss of Support
Cement-treated granular base (E = $1x10^6$ to $2x10^6$ psi)	0.0 to 1.0
Cement aggregate mixtures (E = 500,000 to $1x10^6$ psi)	0.0 to 1.0
Asphalt-treated bases (E = 350,000 to $1x10^6$ psi)	0.0 to 1.0
Bituminous-stabilized mixture (E = 40,000 to 300,000 psi)	0.0 to 1.0
Lime-stabilized materials (E = 20,000 to 70,000 psi)	1.0 to 3.0
Unbound granular materials (E = 15,000 to 45,000 psi)	1.0 to 3.0
Fine-grained or natural subgrade materials (E = 3,000 to 40,000 psi)	2.0 to 3.0

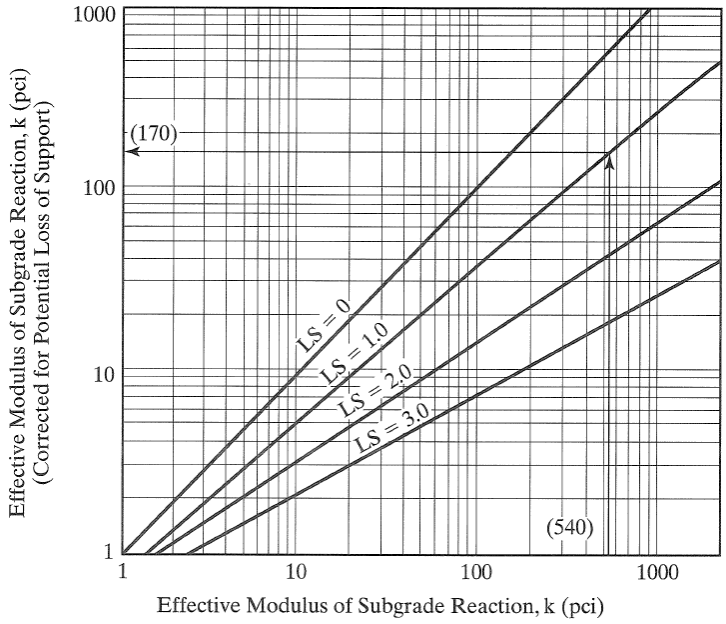

Figure 2-12 Correction of Effective Modulus of Subgrade Reaction Due to Loss of Foundation Contact (*13*).

Load transfer and drainage coefficients are also related with erosion; a lower deflection caused by better load transfer would reduce shear stress at the interface between the slab and base/subgrade and in the vicinity of a joint or crack, as well as minimization of the time water is present on the interface due to better drainage; both situations should decrease the potential for pumping. These factors affecting erosion are considered indirectly through the slab thickness design.

PCA Design Method

PCA procedure developed Equations 2-10 and 2-11 to compute the allowable load repetitions by erosion damage. Separate sets of tables for erosion factors and charts are used for doweled and aggregate interlock joints with or without concrete shoulders.

Figure 2-13 shows approximate k-value that could be used for design purpose based on soil classification or other test methods. Table 2-4 also suggests a simple guide for approximate range of k-value based on subgrade soil types but the vagueness associated with this classification reduces its sensitivity to the erosion mechanism.

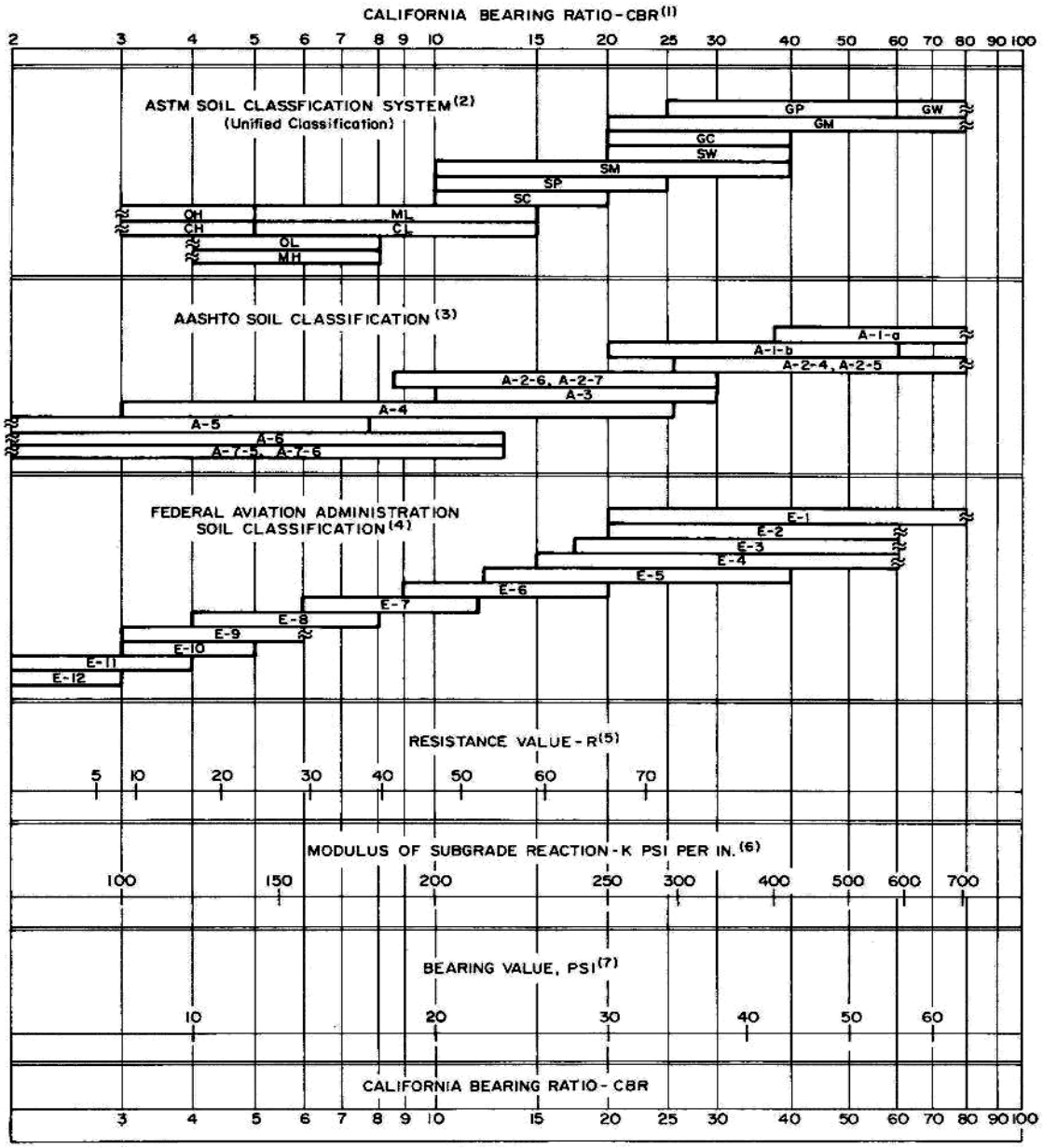

Figure 2-13 Approximate Interrelationships of Soil Classifications and Bearing Values (*9*).

Table 2-4 Subgrade Soil Types and Approximate *k*-Values (*9*).

Type of Soil	Support	k values Range, pci
Fine-grained soils in which silt and clay-size particles predominate	Low	75 – 120
Sand and sand-gravel mixtures with moderate amounts of silt and clay	Medium	130 – 170
Sand and sand-gravel mixtures relatively free of plastic fines	High	180 – 220
Cement-treated subbases	Very high	250 – 400

Table 2-5 shows adjustment of k-value for subbases that could be construed for determining an effective or composite k-value. It is well accepted that cement-treated subbases significantly increase the effective k-value over a subgrade k-value or that caused by use of untreated subbases but only in regard to curling and warping behavior. As mentioned early in AASHTO design guide, the analysis using a 30-in. plate test on a two-layer system may result in a high k-value, which may not represent actual foundation behavior.

Table 2-5 Design *k*-Values for Untreated and Cement-Treated Subbases (*9*).

Subgrade k-value, pci	Untreated Subbase k-value, pci				Cement-treated Subbase k-value, pci			
	4 in.	6 in.	9 in.	12 in.	4 in.	6 in.	8 in.	10 in.
50	65	75	85	110	170	230	310	390
100	130	140	160	190	280	400	520	640
200	220	230	270	320	470	640	830	-

NCHRP 1-37A MEPDG

The NCHRP (*15, 16, 17*) categorize three different design input levels. Level 1 classification is site-specific material inputs obtained through direct testing or methods of measurements that may not be fully developed at this time. Level 2 classification use correlations to establish or determine the required inputs as shown in Table 2-6. Level 3 classification is based on material type description as other design guides.

Table 2-6 Level 2 Recommendations for Assessing Erosion Potential of Base Material *(15, 17)*.

Erodibility Class	Material Description and Testing
1	(a) Lean concrete with approximately 8 percent cement; or with long-term compressive strength > 2500 psi (>2000 psi at 28 days) and a granular subbase layer or a stabilized soil layer, or a geotextile fabric is placed between the treated base and subgrade, otherwise Class 2. (b) Hot-mixed asphalt concrete with 6 percent asphalt cement that passes appropriate stripping tests and aggregate tests and a granular subbase layer or a stabilized soil layer (otherwise Class 2).
2	(a) Cement-treated granular material with 5 percent cement manufactured in plant, or long-term compressive strength 2000 to 2500 psi (1500 to 2000 psi at 28 days) and a granular subbase layer or a stabilized soil layer, or a geotextile fabric is placed between the treated base and subgrade, otherwise Class 3. (b) Asphalt-treated granular material with 4 percent asphalt cement that passes appropriate stripping test and a granular subbase layer or a treated soil layer or a geotextile fabric is placed between the treated base and subgrade, otherwise Class 3.
3	(a) Cement-treated granular material with 3.5 percent cement manufactured in plant, or with long-term compressive strength 1000 to 2000 psi (750 to 1500 psi at 28 days). (b) Asphalt-treated granular material with 3 percent asphalt cement that passes appropriate stripping test.
4	Unbound crushed granular material having dense gradation and high quality aggregates.
5	Untreated soils (PCC slab placed on prepared/compacted subgrade).

The NCHRP 1-37 A MEPDG addresses erosion through modeling faulting distress (Equations 2-13 and 2-14). Classes of erodibility are formulated based on a modification of Permanent International Association of Road Congresses (PIARC) specifications relative to material type and stabilizer percent. Five levels of erosion resistance listed in Table 2-6, distinguish between material types based on stabilizer type and content (asphalt or portland cement) as well as long-term compressive strength (later than 28 days). Prediction of erodibility is closely associated with the material compressive strength. Each class of erosion is assumed to offer five times the resistance to erosion than the next class (i.e., Class 1 materials are five times more erosion resistant than Class 2 and so on).

However, field performance of lower strength subbase material has been good perhaps because of low friction interface bases. For instance, a 2-in. asphalt concrete (AC) overlaid 8-in. thick CRC pavement of IH 30 in Fort Worth constructed in the 1950s over a seal-coated flexible base has been performing well for 50 years. Little guidance is provided addressing the degree of friction that should exist between the concrete and an underlying base layer or its contribution to erosion of the interface via load-induced shear stress. Moreover, PIARC uses the classification based on brush test results (previously noted) under dry conditions, which yields conservation results compared to erosion action under saturated conditions.

$$FAULTMAX_i = FAULTMAX_0 + C_7 * \sum_{j=1}^{m} DE_j * Log(1 + C_5 * 5.0^{EROD})^{C_6} \quad \textbf{(2-13)}$$

$$FAULTMAX_0 = C_{12} * \delta_{curling} * \left[Log(1 + C_5 * 5.0^{EROD}) * Log(\frac{P_{200} * WetDays}{P_s}) \right]^{C_6} \quad \textbf{(2-14)}$$

where: $FAULTMAX_i$ = maximum mean transverse joint faulting for month i, in.

$FAULTMAX_0$ = initial maximum mean transverse joint faulting, in.

DE_i = differential deformation energy accumulated during month i

$EROD$ = base/subbase erodibility factor

C_{12} = $C_1 + C_2 * FR^{0.25}$

C_i = calibration constants

FR = base freezing index defined as percentage of time the top base temperature is below freezing (32 °F) temperature

$\delta_{curling}$ = maximum mean monthly slab corner upward deflection PCC due to temperature curling and moisture warping

P_s = overburden on subgrade, lb

$P200$ = percent subgrade material passing #200 sieve

$WetDays$ = average annual number of wet days (greater than 0.01in. rainfall)

Table 2-6 also can be used to estimate erosion width in CRC pavement and incorporated into the punchout prediction model. An empirical model for expected erosion width (Equation 2-15) is developed from expert opinion since no model, procedure, or field data are available for developing relationships between the erosion class, precipitation, and eroded area.

$$e = -7.4 + 0.342P_{200} + 1.557BEROD + 0.234PRECIP \quad \textbf{(2-15)}$$

where: e = maximum width of eroded base/subbase measured inward from the slab edge during 20 years, in. (if $e < 0$, set $e = 0$)

P_{200} = percent subgrade soil (layer beneath treated base course) passing the No. 200 sieve

$BEROD$ = base material erosion class (1, 2, 3, or 4)

$PRECIP$ = mean annual precipitation, in.

The NCHRP design guide provides general recommendations for subbase class selection based on load transfer efficiency and traffic level but there is no guide for the determination of layer thickness. A high volume lane requires high joint load transfer with an erosion-resistant base as shown in Table 2-7.

Table 2-7 Recommendations for Base Type to Prevent Significant Erosion (*15*).

Design Lane Initial ADTT	JPCP		CRCP
	Nondoweled	Doweled	
> 2,500	n/a – nondoweled design not recommended	Class 1	Class 1
1,500 – 2,500	n/a – nondoweled design not recommended	Class 1	Class 1
800 – 1,500	n/a – nondoweled design not recommended	Class 2, 3, or 4	Class 1
200 – 800	Class 2 or 3	Class 3 or 4	Class 2
< 200	Class 4 or 5	Class 4 or 5	Class 3

SUMMARY AND DISCUSSIONS

Previous erosion test methods are reviewed and summarized in Table 2-8. The strong points such as generating erodibility index and simulating field condition with no coarse aggregate loss were considered for new test method therefore, a test method like rolling wheel erosion test device is selected and shortcomings of previous test methods such as long test time, no void under slab, and sample surface damage would be improved in new test method.

Table 2-9 shows summarized reviews of previous erosion models. The mechanistic model by Jeong and Zollinger was selected to be improved based on the calibration through out the lab tests and field data since a general mechanistic model was not developed properly. Lab test results using new test method and LTPP data would be applied for model calibration process.

According to the review of previous subbse design guides in Table 2-10, NCHRP 1-37A MEPDG presented some of the most comprehensive guidance with erodibility class which is determined based on dry condition brush test results and strength test. However, erosion occurs mostly under saturated condition, therefore, new design guide would provide new criteria for subbse erosion based on wet condition test results using site specific material. Moreover, all design factors in AASHTO and PCA design that affect the performance of subbase would be reconsidered in the advanced design guides.

Table 2-8 Summary of Erosion Test Methods.

Test method	Features	Strengths	Weaknesses
Rotational shear device	Stabilized test samples are eroded by application of hydraulic shear stress. The critical shear stress is recommended as an index of erosion resistance	Easy and precise to control shear stress	No consideration of crushing or compressive failure. Overestimation of weight loss by coarse aggregates loss
Jetting device	Pressurized water at an angle to the upper surface of unstabilized samples generating weight loss over time	Easy to test	Shear stress is not uniform and inaccurate. Overestimation of weight loss by coarse aggregates loss
Brush test device	Rotational brush abrasions generate fines. An erosion index, IE is defined as the ratio of the weight loss to that of a reference material	Easy to test. Consider durability of wet and dry cycle. Relative erodibility of each material is defined using an erosion index, IE	Long test time and overestimation of weight loss by coarse aggregates loss
Rolling wheel erosion test device	Wheel movements over a friction pad on sample induce erosion. Measure average erosion depth after 5000 wheel load applications	Simulate field conditions for flexible pavement. No coarse aggregate loss.	Voiding of the subbase under concrete slab can not be considered. Sample saw-cut can damage surface of sample

Table 2-9 Summary of Erosion Models.

Erosion model	Features	Strengths	Weaknesses
Rauhut model	Empirical model using COPES data	Include many erosion related factors	Rough categories for each material factor
Markow model	Empirical model using AASHO data: traffic, slab thickness, drainage	Consider more detail drainage condition	Subbase material properties are ignored
Larralde model	Empirical model using AASHO data: traffic, slab thickness	Normalized pumping index to eliminate the effect of slab length and reinforcement	No consideration about many erosion related factors

Table 2-9 (continued).

Erosion model	Features	Strengths	Weaknesses
Van Wijk model	Fusion model of Rauhut and Larralde models with more field data	Consider various erosion related factors and four types of climates	Rough categories for each material factor
PCA model	Mechanistic-empirical model using AASHO data	Significant advancement in the mechanistic analysis	Application of the model is limited to subbase types used in AASHO test
Jeong and Zollinger model	Mechanistic model using theoretical hydraulic shear stress model	Predict erosion depth based on feasible mechanistic equations	Calibration require through lab tests and field performances

Table 2-10 Summary of Subbase Design Guides.

Design guide	Features	Strengths	Weaknesses
TxDOT	Select one from two types of stabilized subbase and require minimum 7-day compressive strength	Historical performances and erosion resistance are demonstrated as good	Costly excessive design regardless subgrade and environmental condition
1993 AASHTO	Composite modulus of subgrade reaction considers the loss of support due to the foundation erosion	Accounting structural degradation of support due to erosion using LS factor	k-value obtained from the chart is over estimated and LS is insensitive to various stabilized materials
PCA	Provide erosion factor as a function of the slab thickness, composite k-value, dowel, and shoulder type	Consider erosion analysis in design procedures as the most critical distress in rigid pavement performance	Proposed composite design k-values for treated bases are overestimated and need discrimination for different stabilization levels
NCHRP 1-37A MEPDG	Classified erodibility of subbase materials are utilized in JCP faulting prediction model as well as erosion width estimation of CRCP	Employed the erodibility class based on the type and level of stabilization along with compressive strength	Erodibility class is determined based on dry brush test results and strength even erosion occurs mostly under saturated condition

CHAPTER III

FIELD INVESTIGATIONS

Field investigation of pavement condition is the first step to identify the factors associated with the erosion process. It is needed to validate the extent of distress related damage, the quality of drainage, and relative base/subgrade layer strength and pavement distress condition is considered relative to functional and structural performance. The following evaluation techniques are applied:

- visual survey,
- FWD,
- GPR, and
- DCP.

EVALUATION TECHNIQUES

Visual Survey

Selected project sites can be scanned to identify distressed areas to select locations for further inspection. There are many well organized visual pavement condition survey protocols used by highway agencies to monitor and record pavement distresses. However, current survey protocols often require a level of inspection detail greater than what is normally needed; therefore, simplified survey as following information are collected:

- general information about pavement – age, aggregate type,
- condition record information – recent visual and deflection information,
- condition of joint or crack sealing,
- surface and subsurface drainage condition – possible locations for GPR and DCP testing,

- functional conditions – factors affecting riding quality and possible locations for FWD, GPR and DCP testing,
- structural conditions – factors affecting premature failure of pavement,
- possible locations for FWD, GPR and DCP testing, and
- identification of distressed areas for full depth repair (FDR).

FWD Testing

Deflection test using FWD can evaluate the structural condition of pavement such as layer stiffness, LTE, and loss of support below the slab. Therefore, the areas selected from the checklist of visual survey items needs to be evaluated relative to structural capacity for such stiffening measures as load transfer retrofitting. Figure 3-1 shows the example of FWD testing along the edge and center of slab locations. Highly spalled or faulted joints and cracks should be tested to evaluate LTE and continuity of support. Moreover, deflection and LTE at the center of slab should be tested occasionally as a reference of good support conditions.

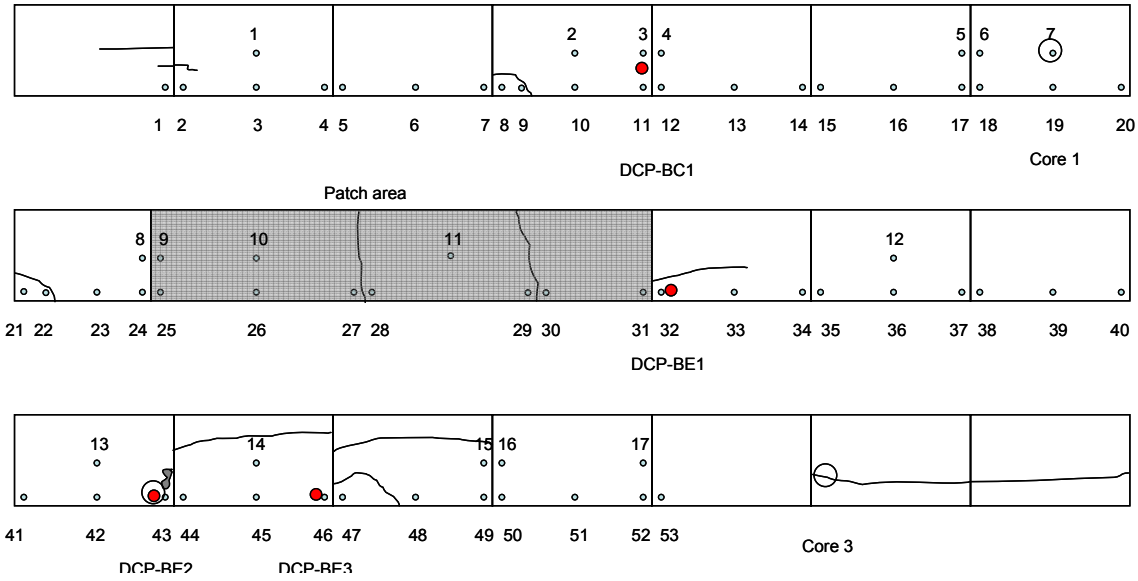

Figure 3-1 Example of the FWD Testing Locations.

LTE

LTE is recommended to check the structural capacity of joints or cracks. Deflections on loaded and unloaded side of a joint or crack are measured, and used to determine the LTE as follows:

$$\text{LTE} = \frac{d_U}{d_L} \times 100 \quad \textbf{(3-1)}$$

where: LTE = Load transfer effectiveness, percent

d_U = Deflection on the unloaded side of the joint or crack, mils

d_L = Deflection at the loaded side of the joint or crack, mils

It is recommended that testing be completed when the ambient air temperature is above 80 ^oF, and below 60 ^oF. Since LTE is generally over 90 percent for temperature expanded concrete pavement, load transfer retrofitting should be considered when LTE is lower than 70 percent a substantial amount of time at the joint or crack.

Effective Thickness

In conjunction with the LTE, the calculated effective thickness, h_e indicates areas of deterioration. The locations show low effective thicknesses are interpreted as areas of low stiffness. The deflection basin area based on seven sensors is used to determine the effective radius of relative stiffness as a function of the effective thickness using Equation 3-2 (*18*).

$$h_e = \left[\ell_m^4 \cdot \frac{12\left(1-\nu^2\right)k_{dyn}}{E_c} \right]^{\frac{1}{3}} \quad \textbf{(3-2)}$$

where: h_e = effective slab thickness, in.

ℓ_m = radius of relative stiffness, in.

$= 0.0284 \cdot BA^2 - 0.2891 \cdot BA + 0.992$

ν = Poisson's ratio of the concrete

k_{dyn} = dynamic modulus of subgrade reaction, psi/in.

$$= \frac{d_0^* \cdot P}{d_0 \cdot \ell^2} \cdot 1000$$

Ec = elastic modulus of the PCC layer, psi

d_0^* = dimensionless deflection

$$= \frac{1}{8}\left[1 + \frac{1}{2\pi}\left(\ln\left(\frac{a}{2\ell}\right) - 0.673\right)\left(\frac{a}{\ell}\right)^2\right]$$

P = wheel load, lb

d_0 = deflection at the loading position, mils

a = radius of loading plate, in.

BA = basin area calculated from 7 sensors, in.

$$= 6\frac{d_0 + 2(d_1 + d_2 + d_3 + d_4 + d_5) + d_6}{d_0}$$

d_1, d_2, d_3, d_4, d_5, d_6 = Deflection at 1, 2, 3, 4, 5 and 6 ft from the loading position, mils

Basin Area

Deflection basin area is a simple means to detect possible deteriorated areas. The locations which show low deflection basin areas could be interpreted as problematic as the same meaning of a low LTE. The typical range of basin area for rigid pavements is between 24 and 33 in., and load transfer retrofitting may be recommended when basin area is lower than 25 in. Deflection basin area can be calculated by Equation 3-3 (*19*):

$$\text{Basin area} = \frac{6(D_0 + 2D_1 + 2D_2 + D_3)}{D_0} \quad \textbf{(3-3)}$$

where: Basin area = FWD deflection parameter, in.

D_0 = Deflection at the loading position, mils

D_1 = Deflection at 12 in. from the loading position, mils

D_2 = Deflection at 24 in. from the loading position, mils

D_3 = Deflection at 36 in. from the loading position, mils

GPR Testing

GPR testing is a fast and effective test method to determine base conditions such as voids and the presence of water trapped in and between underlying pavement layers. Moreover, GPR survey can be used for PCC pavement layer thickness estimation, layer interface condition assessment, and dowel misalignment evaluation. In pumping areas, dowel locations, voids, and subsurface water under the slab could be detected using an air-coupled system vehicle or ground coupled, as shown in Figure 3-2. Although no standard procedures have been documented for detection of voids under the concrete slab using GPR, image analysis or dielectric constant (DC) analysis could be used to detect void and subsurface moisture for the routine maintenance purpose.

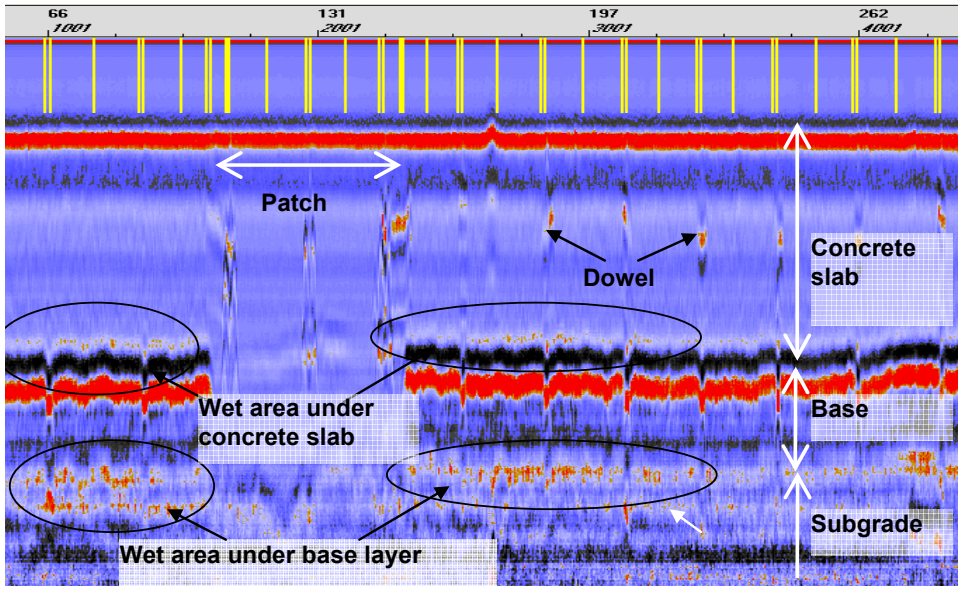

Figure 3-2 Example of the GPR Testing Image.

Image Analysis

Detection of voids under the concrete slabs may require determination by trained personnel, but generally the following can help to analyze GPR images. In the color image, blue strips represent voids and red strips represent moisture, while in the gray scale image, black strips represent voids and white strips represent moisture. Intervallic dots indicate dowel locations.

DC Analysis

The DC value of GPR can be used to detect subsurface moisture. DC values range from 1 (air) to 81 (distilled water), and generally DC of aggregate base is around 6 to 7. In the pavement system, DC is an efficient indicator of the presence of subsurface water if the DC of base or subgrade is higher than 9.

DCP Testing

DCP testing indicates the in situ strength of base and subgrade soils. The test provides a correlation between the strength of the soil and its resistance to penetration. It is a fast and easy method and can be used to estimate the elastic modulus of each layer and sublayer. Conduct DCP testing on selected areas where visual and GPR surveys indicate the evidence of pumping or subsurface water. Equation 3-4 shows the relationship between the penetration ratio and elastic modulus of soils (*20*).

$$E = 2550 \times CBR^{0.64} \quad \textbf{(3-4)}$$

$$CBR = 292 / PR^{1.12}$$

where, E = Elastic modulus, psi

CBR = California bearing ratio

PR = Penetration ratio, mm/blow

Figure 3-3 shows an example of calculation for penetration ratio. A plot of the DCP data is useful to find the slope of the linear trendline. Typical flexible base modulus is 60 to 80 ksi or PR is 1 to 2 mm/blow (0.05 to 0.1 in./blow). The PR value higher than 2 in./blow indicates a very soft subgrade material which implies the soil modulus < 6000 psi.

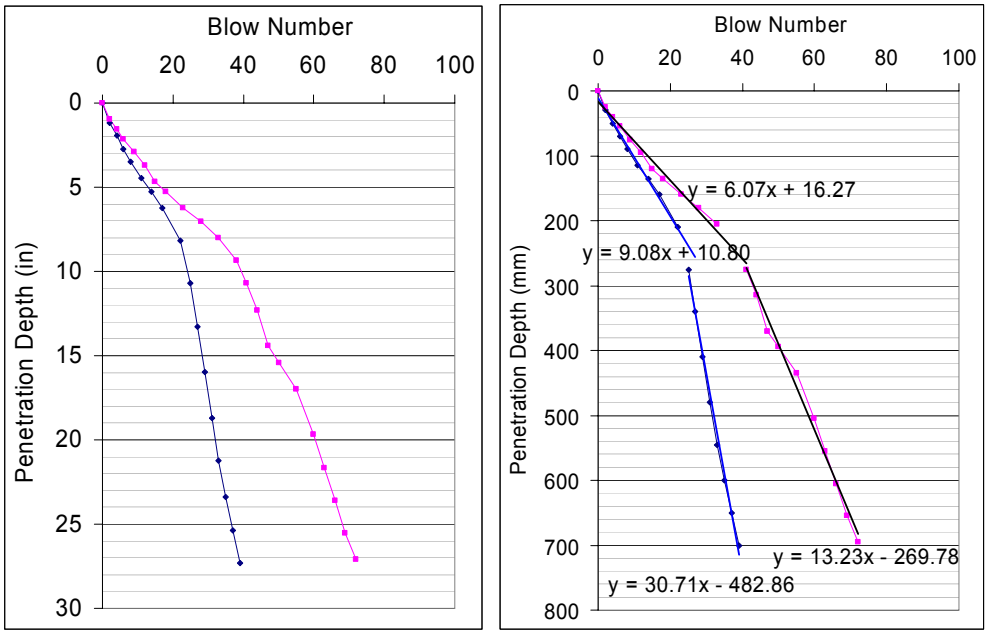

Figure 3-3 Example of the DCP Testing Analysis.

SELECTED FIELD INVESTIGATION RESULTS

The objectives of the field investigation were to identify the factors associated with the erosion process. Sample sections were identified and investigated using a number of techniques including visual survey, nondestructive testing and coring. Table 3-1 shows the performance of non-asphalt treated subbase of selected pavement sections in Texas.

Generally, untreated flexible base and lime-treated subgrade have not performed well under both CRC and JC pavement. These sections were subject to pumping damage through the displacement of fines causing voiding of the subbase layer. However, sections constructed in the 1950s involving a seal-coated flexible base have performed well; these sections were also constructed on elevated ground, which apparently

facilitates good surface drainage and maintains unsaturated conditions in the subgrade. The presence of the seal coat may have helped to reduce moisture intrusion into the base while minimizing the friction between a slab and the flex base. Most cement treated bases in Texas placed without a bond breaker have performed well under both jointed and CRC pavements and various traffic levels since CTB is highly resistant to erosion. However, sections statewide with weakly constructed CTBs built during the 1950s and 1960s have shown premature failures possibly due to the low cement content of these bases.

Table 3-1 Subbase Type and Performance of Highways in Texas.

Poorly Performing Subbases	Well Performing Subbases
Statewide – 8 in. CRC pavement over weak CSB (1950s-1960s)	**IH 30 in Fort Worth** – 8 in. CRC pavement over seal coat and flexible base, built in late 1950s (overlaid with 2 in. Asphalt Concrete Pavement (ACP), still in place)
IH 35E near Waxahachie – 8 in. CRC pavement over flexible base, built in the 1960s	**IH 10 in El Paso** – 8 in. CRC pavement built directly over CSB
US 75 near Sherman – 10 in. concrete pavement contraction design (CPCD) over flexible base, built in the early 1980s	**IH 10 in Houston** – 8 in. CRC pavement over CTB
IH 35W N. of Fort Worth – 8 in. CRC pavement over lime-treated subgrade, built in the 1960s	**Beaumont District** – CPCD over CSB
Various roadways in Atlanta and Childress – 13 in. CPCD (no dowels) over natural subgrade (usually sandy)	**IH 45 in Houston** – 8 in. JRCP over Oyster Shell Base (1945)

An AC base on a lime-treated subgrade on US 81/287 in Wise County has performed reasonably well except in areas where the subbase and subgrade was eroded. The bond condition particularly between CRC and an AC base layer was generally good but erosion at the slab/AC layer and the AC layer/lime-treated subgrade interfaces diminished the structural integrity of the pavement.

The cement stabilized oyster shell base on FM 364 in the Beaumont area showed some erosion at the interface with the PCC (near the joint). No erosion was noted away from the joint as indicated by the good contact between the concrete slab and the base. Distressed areas on the frontage road along IH 10 in Beaumont consisted of severe map cracking, spalling, and pumping due to placement of a CRC pavement over a soft silty and sandy subgrade. Some patched areas had settled and experienced corner breaks due to low LTE and poor support. Most of the damage appeared to be due to a weak subgrade and an insufficient slab thickness for the applied loads.

The key distress types of CRC pavement over CTB on IH 635 in the Dallas area were related to the condition of the full-depth patches and the widened longitudinal joints; nonetheless the overall condition of the pavement appeared to be very good. The patches in the pavement were most likely repairs of either full or partial punchouts that were possibly a result of erosion and loss of support immediately below the slab. Summarized evaluations of selected sections are discussed from Table 3-2 to Table 3-4.

Table 3-2 Performance of Field Test Sections US 75 and US 81/287 in Texas.

Test Section	US 75—Sherman District	US 81/287—Wise County Sections 1 and 2
Pavement Type	10 in. (15 ft joint spacing) JC pavement built in 1983	8 in. CRC pavement on northbound near Decatur constructed in 1971
Subbase Type	6 in. unbound aggregate base	4 in. AC base
Subgrade Type	Weathered soil subgrade	6 in. lime-treated subgrade, sandy soil
Traffic	ADT = 43,000 Total = 25 million equivalent single axle load (ESAL)s	ADT = 23,000 (23% truck) Total = 35 million ESALs
Distress Type	Faulting, pumping	Pumping, faulting, patching
Cause of Distress	Joint sealing deterioration, weak subbase, erosion	Wide crack widths, wide and no longitudinal joint sealing
GPR Analysis Results	Most sections showed voided and eroded areas. Patched sections showed no erosion but slabs adjacent to the patched areas did indicate voided areas	GPR images showed significant amounts of wet or eroded areas in the lime-treated subgrade layer; however, little erosion on the AC base layer was detected
FWD Analysis Results	Patched sections had low LTE and effective thickness due to the lack of aggregate interlock along the joints and consequently potential problem locations for future repair	Section with wetter subgrade conditions showed a greater mean deflection. Some cracks have a relatively low LTE and may hold a higher possibility of erosion in the future at those locations
DCP Analysis Results	Patched areas showed a base modulus to be about twice the base modulus of the unrepaired sections caused discontinuous base support	Section 1 had the lowest elastic modulus, perhaps due to the wet subgrade conditions as noted by the GPR images
Coring Analysis Results	The evidence of separation due to erosion and pumping action were apparent	Some erosion at the interface between AC and subgrade was detected

Table 3-3 Performance of Field Test Sections US 81/287 and FM 364 in Texas.

Test Section	US 81/287—Wise County Section 3	FM 364—Beaumont Area
Pavement Type	12 in. CRC pavement with 3 ft extended lane width as part of the shoulder constructed in 1985	10 in. (15 ft joint spacing) JC pavement constructed in 1985
Subbase Type	2 in. AC base 2 in. AC subbase	6 in. cement stabilized oyster shell base
Subgrade Type	6 in. lime-treated subgrade, sandy soil	Natural soil subgrade
Traffic	ADT = 23,000 (23% truck) Total = 35 million ESALs	ADT = 21,000 (2.5% truck) Total = 2.5 million ESALs
Distress Type	No major distress	Transverse cracks near the joints
Cause of Distress	Thick Portland Cement Concrete (PCC), extended lane width, good longitudinal joint seal	Late saw-cutting
GPR Analysis Results	Low level of moisture at the interface between two AC base layers and a moderate level of moisture on the subgrade layer, no significant erosion was identified	High chance of water was presented at the interface of the slab and base layer as well as an indication of erosion-related damage
FWD Analysis Results	Low deflection and high effective thickness	Most joints show good LTEs and low deflections except eroded area
DCP Analysis Results	modulus was in the low end of the range of typical values since the untreated natural subgrade material was a low modulus material	Calculated modulus was in the normal range of subgrade material moduli
Coring Analysis Results	Manifest erosion on the AC subbase layer; debonding and the erosion between two AC layers diminishes the structural integrity of the pavement	Damage at the interface between base and subgrade was limited to the vicinity of the joint. The bottom of each layer indicated a debonded condition

Table 3-4 Performance of Field Test Sections IH 10 and IH 635 in Texas.

Test Section	IH 10—Beaumont Area	IH 635—Dallas Area
Pavement Type	6 in. CRC pavement constructed in 1963	8 in. CRC pavement with a concrete shoulder opened to traffic in 1967
Subbase Type	No subbase	4 in. cement stabilized base
Subgrade Type	Silty and sandy subgrade	Sandy and clay subgrade
Traffic	ADT = 100 (3.2 % truck) Total = 130,000 ESALs	ADT = 200,000 (12% truck)
Distress Type	Severe map cracking with spalling and pumping	spalled cracks and patches, widened longitudinal joints
Cause of Distress	No joint sealing, subgrade erosion and saturation to 12 in. depth	erosion and loss of support immediately below the slab
GPR Analysis Results	High degree of moisture and voiding under the slab; some peaks of DC values occurring at the beginning and end of the FDR patches	Some moisture areas under the concrete slab but no significant sign of erosion was identified. DC values of overall sections represented a low level of moisture on the base layer
FWD Analysis Results	Low effective thickness in combination with high deflection was found at the FDR patch joints indicating weakened subgrade conditions at those locations	Good LTEs but there were a few areas where low values of effective thickness exist indicating the integrity of this pavement is beginning to diminish
DCP Analysis Results	The subgrade was very weak; All tested locations showed very high penetration ratios through the top 12 in.. Backcalculated moduli were around 2.5 to 3 ksi	Good subgrade conditions. The pavement support is not presently as issue but could soon become serious if maintenance activities are terminated or diminished
Coring Analysis Results	All cores showed eroded conditions and, of course, no bonding between the concrete and the subgrade. There was no base layer	Erosion was found only at areas where the condition of the longitudinal construction joint was not well maintained and moisture had penetrated the pavement

US 75—Sherman District

US 75 Sherman, TX is a 10 in. 15 ft jointed PCC pavement built over 6 in. unbounded limestone aggregate base and weathered natural soil subgrade in 1983. Traffic information was limited but was found to be 42,760 ADT in 1997. Much of the jointed pavement over the sampled areas has exhibited poor performance since the early 1990s. Slab settlement issues (with limited cracking and shattering) were worsening even though joint sealant repairs were performed in 1996 and then a major rehabilitation involving slab jacking using polyurethane material was undertaken in 2004 to fill voids under the slab and eliminate eroded areas below the affected slabs due to pumping action. After the slab jacking work was completed, generally, very little settlement occurred during the first 2 years; however, some slabs started to crack, and pavement conditions worsened again. Cracks formed between grout injection holes and with the transverse joint or shoulder. This problem could possibly have been caused by overgrouting and being too aggressive with the repair technique, combined with soft and low subgrade strength. Localized slab jacking and stiffening at slab corners may also generate cracks in the middle of the slab due to lifting the slab edges creating a lack of support under the center of the slab.

The sampled data suggested the project could be divided into four sections as noted in Figure 3-4: (a) good performing areas (with no cracks), (b) poor performing condition areas (with more than one crack), (c) newly patched slabs (approximately 1 to 2 years old), and (d) areas with patches more than 5 years old. The good performing and patched areas showed no distress but the joint sealing appeared to be well maintained. Poorly performing sections typically showed significant joint seal deterioration particularly along the joints between the lanes and the shoulder, which apparently lead to significant base and subgrade erosion.

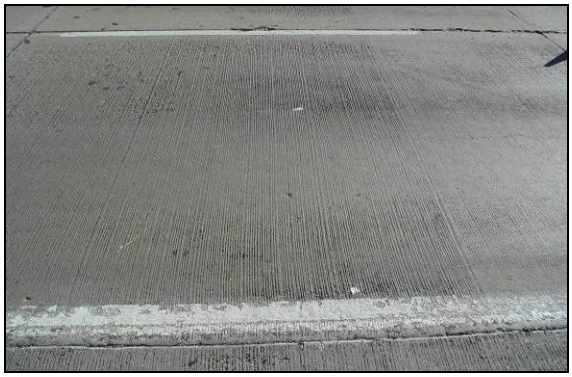

a) Good Performing Section

b) Poorly Performing Section

c) Newly Patched Section

d) Old Patched Section

Figure 3-4 Test Sections on US 75.

FDR in Figure 3-5 was employed as another method to eliminate badly deteriorated sections. However, some FDR or areas adjacent to the FDR failed soon have placement caused perhaps by saturated and weakened base and subgrade materials. Adjacent slab damage was often caused by the FDR itself or because moisture was able to readily penetrate the subgrade because of the improperly placed FDR. Damaged joint seals (especially at shoulder joints) often allowed for the penetration of water or incompressible material into the joint, which can be problematic if there is no edge drain system. Figure 3-5 shows the pictures how quickly patching areas may deteriorate especially with intrusion of water due to a lack of joint sealing. Moreover, rocking of the slab caused by insufficient LTE, uneven support, and poor base/subgrade compaction resulted in significant faulting within the patch sections.

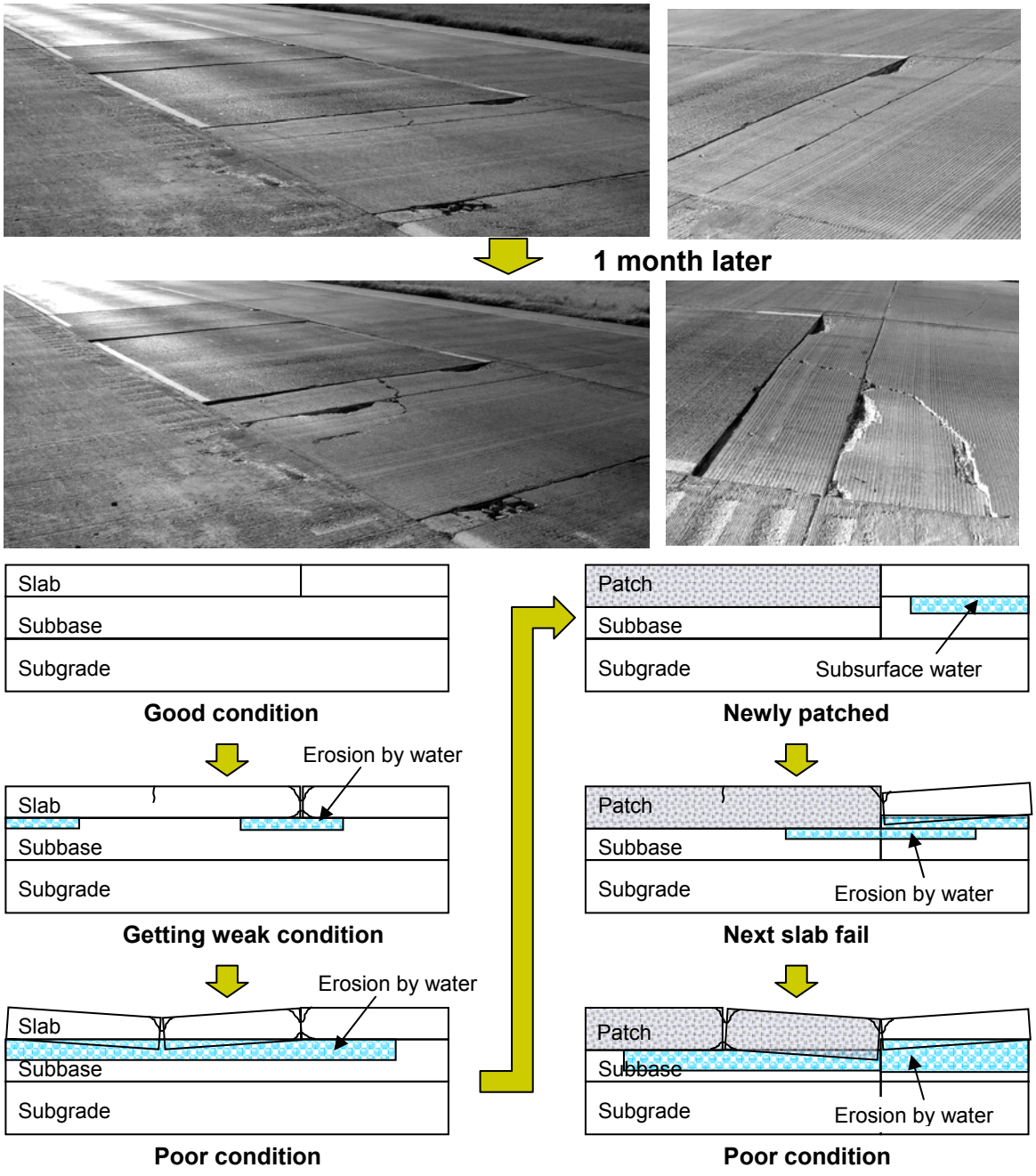

Figure 3-5 Pavement Performance and Deterioration Process of FDR.

Visual survey

Test sections were classified visually as good areas (no cracks), poor areas (slabs with more than one crack), slabs with old patches (patches more than 5 years old), and newly

patched slabs (patches approximately 1 to 2 years old). The good performing areas showed no surface distress particularly where the shoulder joint seals were kept in good condition while the shoulder joint seals in the poor performing sections typically showed significant joint seal deterioration. Based on decision flow chart, joint resealing should be employed to block the surface water intrusion. Table 3-5 shows the visual condition survey results of poor condition sections.

Table 3-5 Concrete Pavement Condition Survey.

No.	Checklist	Notes	More NDT Inspection (Enter all that apply)
1	Pavement age (yr.)	24 yrs, 15 ft joint spacing	
2	Aggregate type (hard or soft)	Soft - limestone	
3	Year of recent pavement distress survey (yr.)	N/A	
4	Year of recent pavement deflection survey (yr.)	N/A	FWD, GPR
5	Joint sealant age (yr.)	N/A	
6	Sealant damage of transverse joint (%)	50%	GPR
7	Sealant damage of longitudinal joint (%)	80%	GPR
8	Sealant damage of sealed crack (%)	No seal on crack	GPR
9	Trapped surface water in depressed area	No	
10	Standing water or slab staining	Yes - on shoulder	GPR, DCP
11	Pumping with or without staining	Positive	FWD, GPR, DCP
12	Bump (stable or unstable; depth, in.)	No	
13	Settlement (stable or unstable; depth, in.)	Repaired	
14	Joint spall (width, depth, % of joint spall > 2 in.)	3 in., 2 in., 20%	FWD, GPR
15	Crack spall (width, depth, % of crack spall > 2 in.)	2 in., 1 in., 5%	
16	Deep spall (depth, in.)	No	
17	Patching (number/mile)	35	FWD, GPR
18	Faulting (depth, in.)	No - Repaired	
19	Transverse crack (width, number/slab)	0.05 in., 2/10	FWD, GPR, DCP
20	Longitudinal crack (width, number/slab)	0.04 in., 1/10	FWD, GPR, DCP
21	Shoulder separation (width, in.)	1/4 in. joint well damage	
22	Corner break (spall width, fault depth, % of slab)	12 in. × 10 in., 5%	
23	Punchout (spall width, fault depth, % of slab)	N/A	
24	Reflection crack in overlay	N/A	

FWD Testing

Figure 3-6 illustrates an example location of FWD testing. Figure 3-7 shows joint LTE and effective thickness along the center and the edge of slab. Interestingly, the patched sections had low LTE and effective thickness as if eroded conditions were present. The reason for low LTE in these sections is perhaps due to the lack of aggregate interlock along the joints. LTE and erosion are typically highly related to each other; joints with low LTE are often associated with high rates of erosion due to independent deflection behavior between two slabs; an eroded base also contributes to higher wear out rates of the aggregate interlock. Patches in pavements tend to create areas of low stiffness and consequently potential problem locations for future repair.

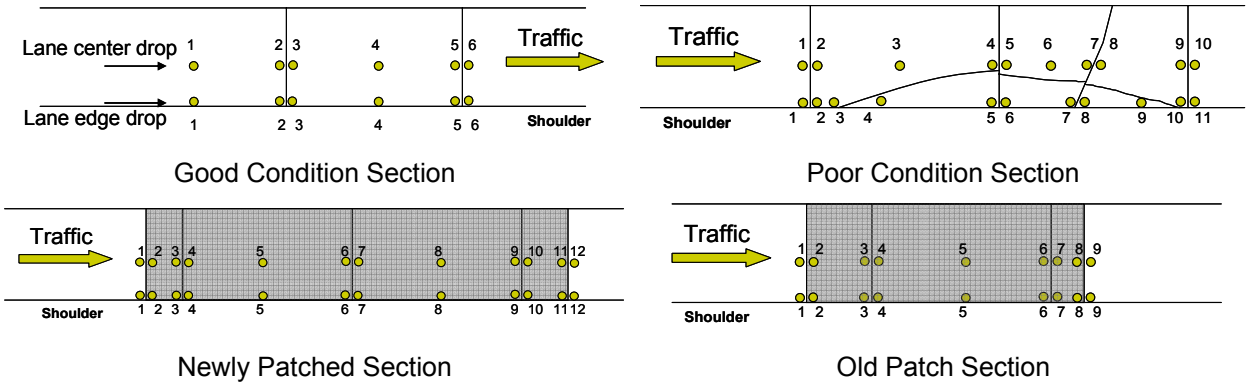

Figure 3-6 Test Sections and FWD Location ID Numbers.

Figure 3-7 LTEs and Effective Thickness of Test Sections.

Figure 3-8 shows the mean and standard deviation of FWD basin areas. Patched sections show a lower mean basin area with a higher standard deviation than the cracked poorly performing areas, which means the general structural capacity of FDR is lower than even the problematic pavement areas manifesting non-uniform support that often results in premature slab cracking. Other existing patched areas should be checked using the FWD for structural adequacy and proper maintenance includes activities such as joint resealing and retrofit doweling to prolong the life of patched areas.

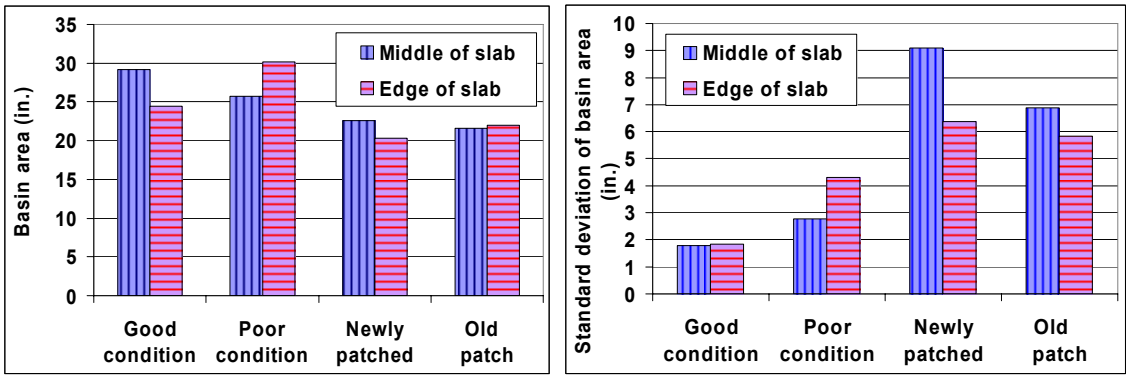

Figure 3-8 Mean and Standard Deviation of Basin Area of Test Sections.

GPR Testing

Figure 3-9 shows GPR images in which voids are represented as black areas and eroded or wet areas represented as bright areas within the base layer. Poor performing sections showed many voided and wet areas while the good performing sections showed some areas with erosion and moisture. The patched areas did not show significant moisture damage, but adjoining areas showed the presence of water which could affect the performance of those areas. The zigzag line in the lower portion of Figure 3-9 is the surface DC value which indicates the moisture level of the base. The good and poor performing sections show high DC values suggesting wet base conditions may exist while patched sections show lower DC values. Edge drain for subsurface water and slab undersealing for voids under the slabs would be feasible solution to reduce pumping – as noted in the decision chart.

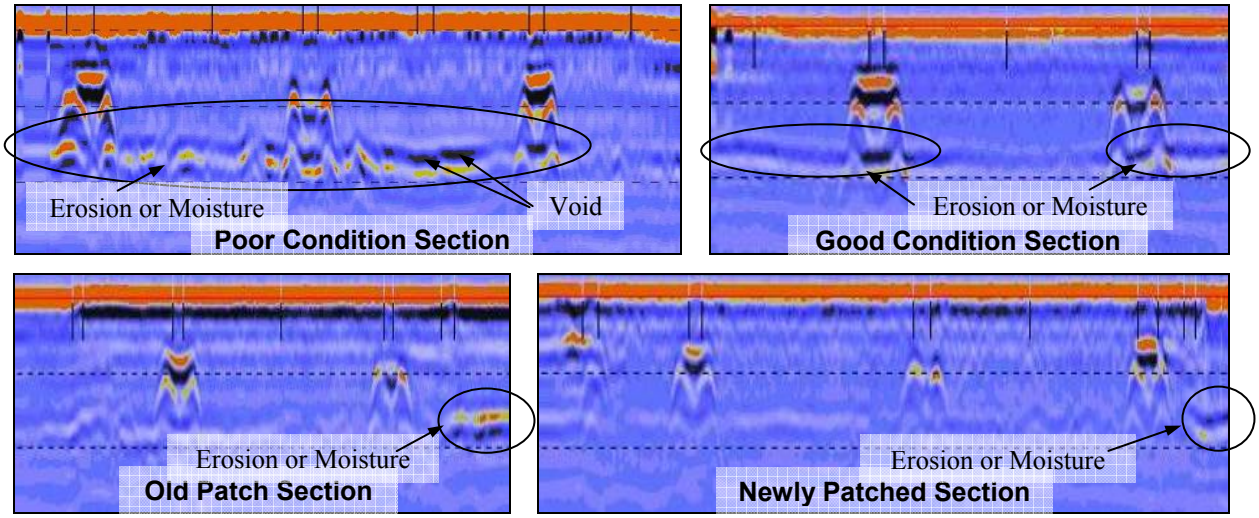

a) GPR along FWD Lane Center Drop Points (Ground-Coupled System)

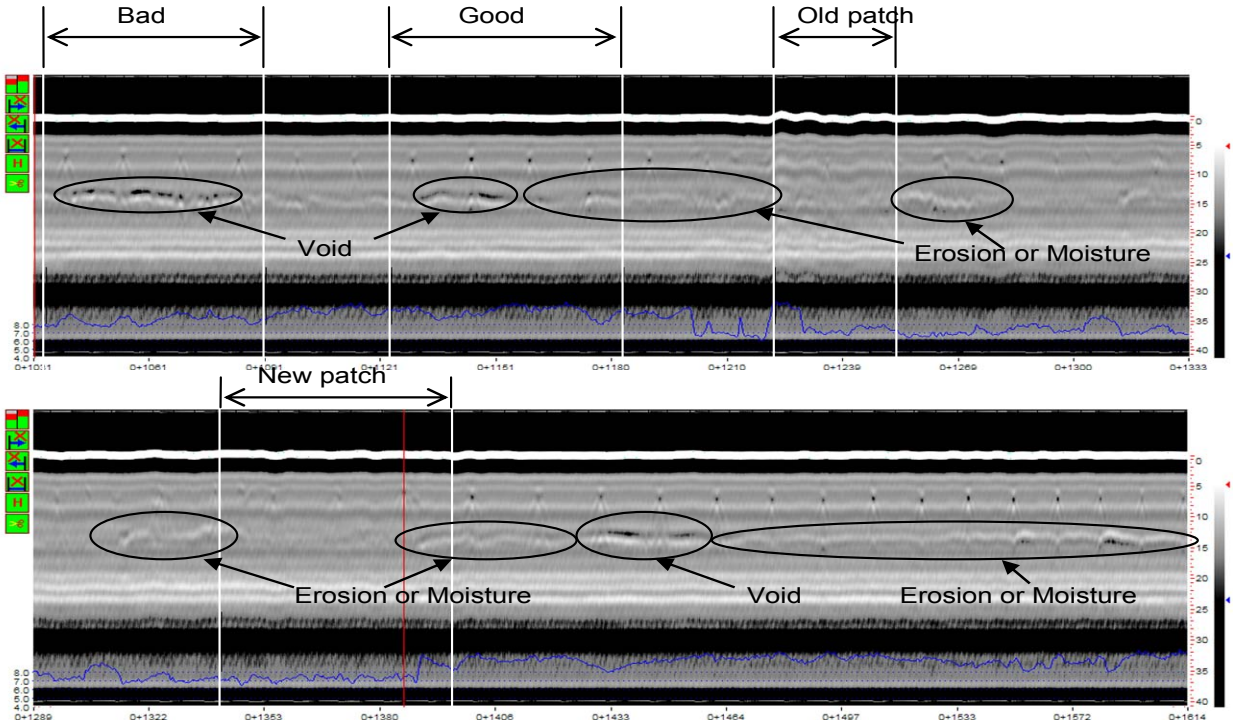

b) GPR along Edge Side Wheel Path (Air-Coupled Vehicle System)

Figure 3-9 GPR Images of Test Sections.

DCP Testing

The base type for all sections investigated was an unbounded aggregate base where the estimated elastic moduli appeared to be quite low, as shown in Figure 3-10. The base in

the good performing areas has nearly the same modulus as that of the subgrade, and there appears to be a significant loss of base strength in unrepaired areas due to subsurface moisture; the typical elastic modulus for an unbounded aggregate base ranges from 15 to 45 ksi *(13)*. The base layer in the good performing areas showed lower modulus than in the poor performing areas based on DCP results. Visually good conditions apparently do not translate to better structural conditions in the subsurface layers.

Patched areas showed relatively higher base layer modulus than the unrepaired sections but there was no significant difference for the subgrade layer. This low subgrade modulus could be due to a wet condition since only the base materials may have been replaced during the installation of the FDR. The presence of standing water along the shoulder joint can indicate poor drainage, contributing to degradation of the modulus for the base and subgrade, particularly when damage to the longitudinal joint seal is present. Some of the patching areas not sealed properly showed very fast deterioration most like due to water intrusion into the replaced base as shown in Figure 3-5. Sufficient LTE and good joint sealing are essentials for effective FDR.

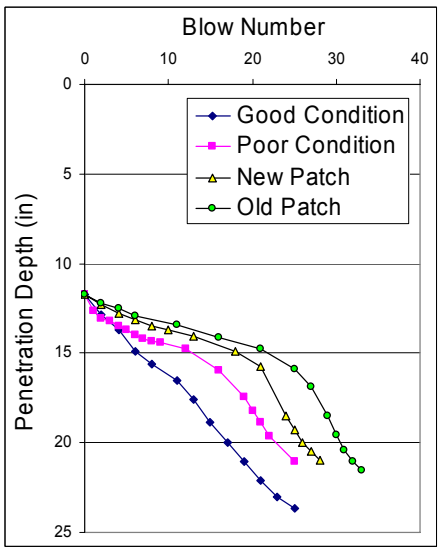

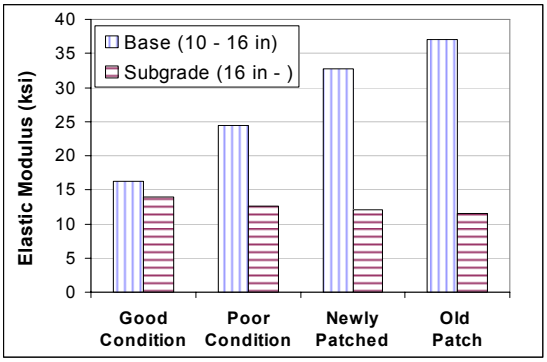

Depth	Good Condition	Poor Condition	Newly Patched	Old Patch
Base (10 - 16 in)	16.3 ksi	24.4 ksi	32.8 ksi	37.1 ksi
Subgrade (16 in -)	13.9 ksi	12.6 ksi	12.1 ksi	11.6 ksi

a) Penetration Ratio b) Elastic Modulus

Figure 3-10 DCP Testing Results of Test Sections.

Core Samples

Core samples provide a means to measure the compressive strength of the concrete and to indirectly estimate the modulus of the concrete layer relative to assessing the performance of the base layer. The core hole also provides a means of visually checking for voids and base erosion.

The illustration shown in Figure 3-11 is of a cored location in a poorly performing section that exposes a voided area at the surface of the base layer due to erosion. Although not entirely evident, Figure 3-11 also shows the bottom surface of individual cores where the bond between the concrete and the base was observed after removal of the core. The core sample from the poor condition section showed evidence of separation (possibly due to erosion and pumping action), while the sample from the good condition section showed partial bonding between the concrete slab and the base. Cores from patched areas did not show evidence of separation.

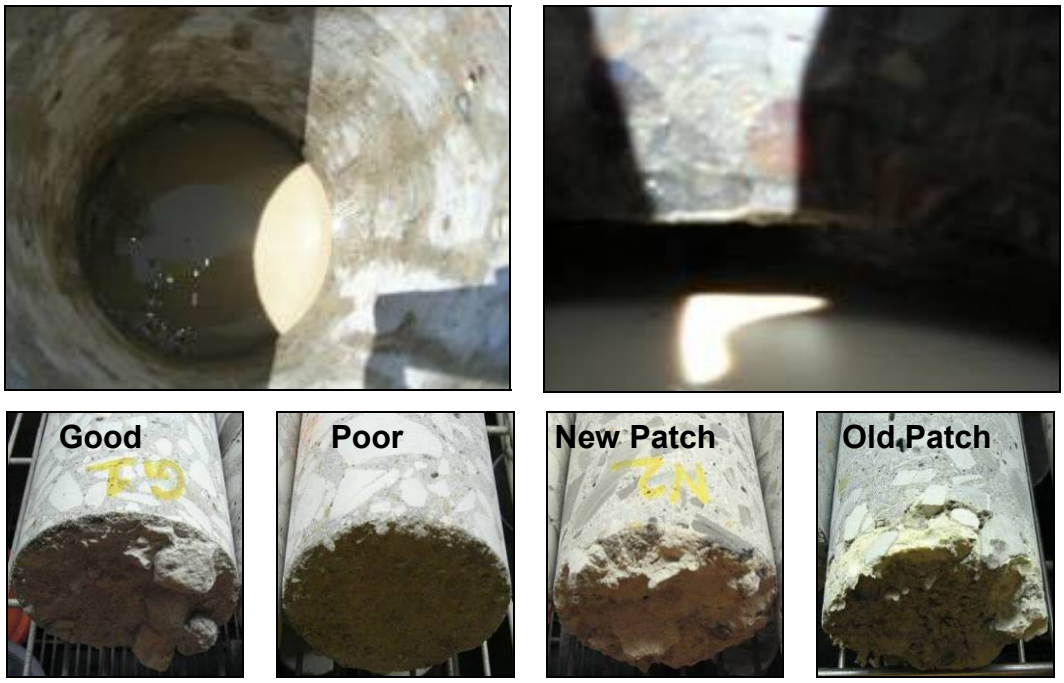

Figure 3-11 Erosion under the Concrete Slab and Cored Sample of Sections on US 75.

US 81/287—Wise County

Sections on CRC pavement on northbound US 81/287 near Decatur, TX were sampled to monitor base or subgrade erosion performance. Traffic was noted to be 23,000 ADT which is estimated to be 1.7 million ESAL per year (with 23 percent trucks), with an estimated 20 million historical ESAL. Figure 3-12 shows a distressed typical area of each section and Table 3-6 shows visual survey results of Section 2.

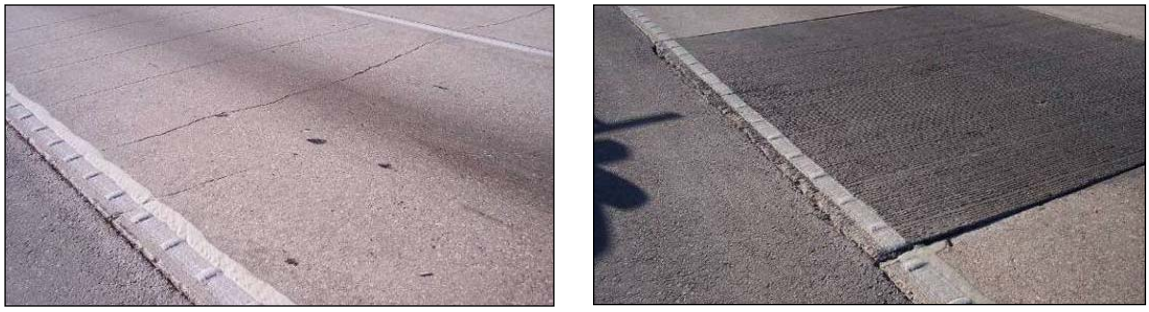

a) Section 1

b) Section 2

c) Section 3

Figure 3-12 Test Sections on US 81/287.

Table 3-6 CRC Pavement Condition Survey of US 81/287 (Sample Section 2).

No.	Checklist	Notes
1	Pavement age (yr)	37 yr 8 in. CRC pavement
2	Aggregate type (hard or soft)	Soft — limestone
3	Year of recent pavement distress survey (yr)	N/A
4	Year of recent pavement deflection survey (yr)	N/A
5	Joint sealant age (yr)	N/A
6	Sealant damage of transverse joint (%)	N/A
7	Sealant damage of longitudinal joint (%)	70%, No seal on shoulder
8	Sealant damage of sealed crack (%)	N/A
9	Trapped surface water in depressed area	No
10	Standing water or slab staining	No
11	Pumping with or without staining	Positive
12	Bump (stable or unstable; depth, in)	No
13	Settlement (stable or unstable; depth, in)	No
14	Joint spall (width, depth, % of joint spall > 2 in.)	N/A
15	Crack spall (width, depth, % of crack spall > 2 in.)	2 in., 3/4 in., 20% 1/4 in., 1/2 in., 80%
16	Deep spall (depth, in.)	No
17	Patching (number/mi)	7
18	Faulting (depth, in.)	Patched area 0.5 in.
19	Longitudinal crack (width, number/slab)	0.05 in., 1/over 4 cracks, 20 ft length
20	Shoulder separation (width, in.)	1/2 in., No joint seal
21	Punchout (spall width, fault depth, % of slab)	No

Sections 1 and 2, constructed in 1971, consisted of 8 in. CRC pavement over a 4 in. AC base and a 6 in. LTS. The pavement had an AC shoulder and showed some evidence of pumping and patching. The crack pattern was fine but the widths of the cracks appeared to be wide in many areas due to the use of a Skidabrader to address surface friction issues. Some of patched sections showed faulting distress at the joints.

Sample Section 3, located 1 mi to the north was opened to traffic in 1985. This section consists of a 12 in. CRC pavement over 4 in. AC base (double layer of 2 in. thick AC) and a 6 in. LTS. Performance has been reasonably good. The pavement also has a 3 ft extended concrete lane as part of the shoulder; the remaining shoulder is AC and the longitudinal joint between the AC and PCC is well sealed, effectively blocking intrusion of water into the pavement section.

GPR Testing

Figure 3-13 shows GPR images where blue areas represent voids and red areas represent eroded or wet condition areas. Generally, the images indicate that the interface between the AC base and the lime-treated subgrade is wet throughout much of the sample section.

GPR images of Section 1 showed significant amounts of wet or eroded areas in the lime-treated subgrade layer; however, little erosion on the AC base layer was detected. GPR images of Section 2 showed some erosion between the concrete slab and the AC layer, which was verified by coring. Wide crack widths, no longitudinal joint sealing as well as a wide shoulder joint possibly contributed to the occurrence of erosion. Even though GPR images of Section 3 showed a low level of moisture at the interface between two AC base layers and a moderate level of moisture on the subgrade layer, no significant erosion was identified.

DC trends in the subbase layers of Sections 1 and 2 show relatively high DC values (around 8 to 10), while Section 3 DC values indicate lower moisture levels (around 7).

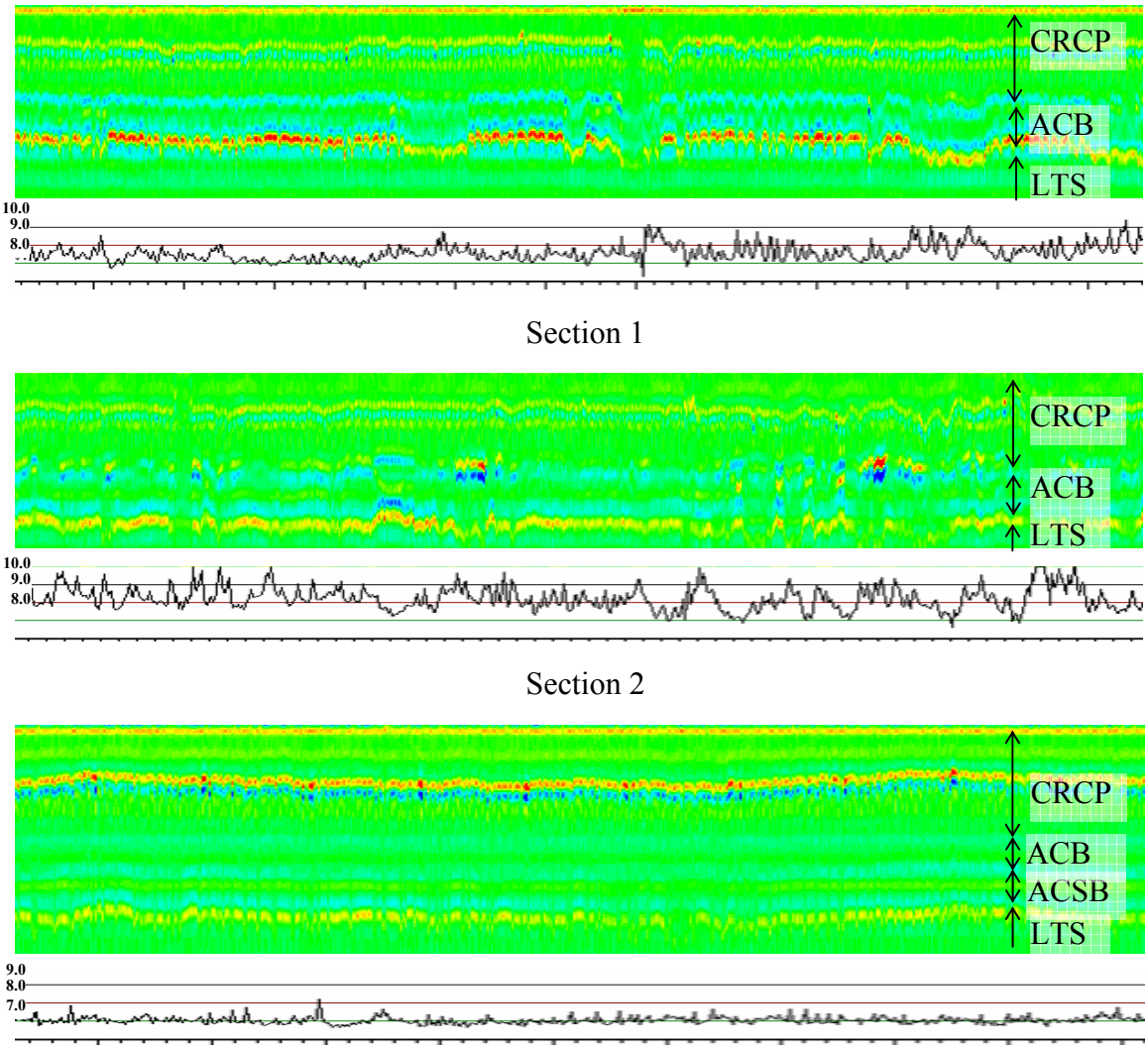

Figure 3-13 GPR Images of Test Sections on US 81/287.

FWD Testing

FWD testing was conducted along the wheel path (1.5 ft inside from pavement edge) in each section where the associated deflections are shown in Figure 3-14. As expected, Sections 1 and 2 showed higher deflections (about 6 times higher) than those measured in Section 3 since the concrete slab thickness is less. However, Section 1 showed a greater mean deflection than those noted for Section 2 even though these sections have the same

layer thickness; the difference may be due to wetter subgrade conditions based on the GPR results.

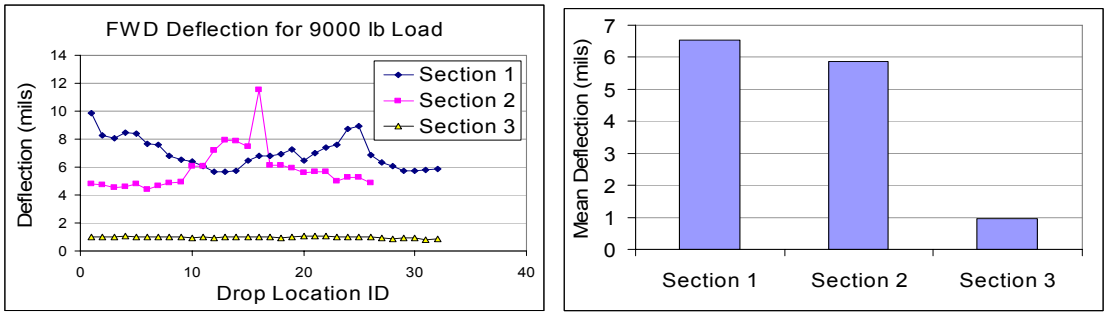

Figure 3-14 Deflections of Test Sections on US 81/287.

Figure 3-15 shows the mean section LTE and effective thickness. Section 3 shows lower LTE than the other sections even though this section has greater effective thickness. The pavement stiffness of this section is good, perhaps since the subgrade conditions are drier based on the GPR results; however, erosion between the AC base layer and the lime-treated subgrade was detected from the core sample. Sections 1 and 2 show good overall LTE and effective thickness, but some cracks have a relatively low LTE and may hold a higher possibility of erosion in the future at those locations.

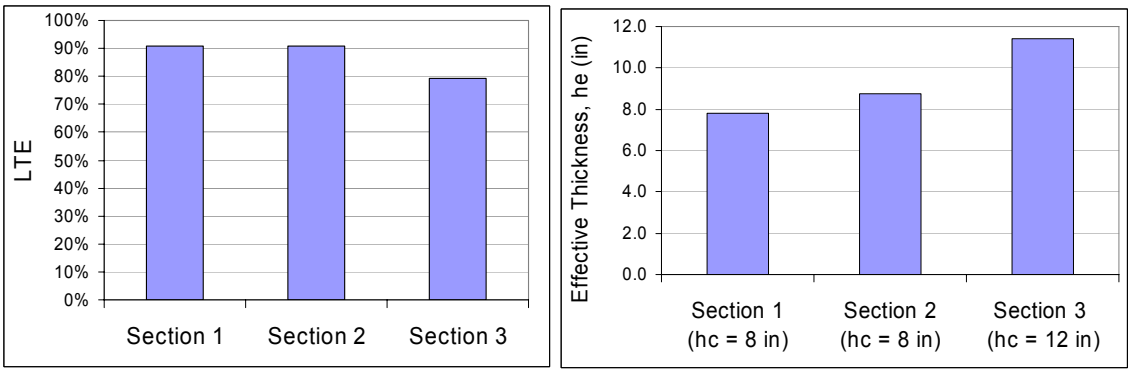

Figure 3-15 LTEs and Effective Thicknesses of Test Sections on US 81/287.

Figure 3-16 suggests evidence of subgrade erosion in portions of Sections 1 and 2. Combinations of low effective thickness and high deflections usually suggest that the base or subgrade layer could be eroded. Moreover, a high deflection condition means greater chance of mechanical and hydraulic shearing action taking place at the interface between the slab and the base under the effect of applied loading. If the LTE is high, erosive action would be reduced, but when LTE is diminished at a crack or joint, the independent vertical movements of adjacent slabs could accelerate the erosion process. The location of low effective thickness and high deflection noted in Section 2 was matched to the wet area noted by the GPR data as well as being verified through coring.

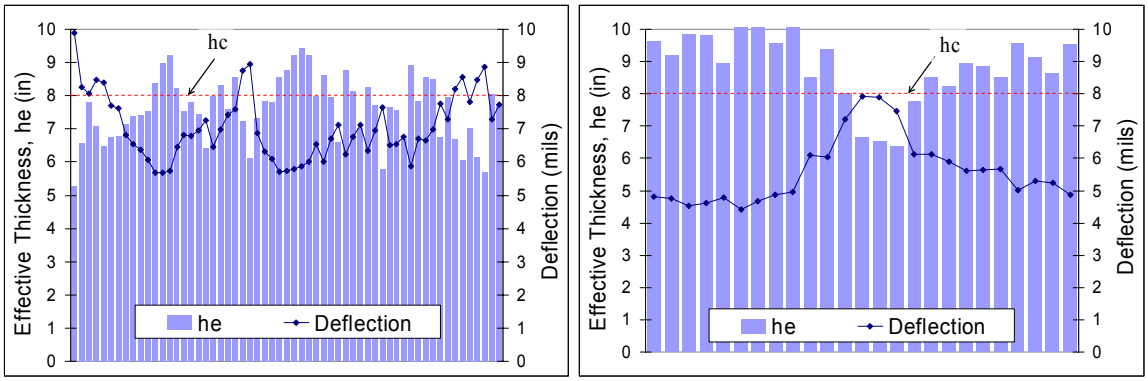

Section 1 Section 2

Figure 3-16 Effective Thicknesses and Deflections of Test Sections on US 81/287.

DCP Testing

All sections were constructed over a 6 in. lime-treated subgrade. Figure 3-17 shows DCP results from the three sample sections. Section 1 has the lowest elastic modulus, perhaps due to the wet subgrade conditions as noted by the GPR images. Section 3 showed the highest modulus although it is in the low end of the range of typical values. The natural subgrade material (sandy soil) is perhaps a low modulus material with a low resistance to erosion.

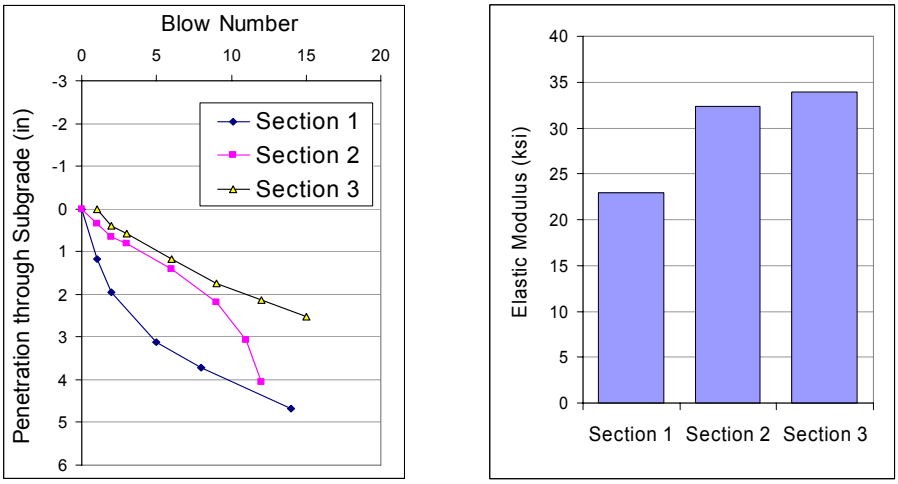

a) Penetration Ratio of Lime-Treated Subgrade

b) Elastic Modulus of Lime-Treated Subgrade

Figure 3-17 DCP Testing Results of Test Sections on US 81/287.

Core Samples

Figure 3-18 shows core samples taken from Section 1 and a view of the interface condition between the AC base and the subgrade. Contact between the concrete slab and the AC base was good with little wear within the sample. However, some erosion at the interface between AC and subgrade was detected as shown.

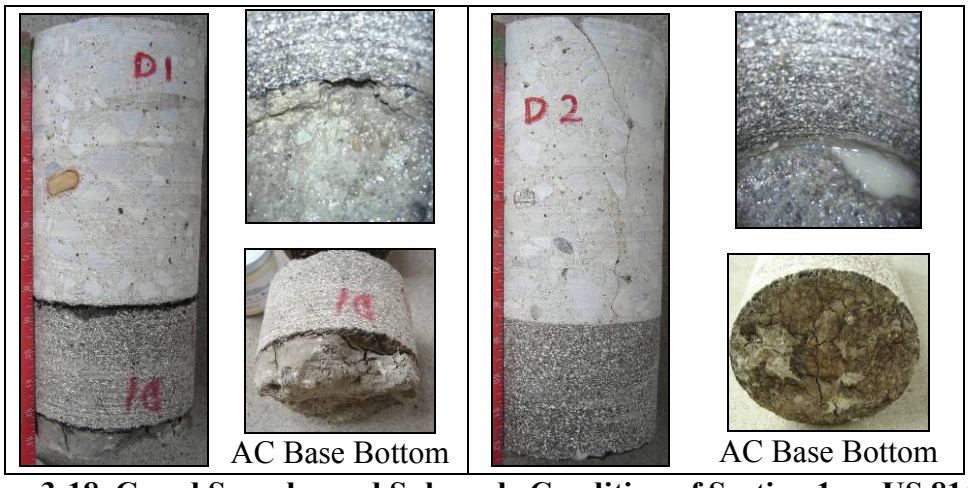

Figure 3-18 Cored Samples and Subgrade Condition of Section 1 on US 81/287.

Sampling in Section 2 indicated a higher level of erosion between the concrete slab and the AC base as shown in Figure 3-19. The core was located on the transverse crack, but the longitudinal joint between lane and shoulder lacked a joint sealant increasing the propensity for water to intrude the pavement structure and contribute to erosion at the surface of the AC base. The bond between AC base and subgrade was clearly missing as there was light erosion on the interface.

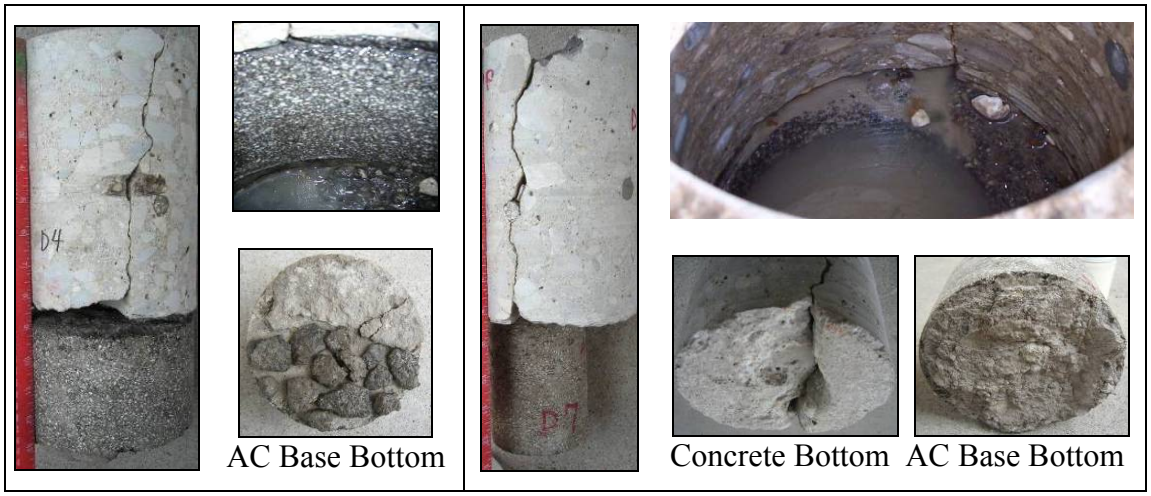

Figure 3-19 Cored Samples and Subgrade Condition of Section 2 on US 81/287.

The core from Section 3 shown in Figure 3-20 manifest erosion on the AC subbase layer; the bond condition between PCC and AC base layer was good, but the debonding and the erosion between two AC layers diminishes the structural integrity of the pavement. The subgrade layer did not show significant erosion even though it was debonded with the AC subbase. Nonetheless, this section presently manifests a relatively high effective thickness but with the joint seal being in good condition has helped maintain a sound subgrade condition with voiding beneath the base.

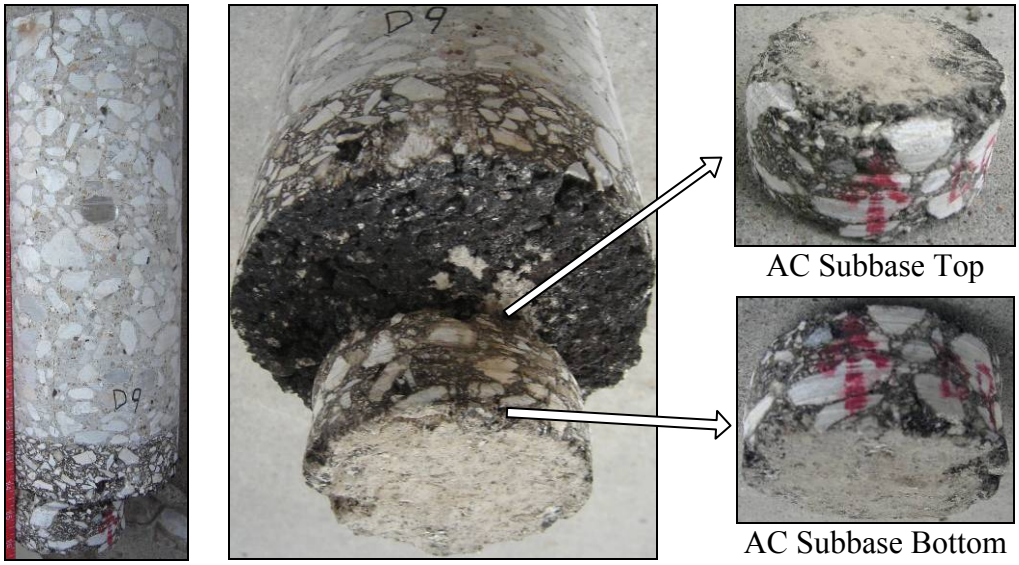

Figure 3-20 Cored Samples and AC Base Condition of Section 3 on US 81/287.

FM 364—Beaumont Area

A sample section on FM 364 in Beaumont consisted of a jointed 10 in. thick pavement with a 15 ft joint spacing over 6 in. cement stabilized oyster shell base. It was opened to traffic in 1985 and current traffic is 21,000 ADT with 2.5 percent trucks. Figure 3-21 shows the surface condition of the sample section. Some slabs had transverse cracks near the joints (about 1 ft apart) possibly due to late sawcutting. The joint seal condition was generally good, but not all the cracks were sealed properly promoting water intrusion and erosion of the base.

GPR Testing

Core sampling was selected based on the presence of the red strip in the GPR image (Figure 3-22) as an indication of erosion-related damage. However, moisture was scarcely present in the base, where there was little evidence of erosion damage. DC values were around 7 to 9 and fluctuated as shown at the bottom of the scanned image suggesting a high chance of water being present at the interface of the slab and base layer.

Figure 3-21 Surface Conditions of Sampled Section on FM 364.

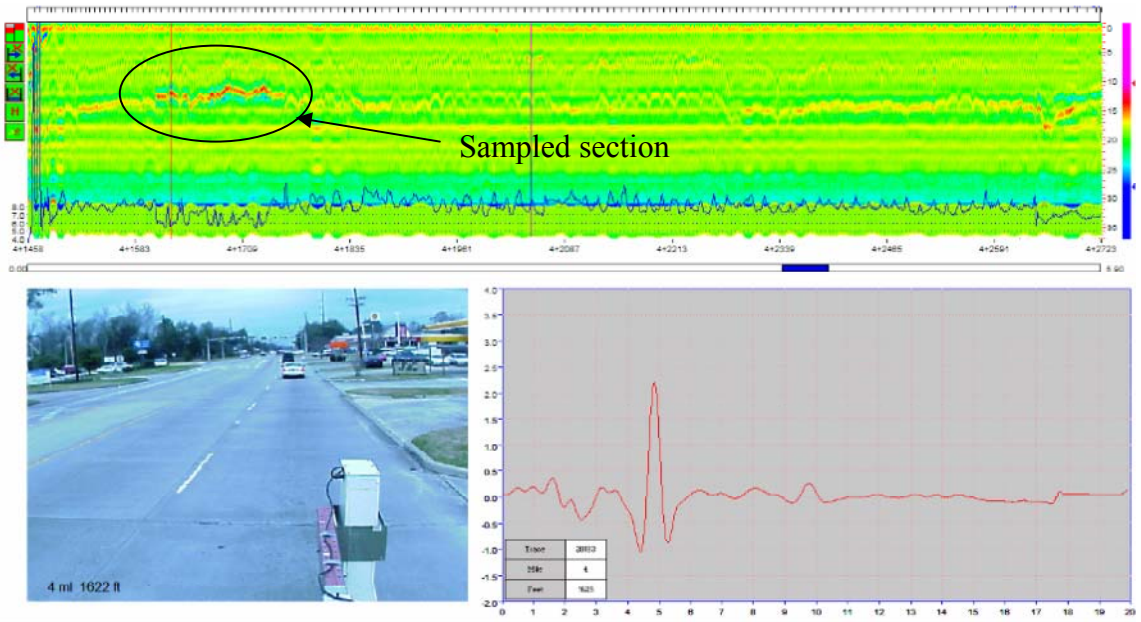

Figure 3-22 GPR Image of Test Section on FM 364.

FWD Testing

FWD testing was employed in the outside wheel path of the outside lane since there is no shoulder; Figure 3-23 shows the LTEs, effective thickness, and deflections. Most joints show good LTEs and deflections in the range of interior loading conditions. As discussed before, low effective thickness with high deflection are indicators of erosion damage at that location, which was verified through the coring.

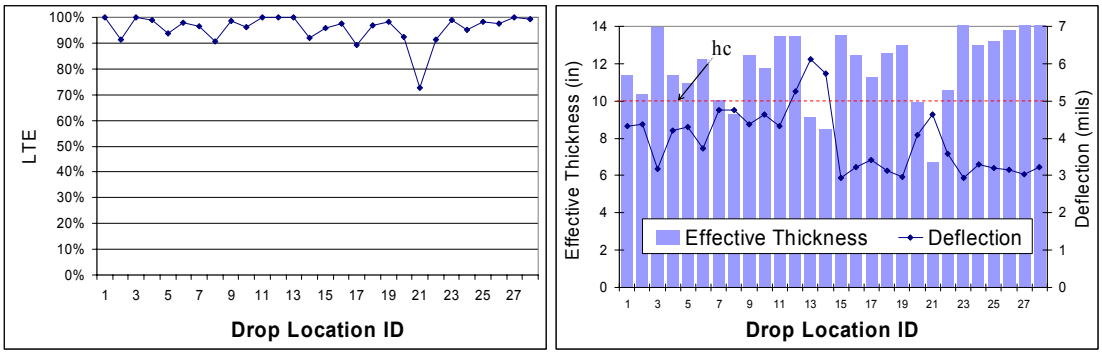

Figure 3-23 LTE, Effective Thicknesses, and Deflection of Test Section on FM 364.

DCP Testing

Figure 3-24 shows DCP results from two core holes made on site. Calculated modulus was around 12 ksi which is in the normal range of subgrade material moduli (3 to 40 ksi).

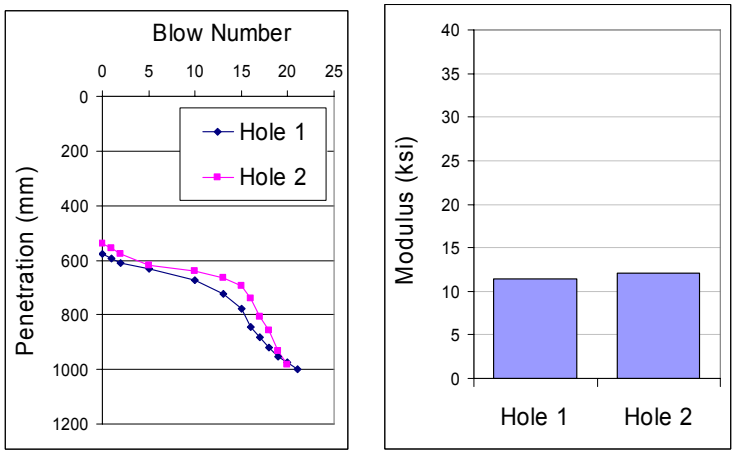

Figure 3-24 DCP Testing Results of Test Section on FM 364.

Core Samples

Figure 3-25 shows views of the interface condition of all the layers in the pavement. Erosion was detected at the interface between the PCC and the cement stabilized oyster shell base near the joint but no erosion was noted away from the joint as indicated by the good contact between the concrete slab and the base. Water intrusion near the joints probably contributed to erosive action but the damage at the interface between base and subgrade was limited to the vicinity of the joint. The bottom of each layer as shown indicates a debonded condition.

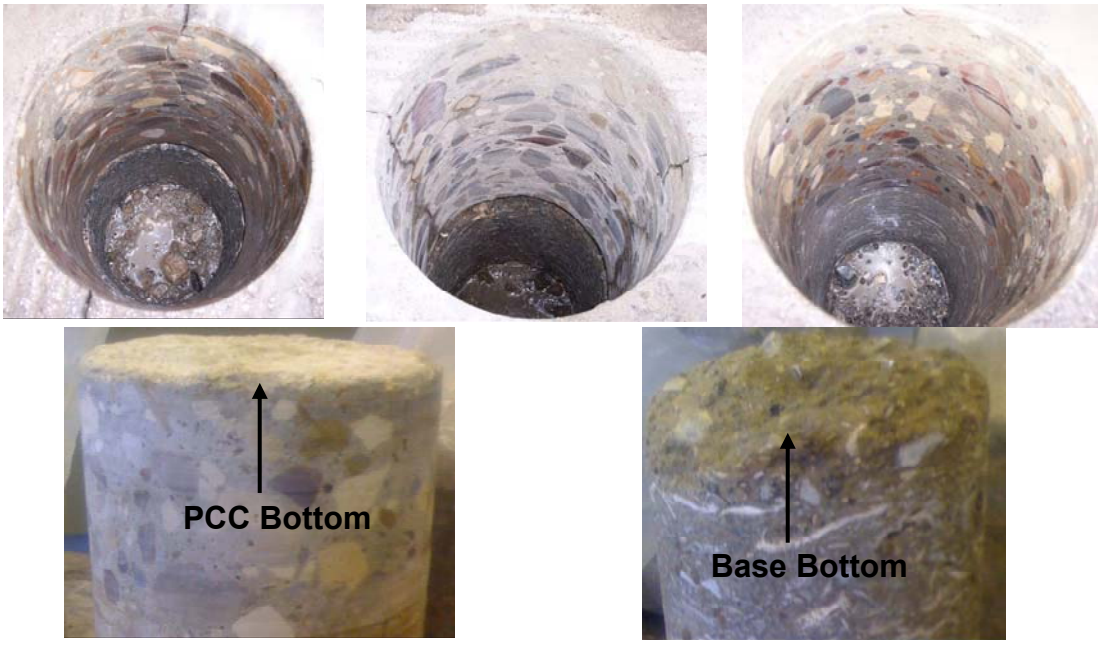

Figure 3-25 Interface and Subgrade Condition of Section on FM 364.

IH 10—Beaumont Area

The support conditions of a frontage road along IH 10 located in Beaumont, TX, which consisted of a 6 in. CRC pavement over silty and sandy subgrade (no base layer) that was constructed in 1963 was investigated. The pavement carries approximately 100 ADT with 3.2 percent truck traffic. Distressed areas indicate signs of overloading are shown in Figure 3-26 and consist of severe map cracking with spalling and pumping. Joint or crack sealing was practically nonexistent and the pavement was severely deteriorated in

the vicinity of the expansion joints. Some patched areas had settled and broken at the corner or in the wheel path; areas adjoining to the patches typically had low LTE and poor support. Most of the damage appeared to be due to a weak subgrade.

Figure 3-26 Surface Conditions of Sampled Section on IH 10.

GPR Testing

Most of the survey sample area showed a high degree of moisture and voiding under the slab based on the GPR results in Figure 3-27. DC values were around 7 to 9 and fluctuated (with high DC values near crack locations) as shown at the bottom of the scanned image. Some peaks occurring at the beginning and end of the FDR patches may indicate the presence of moisture (there was no joint seal between patches and surrounding pavement) possibly leading to more settlement and discontinuous support conditions.

Figure 3-27 GPR Image of Test Section on IH 10.

FWD Testing

Figure 3-28 shows the deflections and LTEs from FWD testing along the center of the outside wheel path of the sampled section lane. FWD testing on the approach side of the patched area showed more uniform and lower deflection conditions compared with the leave side of the patch because the approach side consisted of tighter cracks which did a better job of shedding water off the pavement surface. LTE was generally good (even though deflections were high) except at the FDR joints. Effective thickness trends were similar as the deflection trends. Low effective thickness in combination with high

deflection was found at the FDR patch joints indicating weakened subgrade conditions at those locations.

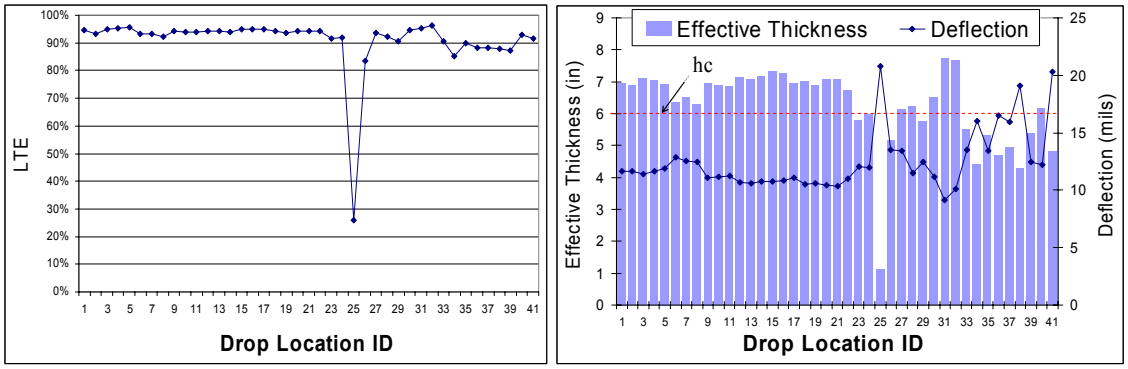

Figure 3-28 LTE, Effective Thicknesses, and Deflection of Test Section on IH 10.

DCP Testing

Figure 3-29 shows DCP results from four core hole locations. All four tested locations showed very high penetration ratios through the top 12 in.. Calculated moduli were around 2.5 to 3 ksi. The subgrade is very weak; however, smaller penetration ratios were detected below 14 in. from the top of the subgrade layer (calculated moduli were approximately 12 to 13 ksi) indicated this part of subgrade was highly saturated.

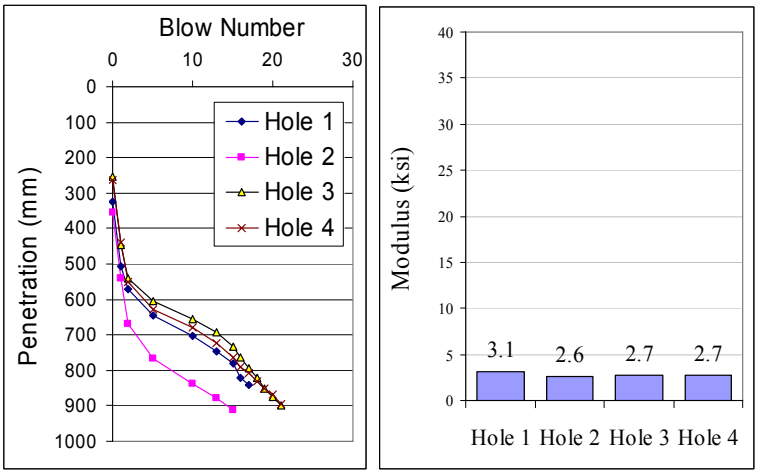

Figure 3-29 DCP Testing Results of Test Section on IH 10.

Core Samples

All four cores showed eroded conditions and, of course, no bonding between the concrete and the subgrade (Figure 3-30). Since there is no base layer, subgrade material was directly subjected to subsurface water through cracks and spalling in the concrete surface exposing it to pumping action and vehicle loading. However, pumping was not excessive since the traffic loading was only approximately three trucks per day. The coring in Figure 3-30 shows horizontal cracking along the reinforcing bar.

Figure 3-30 Interface and PCC Layer Condition of Section on IH 10.

IH 635—Dallas Area

A CRC pavement section on IH 635 from IH 35E to US 75 was sampled to evaluate the base condition. Sampled sections consist of an 8 in. CRC pavement with a concrete shoulder over a 4 in. CSB that was opened to traffic in 1967 that currently carries an ADT of 200,000 with 12 percent trucks. Surface conditions shown in Figure 3-31 were generally good except some spalled cracks and patchs. The key distress types are the full-depth patches and the widened longitudinal joints although the overall condition of the pavement appears to be very good. The patches in the pavement are most likely repairs of punchout distress that are possibly a result of erosion and loss of support immediately below the slab since widened longitudinal joints are evident at a few locations. The patch density is not high, but in places, it is as high as 5 per mile.

Figure 3-31 Surface Condition of Sampled Section on IH 635.

GPR Testing

GPR image in Figure 3-32 showed some moisture areas under the concrete slab but no significant sign of erosion was identified. DC values of overall sections are around 7 to 8 representing a low level of moisture on the base layer.

Figure 3-32 GPR Image of Sampled Section on IH 635.

FWD Testing

The results of FWD testing along the wheel path of the outside lane shown in Figure 3-33 indicates good LTEs but there are a few areas where low values of effective thickness exist indicating the integrity of this pavement is beginning to diminish although the performance over the life of this pavement has been very good. Where effective thickness is less than the existing concrete slab thickness indicates a lack of support possibly due to erosion of the base.

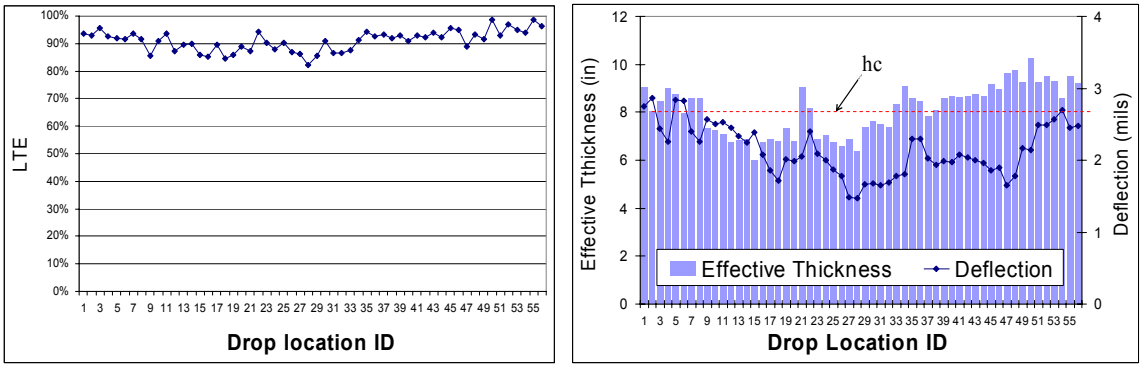

Figure 3-33 LTE, Effective Thicknesses, and Deflection of Test Section on IH 635.

DCP Testing

DCP testing was performed at core locations to assess the insitu strength characteristics of undisturbed soil and/or compacted materials below the subbase. The results of six representative holes in Figure 3-34 show good subgrade conditions except for one area showing a calculated modulus of 12.4 ksi.

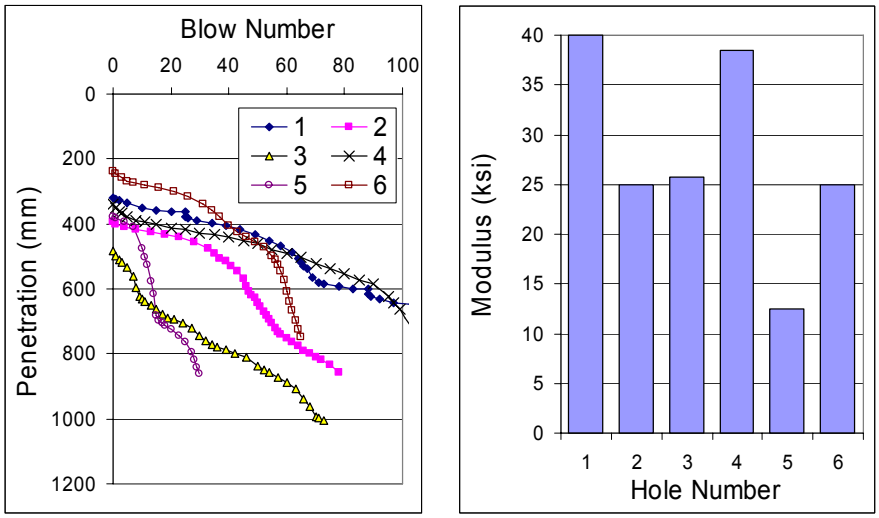

Figure 3-34 DCP Testing Results of Test Section on IH 635.

Core Samples

Erosion was found only at areas where the condition of the longitudinal construction joint was not well maintained and moisture had penetrated the pavement (Figure 3-35). The stabilized base consisted of cemented sand with gravel and ranged in thickness from 3 to 5 in., while the subgrade mainly consisted of clay material. The pavement support is not presently as issue but could soon become serious if maintenance activities are terminated or diminished for an extended period of time. Life extension could be facilitated by addressing the areas in the pavement structure that do not drain well and allow water to penetrate below the surface of the pavement.

Figure 3-35 Cores of Sampled Section on IH 635.

CHAPTER IV

MODEL ADVANCEMENT AND CALIBRATION

A mechanistic model for subbase erosion is advanced based on the model proposed by Jeong and Zollinger (*10*). Lab test results using new test method and LTPP data analysis are applied for model calibration process.

NEW METHOD OF EROSION TESTING

A new laboratory test procedure was configured to determine the erodibility of subbase materials under different moisture conditions. A dry condition test configuration was formulated using the rapid tri-axial test (RaTT) and the wet condition test configuration was formulated using the HWTD. Both tests consist of a two component layer system; one being concrete and the other the subbase material of interest such as a cement-treated or flexible (define abbreviation as Flex) subbase.

Erosion Testing Devices

The dry condition testing method is a mechanical abrasive erosion test using the RaTT where the load levels of σ_1 and σ_3 are controlled through a rubber bladder to provide a cyclic deviatory stress at specified levels as shown in Figure 4-1. This configuration provides mechanical abrasion and compression under an 80 psi normal stress where weight loss occurs due to frictional erosion and compressive fracture of the subbase material at the interface of the two layers. Various shear stresses and load repetitions are applied to evaluate the rate of erosion under dry conditions.

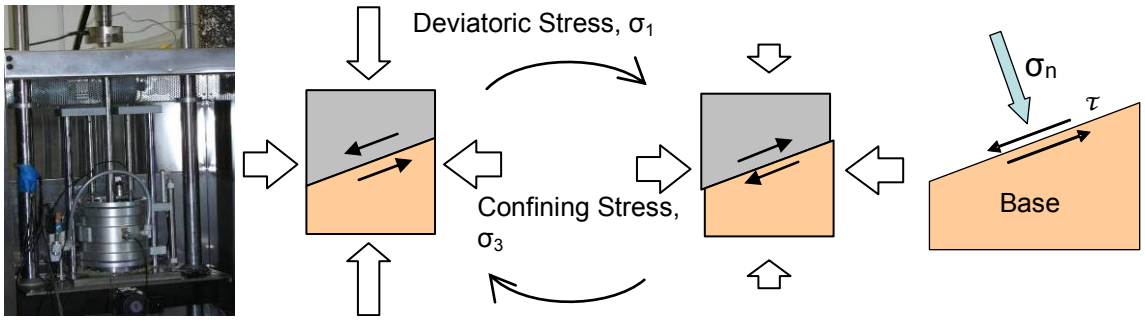

Figure 4-1 Schematic of Erosion Test Using RaTT Device.

The wet condition erosion test uses the HWTD device since water in easily incorporated to transport abraded material due to mechanical and hydraulic shear generated by slab movement under an applied load away from the erosion site on the surface of the base layer. The configuration of the test device is the same as normally used with the HWTD except for the multi-layered sample shown in Figure 4-2. The test configuration consists of a 1-in. thick subbase material placed on a neoprene material below a 1-in. thick jointed concrete block. The test device allows for testing a laboratory compacted specimen or a core obtained from the field. A 158 lb wheel load (11.2 psi normal stress) is applied to the test samples at a 60 rpm load frequency up to 5,000 load repetitions under submerged condition at a temperature of 77 °F. Measurements consist of the depth of erosion at 11 locations versus number of wheel load passes (detailed in Appendix A).

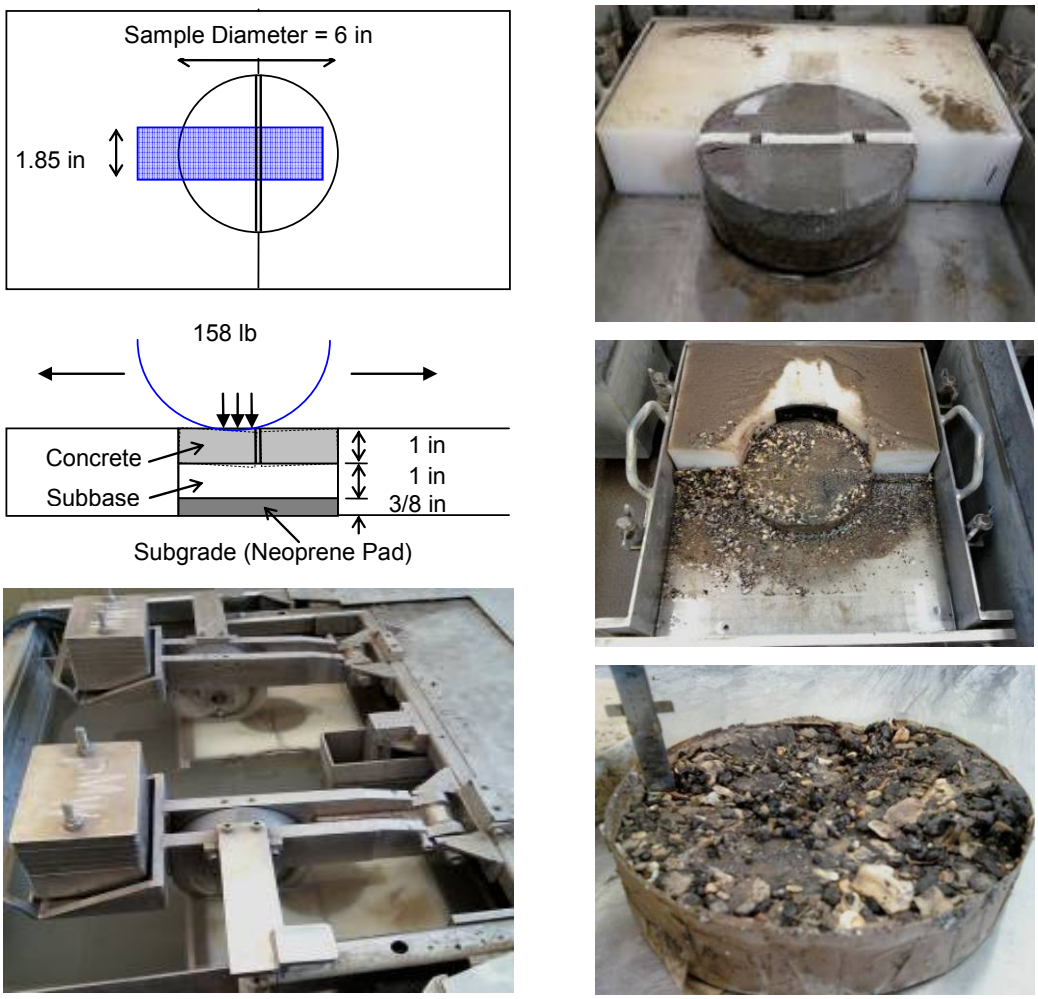

Figure 4-2 Erosion Test using Hamburg Wheel-tracking Test Device.

Sample Preparation

The following three different sample types were selected for erosion testing. All samples were stabilized with different binder contents (0, 2, 4, and 6 percent cement) at optimum moisture content by weight:

1. Flex sample–limestone base material (from the Bryan District);
2. RC sample–Recycled crushed concrete; and
3. RAP sample–30 percent RAP + base material (shell/dark soil) (from the Beaumont District).

All samples were prepared according to the test method "Tex-120-E, Soil-Cement Testing" and compacted according to the test method "Tex-113-E, Laboratory Compaction Characteristics and Moisture-density Relationship of Base Materials," using a 10-lb hammer, with an 18-in. drop, at 50 blows/layer in a 6 x 6-in. mold (with 5-in. disk insertion). All samples were cured more than 90 days under 100 percent relative humidity conditions except for the untreated (0 percent cement treated) samples.

Test Results Using RaTT

The 3 percent cement treated base materials were tested with the RaTT device to examine the effects of shear stress and load repetition under dry conditions in which weight loss occurs due to frictional abrasion and compressive fracture of exposed material on the surface. The aggregate size distributions of the samples varied to some extent as shown in Figure 4-3; the Flex and recycled concrete (RC) grading met the requirements of American Society of Testing Materials (ASTM) D 2940-03 but the reclaimed asphalt pavement (RAP) material grading consisted of an oversized distribution containing more fines than other materials.

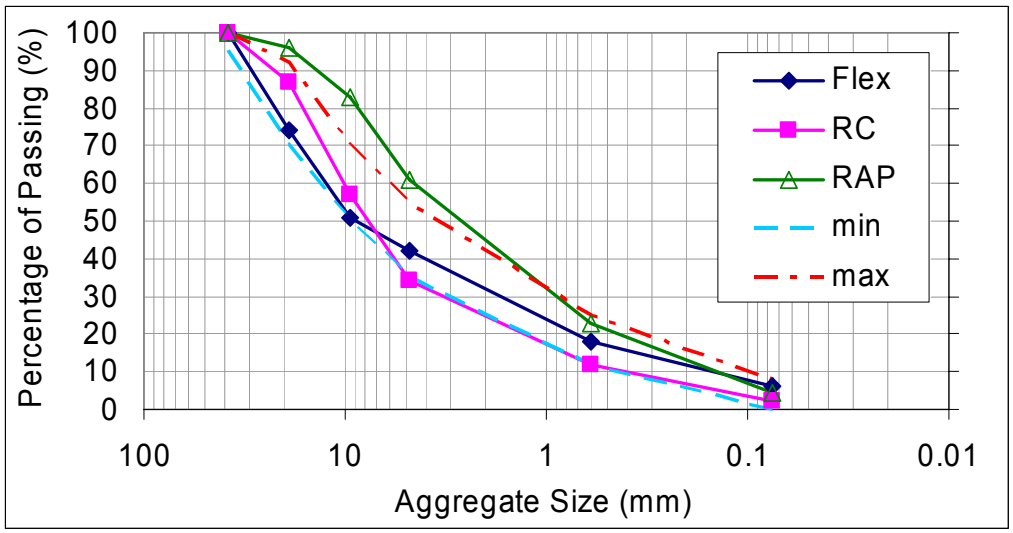

Figure 4-3 Aggregate Size Distributions of RaTT Erosion Test Samples.

Figure 4-4 shows weight loss after 1,000 RaTT test load repetitions under various shear stress levels as shown Table 4-1. As expected, the greater the shear stress the greater the weight loss. However, the rate of weight loss dropped off to some extent at higher stress levels presumably due to a buildup of loose material on the interface effectively reducing the interlayer coefficient of friction. RAP base samples experienced a greater weight loss than the RC base because of a higher fines content. It is clear the aggregate size distribution at the surface significantly affects the rate of abrasive erosion under dry test conditions.

Table 4-1 Stresses in RaTT Test

Normal Stress, N (psi)	Shear Stress, τ (psi)	Ratio of $\frac{\tau}{N}$	Vertical Stress, σ_1 (psi)	Confining Stress, σ_3 (psi)
80	16.8	0.21	94.1	60
80	25.2	0.32	101.1	50
80	33.6	0.42	108.2	40
80	42.0	0.53	115.2	30
80	50.3	0.63	122.2	20

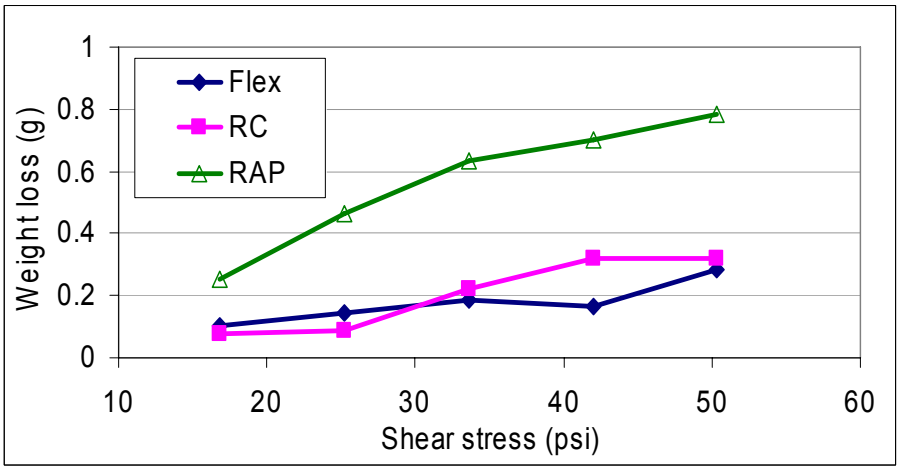

Figure 4-4 Weight Loss versus Various Shear Stress by RaTT Test.

Figure 4-5 shows the effect of the number of loadings with a shear stress of 33.6 psi. Weight loss increased with loading repetition but the rate again diminished after 3,000 load repetitions. The one possible reason is the amount of generated fines causes a reduction in shear stress at the interface of the two layers. To minimize the effect of the accumulated fines on the induced shear stress, periodical cleaning of the interface should be conducted as would take place under pumping action. The spikes in the results (Flex and RAP 3,000 repetition and RC 5,000 repetition) were caused by removal of large-sized aggregate in the mixture relative to other generated fines.

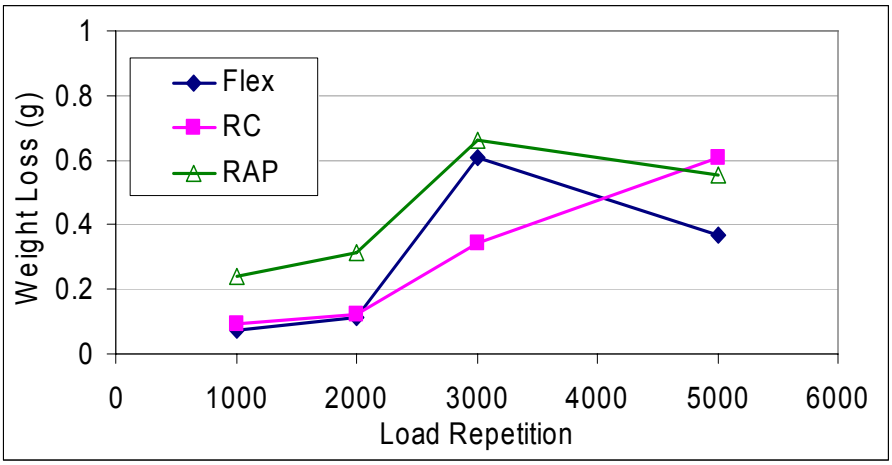

Figure 4-5 Weight Loss versus Various Number of Loading by RaTT Test.

Test Results Using HWTD

As discussed in the RaTT test results, erosion aspects are highly affected by the ratio of the larger sized aggregates exposed on the surface. Therefore, grading could be a factor for all material types in performance among the sample specimens. Figure 4-6 shows various grading distributions of different HWTD test specimens. The maximum aggregate size is changed from 0.8 in. (20 mm) to 0.4 in. (10 mm), 0.2 in. (5 mm), and 0.08 in. (2 mm). Also other aggregate size distributions were examined while maintaining a constant similar sample density and percentage of fines (less than 0.006 in. (0.15 mm), No. 100 sieve size).

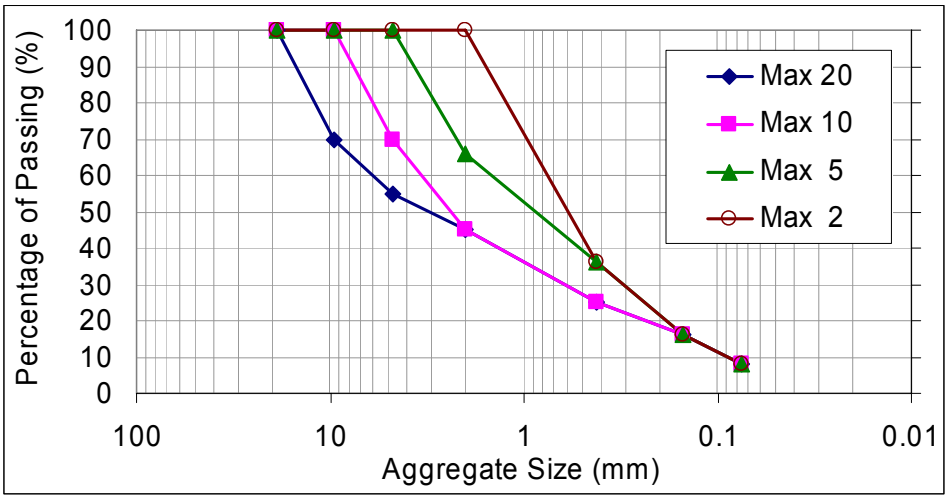

Figure 4-6 Aggregate Size Distributions of HWTD Erosion Test Samples.

Figure 4-7 shows there is no significant difference in the erosion depth and trend when maximum aggregate size is larger than 0.2 in. (5 mm) and the small sized aggregate percentage is held constant. "Max 5" gradation may serve as an optimum grading for specimens graded to generate a greater degree of uniformity at the surface that consequently reduces irregularity and uncertainty in the test data. "Max 2" gradation resulted in significant erosion.

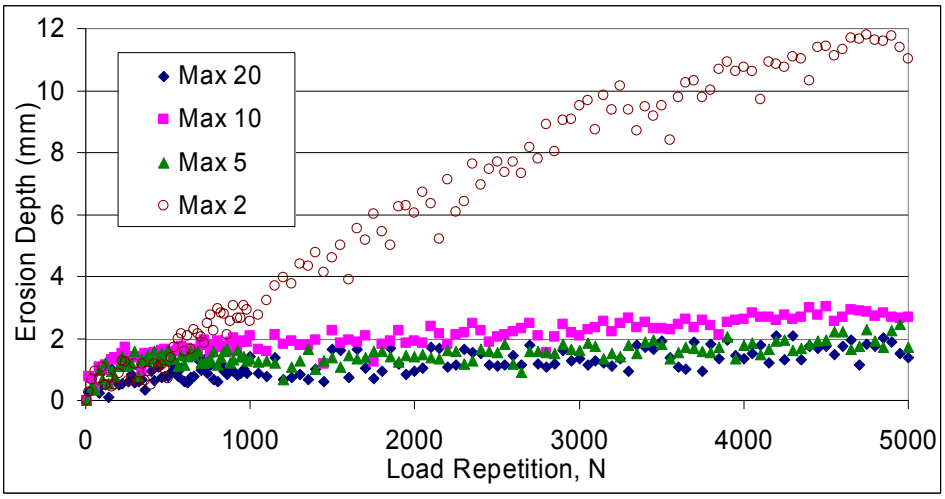

Figure 4-7 Erosion versus Number of Loading by HWTD Test.

Detailed Test Program

Based on the effect of aggregate grading, the samples for cement treated base materials followed the "Max 5" aggregate size distribution. Figure 4-8 shows the RaTT test results of cement treated samples under the shear stress of 21.1 psi where the erosion rate decreased with greater cement content. By the change of the aggregate size distribution from the grading shown in Figure 4-3, test results show a different erosion rate for each sample type. The RC base shows the highest erosion rate, and the RAP base shows the least erosion rate under dry conditions while maintaining the fine-size aggregate fraction constant (i.e., 16 percent passing the 0.006 in. (0.15 mm), No.100 sieve size) since the amount of asphalt mastic increases shear strength.

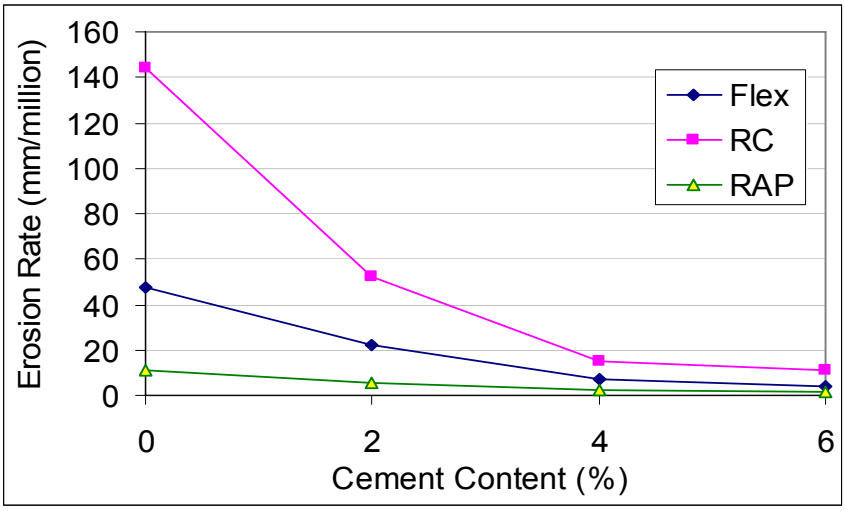

Figure 4-8 Erosion versus Change of Cement Percentage by RaTT Test.

HWTD test results shown in Figure 4-9 indicate as the percentage of cement increases the erosion rate decreases. Two percent cement for Flex and RAP subbases, however, does not reduce the erosion rate significantly but 4 percent cement reduces erosion remarkably when compared with unstabilized materials.

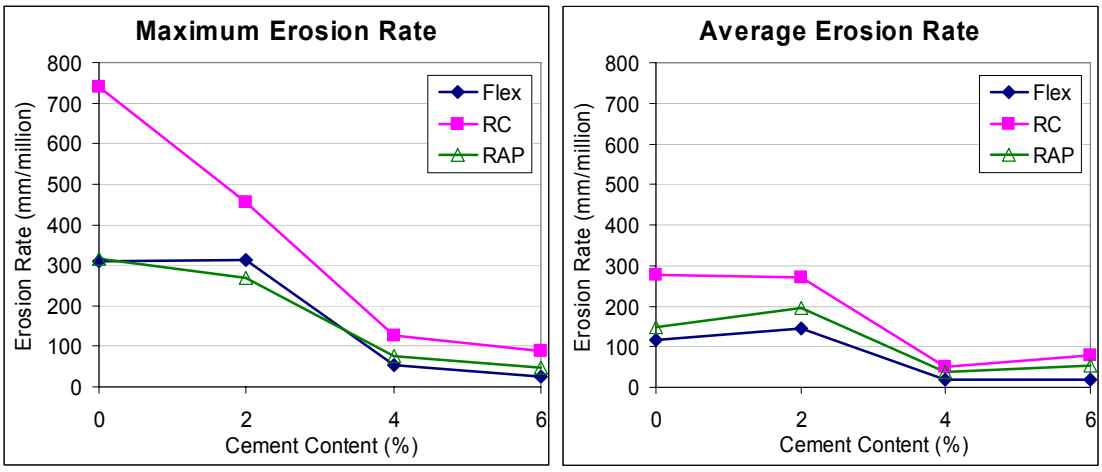

Figure 4-9 Erosion versus Change of Cement Percentage by HWTD Test.

Figure 4-10 and Figure 4-11 show erosion of samples with respect to load application under HWTD testing. Erosion occurred rapidly from the start of the test but its rate decreased as the void deepened since the sample was saturated, and the hydraulic shear was higher when the void between concrete and sample was smaller. (Phu and Ray (*21*) indicated (at a constant slab deflection speed) that if the void is larger than 0.04 in. (1 mm) the rate of erosion will diminish with an increase in void depth). Test results show a fluctuation of erosion depth with the number of loading most likely due to relatively large aggregates being dislocated by pumping action while small fines are more uniform hydraulically transported from the subbase surface.

The dry and wet conditions under which the RaTT and HWTD erosion tests were conducted represent free edge conditions (i.e., no load transfer). However, separation between the slab and the base must occur for sufficient pumping action to initiate erosion (over dry and wet periods). In design, the calculated erosion rate should therefore be weighted over dry and wet performance periods as well as load magnitude and applied interfacial shear. Calibration for local conditions are necessary to represent such factors as LTE, frequency of joint sealing maintenance, changes in drainage conditions, and annual precipitation in estimates of performance.

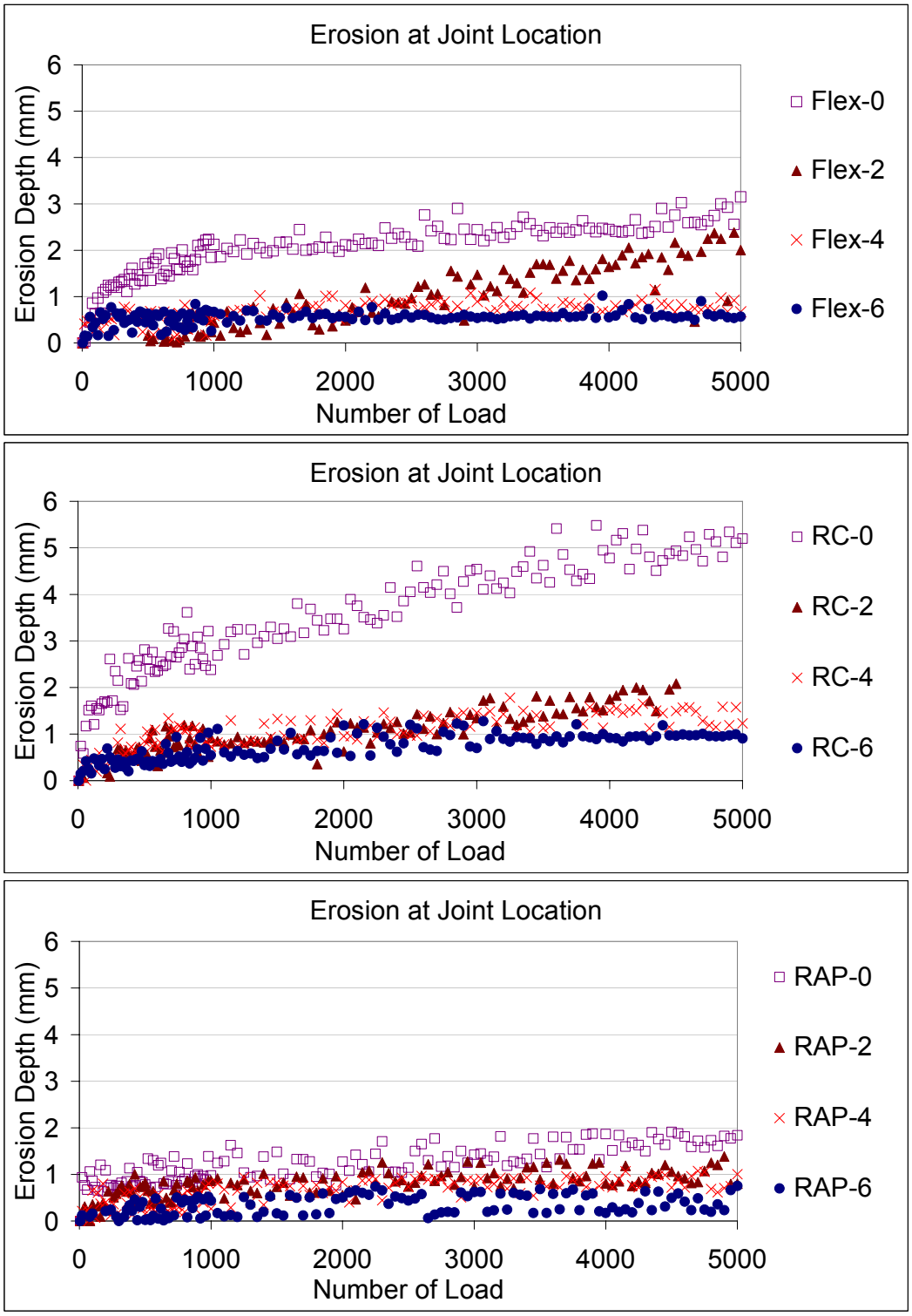

Figure 4-10 Erosion at Joint versus Number of Load by HWTD Test.

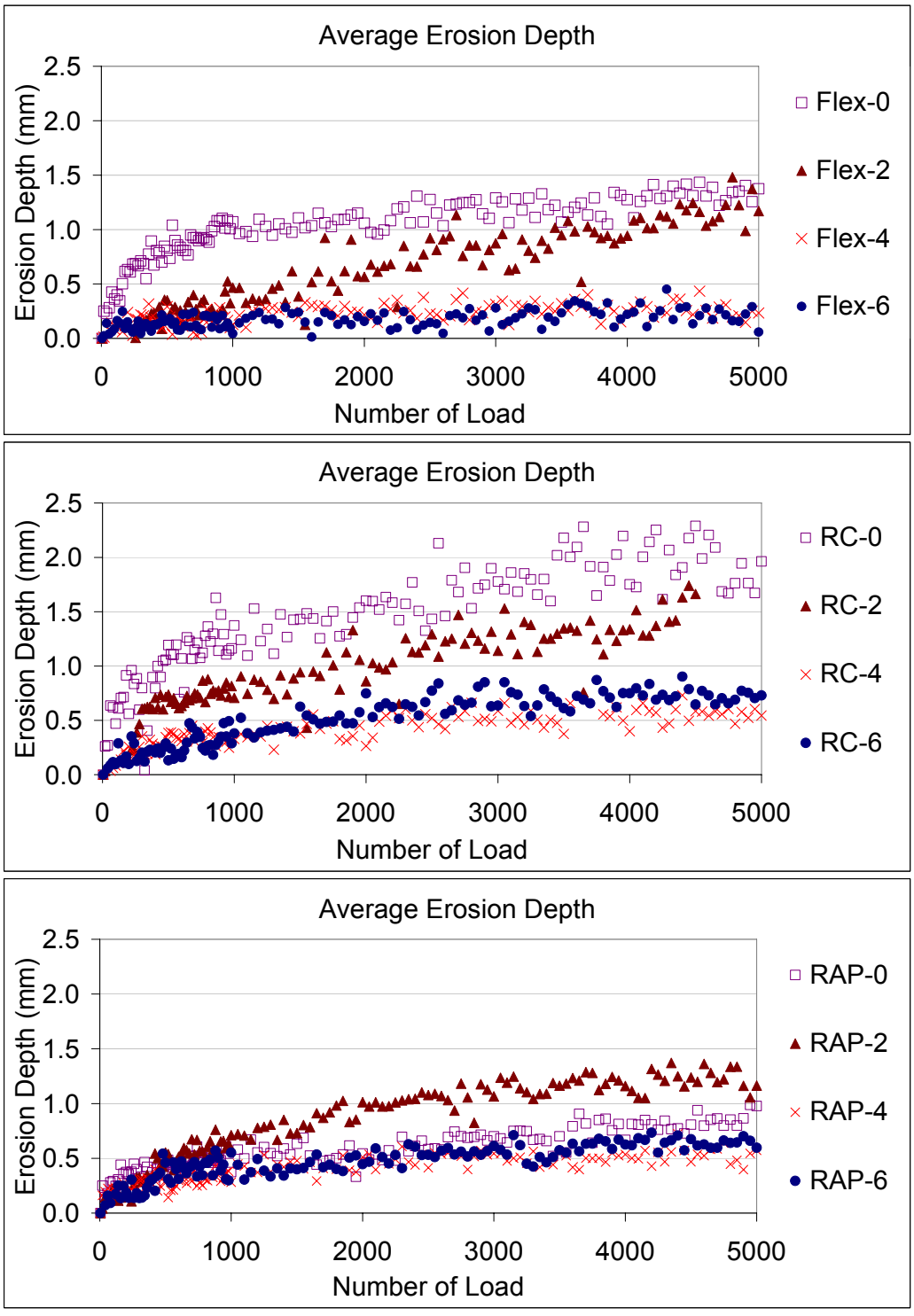

Figure 4-11 Mean Erosion of 11 Measuring Spots versus Number of Load by HWTD Test.

EROSION MODEL

Slab movement acting on the surface of a subbase layer mechanically creates a loosen layer of subbase material. This layer of material is easily saturated and liquidized in the presence of water. Figure 4-12 shows the schematic view of the stress distribution of the approach slab under loading and the fines generating mechanism caused by deflection-induced shear at the interface after debonding of concrete slab and subbase layer. The thermal movement of concrete on the opening and closing of the joint along with repeated loading across the joint diminishes the load transfer over time between adjoining slabs while enhancing the independent deflection movement of the slab.

In the case of bound (stabilized) bases, the frictional interface is a key factor in the deterioration process. A stiff base may undergo high frictional stress along the interface especially in the vicinity of a corner of a slab. This frictional stress generates mechanical abrasion or fracturing of the surface material when the shear stress exceeds the shear strength. As unbound bases deform under slab deflection internal friction is generated through aggregate-to-aggregate grinding inducing fine material internally.

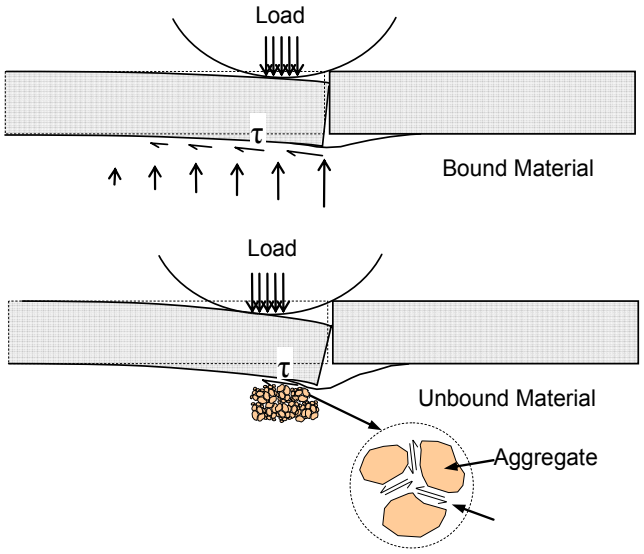

Figure 4-12 Shear Induced Erosion.

Water induced shear stresses on the subbase surface are developed as a function of the up and down slab movement which is simulated by a stiff plate rotating about an axis. A transport potential increases with higher hydraulic shear stress at the surface of the base layer by pumping of trapped water. The advantage of this model (Equation 4-1) is its capability of translating the laboratory test results to any layer combination or thickness in the field.

$$f_i = f_0 e^{-\left(\frac{\rho}{N_i - \Delta}\right)^a} \qquad \textbf{(4-1)}$$

where: f_i = erosion depth at the number of ESAL, (L)

N_i = number of ESAL contributing to erosion, (ESAL)

f_0 = ultimate erosion depth, (L)

ρ = calibration erosion coefficient based on local performance

a = $a' a_f$

a' = environmental calibration coefficient

a_f = rate of void development

$$= \frac{Log^{-1}(a_m \tau + b_m)}{\gamma_b}$$

a_m, b_m = void development constants from lab test

τ = $\left[\tau_{wet} + \tau_{dry}\right]\left(1 - \frac{LTE}{100}\right) = \left[\frac{\eta B}{\delta_{void}} + \mu\left(\frac{h}{12} + \sigma_v\right)\right]\left(1 - \frac{LTE}{100}\right)$, ($FL^{-2}$)

γ_b = unit weight of subbase, (FL^{-3})

τ_{wet}, τ_{wet} = shear stress while wet condition and dry condition of subbase

LTE = joint or crack load transfer efficiency, (%)

η = dynamic viscosity of water, ($FL^{-2}t$)

$$= \left\{2056.82 + 10.56T - 284.93\sqrt{T} - 265.02e^{-T}\right\}10^{-6}$$

T = water temperature, (°C)

B $= V_{z_i} \sin\theta + 6V_{z_i}\left[\frac{\sin\theta}{2} + \frac{\cos^2\theta}{\sin\theta}\right]$, ($Lt^{-1}$)

δ_{void} = void space below slab for water movement, (L)

μ = coefficient of friction of subbase

h = PCC layer thickness, (L)

σ_v = vertical stress over subbase

V_{z_i} = slab deflection velocity, (LT^{-1})

$$= \frac{\delta_{\text{int}}}{s/V_i}$$

V_i = vehicle speed, (LT^{-1})

δ_{int} = slab deflection by interior loading, (L)

$$= \frac{P_i}{8k\ell}\left\{1 + \left[0.3665\log\left(\frac{a_L}{\ell}\right) - 0.2174\left(\frac{a_L}{\ell}\right)^2\right]\right\}$$

P_i = axle load, (F)

k = modulus of sublayer reaction, (FL^{-3})

ℓ = radius of relative stiffness of sublayer, (L)

a_L = loaded radius, (L)

θ = slab angle = $\tan^{-1}\left[\frac{z_o}{s}\right]$

s = slab liftoff distance, (L)

$$= \sqrt{2}\ell(\chi - 1)$$

$$\chi = \sqrt{\frac{z_o}{w_o}}$$

z_o = edge gap, (L)

$$= \frac{(1+\nu)}{h}\Delta\varepsilon_{eqv}\ell^2$$

ν = Poisson's ratio

$\Delta\varepsilon_{eqv}$ = total strain due to moisture and temperature gradient

w_o = deflection of slab by self weight, (L)

$= \frac{\rho h_c}{k}$

ρ = density of concrete, (FL^{-3})

Δ = coefficient represents the number of ESAL for layer debonding to occur and erosion to initiate, 0 for lab test (ESAL)

$= \alpha_1 \cdot (\alpha_2 \cdot DAYS90 - WETDAYS) \cdot ADT \cdot \frac{h_c \cdot h_b}{L_x \cdot L_y}$: JPCP and JRCP

$= \alpha_1 \cdot (\alpha_2 \cdot DAYS90 - WETDAYS) \cdot ADT \cdot \frac{h_c \cdot h_b}{D_{steel} \cdot L_y}$: CRCP

α_1, α_2 = calibration coefficient based on field performance

DAYS90 = number of days per year with the maximum temperature greater than 90 °F in LTPP database (t)

WETDAYS = average annual number of days with rainfall greater than 0.01in. in LTPP database (t)

ADT = average daily traffic (Ct^{-1})

h_b = subbase layer thickness (L)

L_x = joint spacing (L)

L_y = lane width (L)

D_{steel} = diameter of reinforcing steel of CRCP (L)

CALIBRATIONS OF MODEL PARAMETERS

The proposed erosion model parameters (a and ρ) are isolated and calibrated using test data as a function of material type and the percentage of cement treatment. The parameter Δ represents the number of wheel loads to initiate erosion as a result of layer debonding of the slab from the subbase. This parameter is considered to be zero for the laboratory test unbonded conditions exist throughout the duration of the test. Therefore, Equation 4-1 can be rewritten as:

$$\frac{f_i}{f_0} = e^{-\left(\frac{\rho}{N_i}\right)^a} \tag{4-2}$$

$$\ln f_i = \ln f_0 - \left(\frac{\rho}{N_i}\right)^a \tag{4-3}$$

Taking the derivative of Equation 4-3 with respect to N_i:

$$\frac{\partial \ln f_i}{\partial N_i} = \frac{\partial \ln f_i}{\partial f_i} \cdot \frac{\partial f_i}{\partial N_i} = \frac{1}{f_i}\frac{\partial f_i}{\partial N_i} \tag{4-4}$$

Combining Equation 4-3 and Equation 4-3:

$$\frac{\partial f_i}{\partial N_i} \cdot \frac{1}{f_i} = \frac{\partial\left(\ln f_0 - \left(\frac{\rho}{N_i}\right)^a\right)}{\partial N_i} \tag{4-5}$$

Since f_0 is assumed to also be a material parameter (i.e. constant), its derivative with respect to N_i is assumed to be zero. Hence, Equation 4-5 is converted as:

$$\frac{\partial f_i}{\partial N_i} \cdot \frac{1}{f_i} = \frac{\partial\left(-\left(\frac{\rho}{N_i}\right)^a\right)}{\partial N_i} = a \cdot \left(\frac{\rho}{N_i}\right)^{a-1} \frac{\rho}{N_i^2} = a \cdot \left(\frac{\rho}{N_i}\right)^a \frac{1}{N_i} \tag{4-6}$$

$$\left(\frac{N_i}{f_i}\left(\frac{\partial f}{\partial N}\right)_i\right) = \left(\frac{\partial f \big/ f_i}{\partial N \big/ N_i}\right) = \frac{a\rho^a}{N_i^a} \tag{4-7}$$

Taking logarithm for both sides of Equation 4-7, we get:

$$\ln\left(\frac{\partial f / f_i}{\partial N / N_i}\right) = \ln\left(\frac{\partial \ln f_i}{\partial \ln N_i}\right) = \ln a\rho^a - a \ln N_i \quad \textbf{(4-8)}$$

Considering Equation 4-8 to be in the form of $y = mx + b$, $-a$ is the slope m of values of $x = \ln N_i$ plotted against values of $y = \ln\left(\frac{\partial \ln f_i}{\partial \ln N_i}\right)$, and $\ln a\rho^a$ is the intercept b. The slope and intercept from linear regression analysis of the test data is used as Equation 4-9 and Equation 4-10 to determine a and ρ.

$$a = -m \quad \textbf{(4-9)}$$

$$\rho = e^{\frac{b - \ln a}{a}} \quad \textbf{(4-10)}$$

Once a and ρ parameters are defined, it is advantageous to determine the coefficients a_m and b_m which characterize the rate of erosion for each material type:

$$a_f = \frac{10^{a_m \tau_i + b_m}}{\gamma_b} \quad \textbf{(4-11)}$$

$$\log a_f = a_m \tau_i + b_m - \log \gamma_b \quad \textbf{(4-12)}$$

If the above expression is in the form of $y = mx + b$, a_m is the slope m of values of $x = \tau_i$ plotted against values of $y = \log a_f$, and $b_m - \log \gamma_b$ is the intercept b. Therefore, a_m and b_m are to Equation 4-13 and Equation 4-14. f_0 can be found by averaging multiple values from Equation 4-1 above.

$$a_m = m \quad \textbf{(4-13)}$$

$$b_m = b + \log \gamma_b \quad \textbf{(4-14)}$$

MODEL CALIBRATION USING LAB TEST RESULTS

In order to validate the proposed erosion model, HWTD test results have been used and Figure 4-13 shows an example plot to estimate a and ρ from slope and intercept of the linearly regressed trends of the HWTD test results.

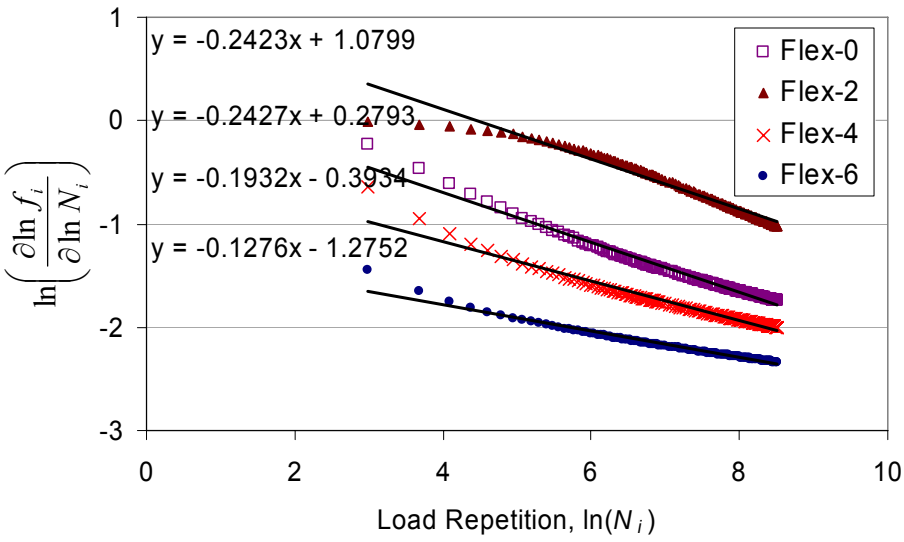

Figure 4-13 Log Plot to Acquire a and ρ from HWTD Test.

Figure 4-14 shows the comparison of the predicted erosions (lines) versus those of the HWTD test results (dots). The prediction results match well with test data for all material type and treatment ratios.

The data in Figure 4-15 shows the correlation between observed and model fitted erosion depth of all test materials. When the data plots closer to a diagonal line, the model fits with the test data more accurately. R-squared value is 93 percent which means good fit of model to the test data. The underestimated erosion near the maximum erosion is perhaps due to the zero load transfer condition in laboratory test although load transfer in the field condition is not zero all the time and retards erosion progress. Fluctuation in the measured data due to random aggregate movements below the concrete slab also induces divergence by scattered test data.

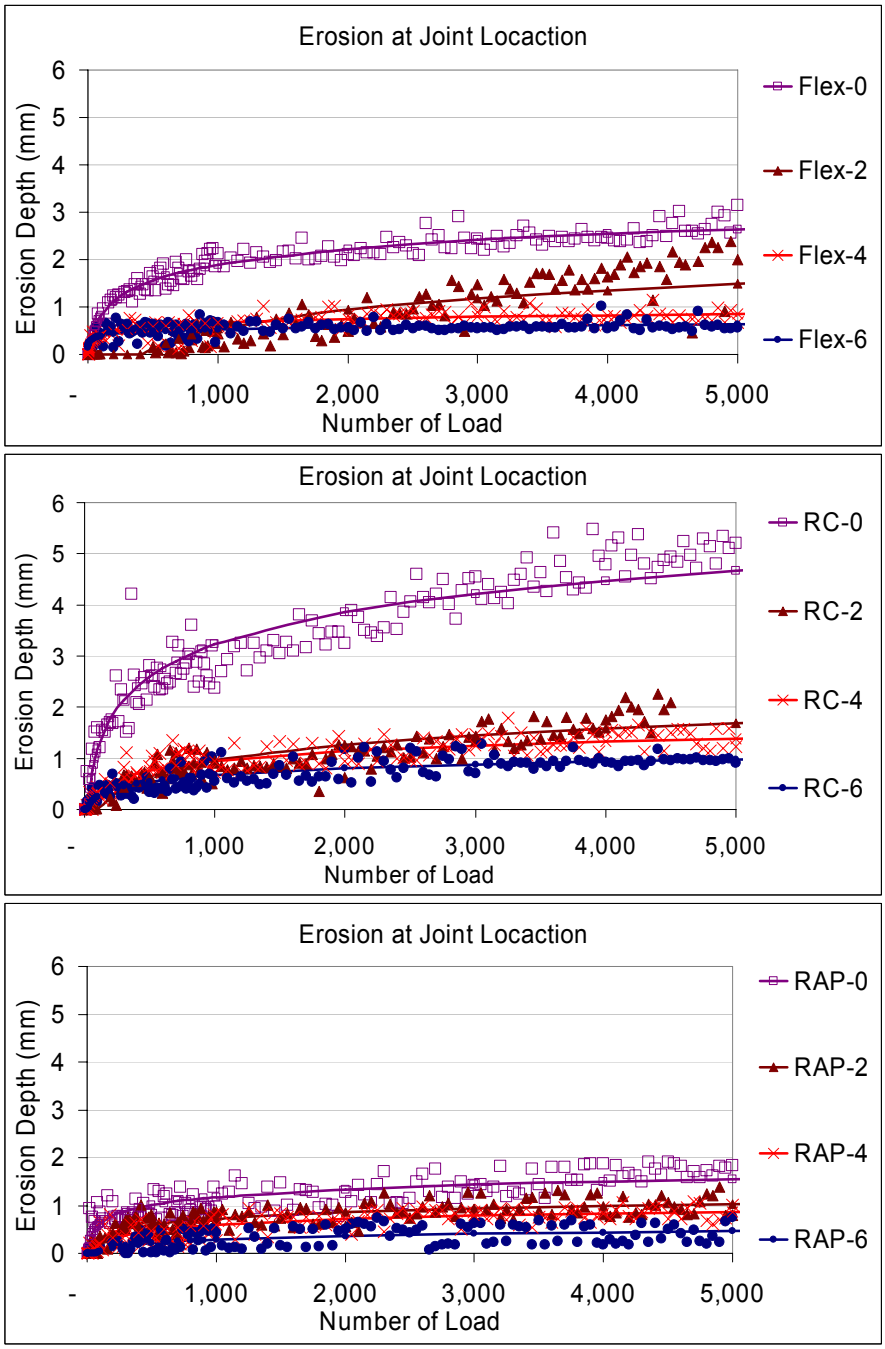

Figure 4-14 Erosion Model Fitting to HWTD Test Results.

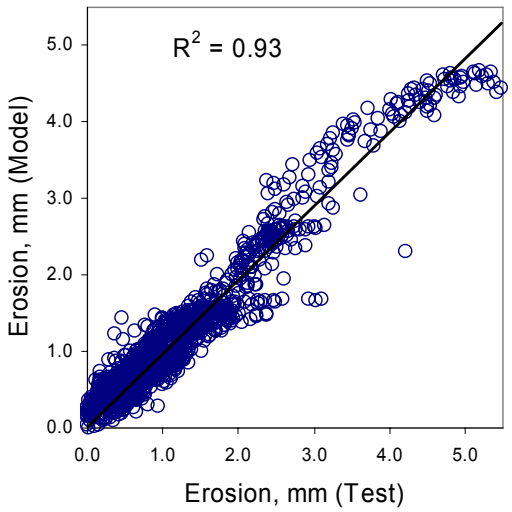

Figure 4-15 Model Fitted Erosion versus Measured Erosion from HWTD Test.

A paired t-test analysis was conducted to validate proposed erosion model at a confidence level of 95 percent based on the null hypothesis of no difference between the means of two data sets. Table 4-2 shows the results of the p-value is greater than 0.05 which indicates there is statistically no difference between measured and fitted values.

Table 4-2 Results of Paired T-test Statistic on Measured and Modeled Erosion.

Statistical quantity	Test Results	Model
Mean	1.13	1.13
Variance	0.95	0.85
Observations	1527	1527
Pearson Correlation	0.97	
Hypothesized Mean Difference	0.00	
df	1526	
t Stat	-0.78	
P(T<=t) one-tail	0.22	
t Critical one-tail	1.65	
P(T<=t) two-tail	0.44	
t Critical two-tail	1.96	

MODEL CALIBRATION USING LTPP DATA

The LTPP is the largest pavement performance research database for faulting and punchout data. The LTPP database was used to compare the proposed erosion model with field performance. There are many factors affecting faulting and punchout, however, erosion is the main factor and the growth rate would trend with the erosion development rate. The results of proposed models generally match well with observed field data.

Calibration of Faulting Model

Faulting data were retrieved from LTPP General Pavement Experiment Study (GPS) number 3 JPCP and GPS-4 JRCP. 20 sections (13 JPCP and 7 JRCP sections) which have significant faulting are selected as feasible data based on availability and reasonableness. Table 4-3 shows summarized section information. Two tables, "TRF_HIST_EST_ESAL" and "TRF_MON_EST_ESAL" are combined to retrieve annual ESALs in the LTPP lane. If any year traffic record is missed, linear interpolation is applied using similar traffic increasing rate with previous years. Since a faulting depth is highly related with the subbase erosion depth under the joint, faulting model is proposed as a function of possibility of erosion in Equation 4-15. Parameters of faulting models are achieved base on LTPP data regression and this correlation is restricted to the cement treated subbases due to the limited material information available in the LTPP data.

$$FAULT_i = FAULT_0 \cdot e^{-\left(\frac{\rho}{N_i - \Delta}\right)^a} \quad \textbf{(4-15)}$$

where: $FAULT_i$ = average faulting depth at the number of ESAL, N_i (mm or in.)

$FAULT_0$ = ultimate average faulting depth (mm or in.)

$e^{-\left(\frac{\rho}{N_i - \Delta}\right)^a}$ = erosion ratio at the number of ESAL, N_i

N_i = number of ESAL contributing to erosion (ESAL)

JPCP:

$$\rho = 327{,}379 \cdot WETDAYS \cdot ADT \cdot \frac{h_c \cdot h_b}{L_x \cdot L_y}$$

$$a_{\text{field}} = 9.3731\ a_f - 6.4999$$

$$a_f = \frac{\log^{-1}(-0.0167\tau - 1.2262)}{\gamma_b}$$

$$\Delta = 4.6 \cdot (1310 \cdot DAYS90 - WETDAYS) \cdot ADT \cdot \frac{h_c \cdot h_b}{L_x \cdot L_y}$$

JRCP:

$$\rho = 4{,}159{,}543 \cdot WETDAYS \cdot ADT \cdot \frac{h_c \cdot h_b}{L_x \cdot L_y}$$

$$a_{\text{field}} = 0.6087\ a_f - 0.1808$$

$$\Delta = 82.5 \cdot (918 \cdot DAYS90 - WETDAYS) \cdot ADT \cdot \frac{h_c \cdot h_b}{L_x \cdot L_y}$$

Table 4-3 Characteristics of LTPP Sections used in Faulting Model Calibration.

State and Section ID	Pavement Type	Construction Date	Last Survey Date	Age to Last Survey Date, year	Estimated Cumulative ESAL to Last Survey Date, millions	Joint Spacing, ft	Lane Width, ft	LTE System	PCC Thickness, in.	PCC Compressive Strength, psi	PCC Flexural Strength, psi
AL 1_3028	JPCP	6/1/1971	2/12/2004	33	11.2	20	12	Aggregate	10.2	4682 (28day)	N/A
CA 6_3013	JPCP	7/1/1982	2/1/2007	25	27.2	13.5	12	Aggregate	9.6	3670 (14day)	585 (14day)
CA 6_3017	JPCP	7/1/1978	1/26/2004	26	4.6	15.5	12	Aggregate	8.1	N/A	N/A
CA 6_3019	JPCP	12/1/1979	1/30/2007	28	40.6	15.5	12	Aggregate	8.6	4340 (28day)	687 (28day)
CA 6_3021	JPCP	4/1/1974	1/29/2007	33	7.1	15.5	12	Aggregate	8.1	3560 (14day)	550 (14day)
CA 6_3024	JPCP	11/1/1980	2/1/2007	27	52.3	15.5	12	Aggregate	10.2	3670 (14day)	625 (14day)
CA 6_7456	JPCP	12/1/1971	6/26/2000	29	18.8	15.5	12	Aggregate	11.7	2975 (14day)	605 (14day)
IN 18_3002	JPCP	8/1/1976	9/13/2002	26	4.9	15.5	12	Dowel	9.5	N/A	546 (14day)
NE 31_3018	JPCP	5/1/1985	12/17/2003	18	22.5	15.5	12	Aggregate	11.9	5980 (28day)	N/A
OK 40_3018	JPCP	6/1/1976	3/25/2004	28	27.8	15	12	Aggregate	8.9	5192 (30day)	N/A
SD 46_6600	JPCP	6/1/1975	7/30/2003	28	0.5	18.5	12	Aggregate	8	4650 (28day)	N/A
WY 56_3027	JPCP	6/1/1981	10/11/2004	23	21.0	13.8	12	Aggregate	10.6	4587 (28day)	787 (28day)
PR 72_3008	JPCP	5/1/1976	11/4/2003	27	37.0	19.7	12	Aggregate	9.9	N/A	N/A
AL 1_4007	JRCP	6/1/1970	12/2/1997	27	6.0	39	12	Dowel	10.5	4633 (7day)	565 (7day)
AL 1_4084	JRCP	6/1/1970	2/11/2004	34	39.8	57.5	12	Dowel	10.5	6287 (28day)	964 (28day)
AR 5_3073	JRCP	1/1/1965	5/21/2003	38	44.6	45	12	Dowel	9.1	4311 (28day)	N/A
AR 5_3074	JRCP	9/1/1966	2/28/2001	35	130.5	45	12	Dowel	10.1	4490 (28day)	N/A
AR 5_4021	JRCP	10/1/1970	3/2/2004	34	13.1	45	12	Dowel	9.7	N/A	N/A
LA 22_4001	JRCP	6/1/1970	7/30/2000	30	14.3	58.5	12	Dowel	9.8	N/A	N/A
NE 31_4019	JRCP	11/1/1976	1/22/2004	28	9.7	45.6	12	Dowel	9.1	4953 (28day)	N/A

Table 4-3 (continued).

State and Section ID	Average Wet-day per Year	Days Above 90 °F	Climatic Region	Shoulder Thickness & Type	Base Thickness, in	Base Type_% Stabilizer	Subbase Thickness, in	Subbase Type_% Stabilizer	Subgrade Type
AL 1_3028	121.6	49.9	WNF	N/A	7	Crush stone	10	Soil-aggregate mixture: Predominantly coarse-grained	Coarse-grained soil: Clayey sand
CA 6_3013	35.2	111.0	DNF	4.2" PCC	4	Lean concrete_8.5%	-	No subbase	Coarse-grained soil: Silty sand with gravel
CA 6_3017	49.1	54.3	WNF	3" AC	3.3	Cement aggregate mixture_4%	6	Soil aggregate mixture	Coarse-grained soil: Silty sand with gravel
CA 6_3019	48.9	105.8	DNF	AC	4.4	Cement aggregate mixture_5.5%	8.8	Soil-aggregate mixture: Predominantly fine-grained	Coarse-grained soil: Clayey sand
CA 6_3021	49.7	90.0	DNF	3.6" AC	5.4	Cement aggregate mixture_5.4%	5.4	Soil-aggregate mixture: Predominantly coarse-grained	Coarse-grained soil: Silty sand with gravel
CA 6_3024	36.8	110.9	DNF	9.6" PCC	6.2	Cement aggregate mixture_4%	5.2	Soil-aggregate mixture: Predominantly coarse-grained	Coarse-grained soil: Clayey gravel with sand
CA 6_7456	61.1	72.1	DNF	3" AC	4.8	Cement aggregate mixture	35.6	Soil-aggregate mixture: Predominantly coarse-grained	Coarse-grained soil: Clayey gravel with sand
IN 18_3002	152.2	15.0	WF	7.5" PCC	5.5	Crushed stone	-	No subbase	Fine-grained soil: Silty lean clay
NE 31_3018	90.6	34.6	WF	12" PCC	5.6	Soil cement_10%	-	No subbase	Coarse-grained soil: Poorly graded soil
OK 40_3018	112.2	65.0	WF	1.5" AC	3.6	Sand asphalt	6.1	Lime-treated soil_5%	Fine-grained soil: Lean inorganic clay
SD 46_6600	101.2	29.0	WF	2" AC	3.2	Gravel (uncrushed)	-	No subbase	Fine-grained soil: Silty clay
WY 56_3027	93.5	7.4	DF	10" PCC	6.6	Crushed gravel	-	No subbase	Coarse-grained soil: Silty sand with gravel
PR 72_3008	242.1	73.9	WNF	2" AC	8.5	Soil-aggregate mixture: Predominantly coarse-grained	-	No subbase	Coarse-grained soil: Well graged gravel with Silt and sand
AL 1_4007	111.1	48.3	WNF	4.2" AC	5.8	Crushed gravel	13.5	Soil-aggregate mixture: Predominantly coarse-grained	Coarse-grained soil: Clayey sand with gravel
AL 1_4084	155.0	66.3	WNF	10" AC	5.6	Gravel (uncrushed)	13.7	Soil-aggregate mixture: Predominantly coarse-grained	Coarse-grained soil: Clayey sand
AR 5_3073	126.6	62.5	WNF	N/A	5.8	Soil-aggregate mixture: Predominantly coarse-grained	12	Soil-aggregate mixture: Predominantly coarse-grained	Coarse-grained soil: Silty gravel with sand
AR 5_3074	132.3	57.7	WNF	N/A	6.1	Cement aggregate mixture_9.5%	-	No subbase	Fine-grained soil: Lean inorganic clay
AR 5_4021	98.0	51.1	WNF	N/A	3.9	Soil-aggregate mixture: Predominantly coarse-grained	4.4	Fine-grained soil	Coarse-grained soil: Silty gravel with sand
LA 22_4001	163.9	80.6	WNF	1" AC	6.7	Cement aggregate mixture_8%	3.4	Fine-grained soil	Fine-grained soil: Sandy silty clay
NE 31_4019	97.7	24.3	WF	2" AC	3.2	Cement aggregate mixture	-	No subbase	Fine-grained soil: Lean inorganic clay

Figure 4-16 shows a plot to get model constants of a_m and b_m of Equation 4-13 and 4-14 from HWTD test results. The rate of field void development a_{field} can be estimated using the constants of a_m and b_m from the lab erosion model, field interfacial shear stress, and unit weight of subbase in the field. These attained parameters require calibrations since shear stresses in the field are much smaller than shear stresses during the HWTD lab tests as well as environmental effects such as dry-period and wet-period. Figure 4-17 shows a good matching of the rates of void development parameters by model and LTPP database. This correlation is limited to the cement treated subbases and more lab tests may broaden its application to other material types.

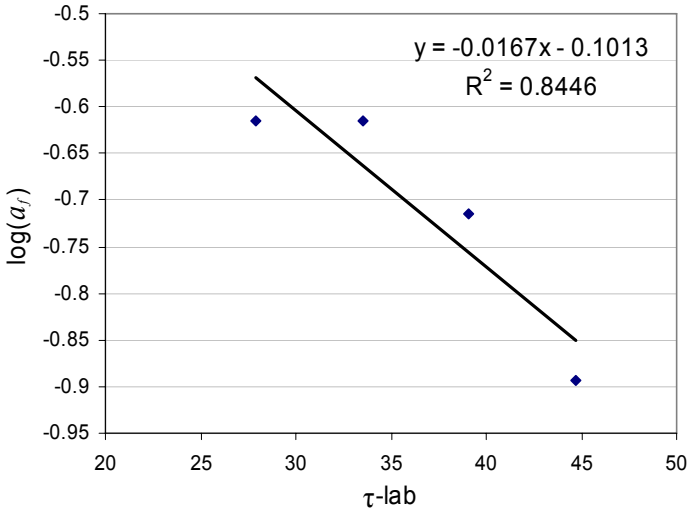

Figure 4-16 Log Plot to Acquire a_m and b_m from HWTD Test.

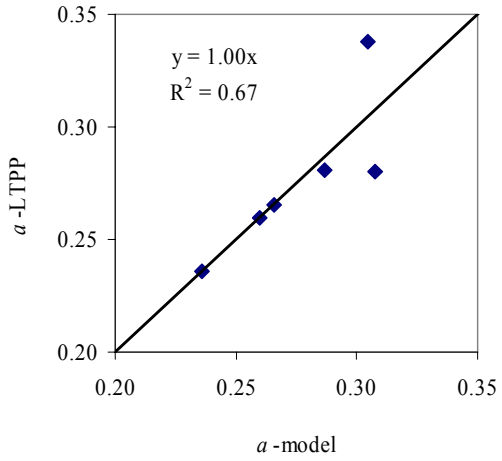

Figure 4-17 Faulting Model Parameters from LTPP Data and Calibrated Model Based on Lab Test.

The q-q plot and a paired two-sample t-test result between observed faulting and model predicted faulting are presented in Figure 4-18 and Table 4-4 . R-squared value is 86 percent representing good fit to the data as well as the null hypothesized of zero mean difference is accepted at a 95 percent confidence level (t statistic is not bigger than t critical two-tail).

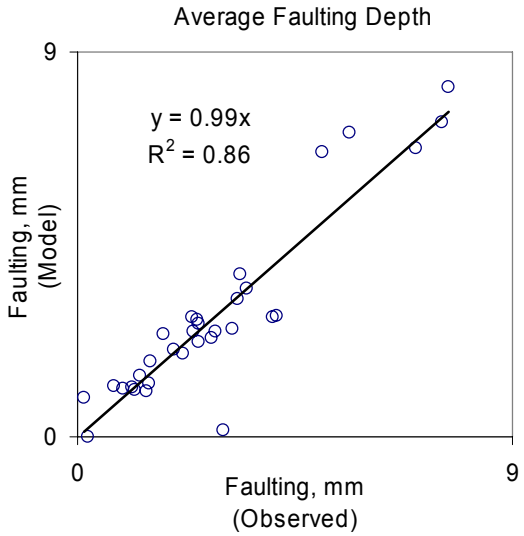

Figure 4-18 Modeled versus Measured Faulting of LTPP data.

Table 4-4 Statistical Analysis for Overall LTPP Faulting Data.

Statistical Quantity	Observed	Model
Mean	2.85	2.81
Variance	3.83	4.55
Observations	32	32
Pearson Correlation	0.93	
Hypothesized Mean Difference	0.0	
df	31	
t Stat	0.34	
P(T<=t) one-tail	0.37	
t Critical one-tail	1.70	
P(T<=t) two-tail	0.74	
t Critical two-tail	2.04	

Calibration of Punchout Model

LTPP GPS-5 CRCP was used to obtain data and two tables are employed to get punchout data: one is "MON_DIS_CRCP_REV" which is distress survey ratings from manual field inspections and the other is "MON_DIS_PADIAS42_CRCP" which is distress interpretations from film using version 4.2 of the PADIAS system. Accordingly, 12 sections are selected as feasible data after analysis for availability and reasonableness. Table 4-5 shows summarized section information.

Table 4-5 Characteristics of LTPP Sections used in Punchout Model Calibration.

State and Section ID	Construction Date	Last Survey Date	Age to Last Survey Date	Estimated Cumulative ESAL to Last Survey Date, millions	PCC Thickness, in.	Lane Width, ft	Reinforcing Steel Bar Diameter, in	PCC Compressive Strength, psi	PCC Flexural Strength, psi	Average Wet-day per Year	Days Above 90 °F	Climatic Region
IL 17_5869	8/1/1979	10/17/2002	23	4.1	8.9	12	0.63	N/A	N/A	139.4	16.0	WF
IL 17_9267	1/1/1966	3/27/1996	30	23.6	8.5	12	0.63	N/A	N/A	144.4	15.6	WF
ND 38_5002	10/1/1973	6/11/1995	22	5.6	8	12	0.63	4,466 (28day)	500 (28day)	125.8	11.5	WF
OR 41_5008	6/1/1972	4/9/2003	31	14.2	8.1	12	0.63	4,739 (28day)	611 (28day)	104.7	24.3	DF
OR 41_5021	7/1/1986	8/6/2002	16	19.4	10.8	13	0.75	4,636 (28day)	312 (28day)	179.6	9.6	WNF
PA 42_5020	3/1/1978	5/6/1999	21	20	9.3	12	0.75	N/A	N/A	144.5	15.4	WF
SC 45_5035	10/1/1975	2/4/2003	28	23.9	7.7	12	0.63	N/A	630 (14day)	150.4	58.3	WNF
SD 46_5025	11/1/1974	9/29/2003	29	1.3	8.1	12	0.63	5,665 (28day)	N/A	95.2	47.5	DF
TX 48_5323	9/1/1980	6/25/2002	22	20.7	8	12	0.75	3,939 (7day)	609 (7day)	85.4	67.2	WF
TX 48_5336	12/1/1986	1/10/2003	16	9.2	9	12	0.75	3,671 (7day)	N/A	78.7	63.7	WNF
VA 51_2564	2/1/1969	3/17/2004	35	20	7.9	12	0.63	N/A	N/A	159.4	25.6	WNF
VA 51_5010	5/1/1988	8/22/2000	12	9.4	9.1	12	0.75	N/A	N/A	131.3	37.2	WNF

Table 4-5 (continued).

State and Section ID	Shoulder Thickness & Type	Base Thickness, in.	Base Type_% Stabilizer	Subbase Thickness, in.	Subbase Type_% Stabilizer	Subgrade Type
IL 17_5869	3" AC	4.1	Lean concrete	-	No subbase	Fine-grained soil: Sandy silty clay
IL 17_9267	5" Surface treated	4.2	HMAC	-	No subbase	Coarse-grained soil: Well graded sand with silt
ND 38_5002	4" PCC	2.3	ATB	6	LTS_4%	Fine-grained soil: Fat inorganic clay
OR 41_5008	3" AC	4.4	CTB_6%	6	Crushed gravel	Coarse-grained soil: Poorly graded gravel with clay
OR 41_5021	3" AC	7.7	CTB_5.5%	6.4	Uncrushed gravel	Coarse-grained soil: Silty sand
PA 42_5020	3" AC	12	Crushed gravel	-	No subbase	Fine-grained soil: Sandy silt with gravel
SC 45_5035	3" AC	5.2	Soil cement_6%	-	No subbase	Coarse-grained soil: Silty sand
SD 46_5025	3" AC	4	Uncrushed gravel	-	No subbase	Fine-grained soil: Fat clay with sand
TX 48_5323	4" PCC	7	ATB	5.7	LTS_6.3%	Fine-grained soil: Lean clay with sand
TX 48_5336	4" PCC	1.6	HMAC	10	4” HMAC & and 6” LTS_1%	Fine-grained soil: Lean clay with sand
VA 51_2564	3" AC	6	Soil cement_10%	-	No subbase	Fine-grained soil: Silt
VA 51_5010	4" PCC	6.9	CTB_4%	-	No subbase	Fine-grained soil: Lean inorganic clay

Since the punchout is highly related with the subbase erosion possibility, punchout model is proposed as a function of possibility of erosion in Equation 4-16. Parameters of punchout models are achieved base on LTPP data regression and this correlation is restricted to the cement treated subbases due to the limited material information available in the LTPP data.

$$PO_i = PO_0 \cdot e^{-\left(\frac{\rho}{N_i - \Delta}\right)^a} \quad \textbf{(4-16)}$$

where: PO_i = number of punchout at the number of ESAL, N_i

PO_0 = ultimate number of punchout

$e^{-\left(\frac{\rho}{N_i - \Delta}\right)^a}$ = erosion ratio in punchout process at the number of ESAL, N_i

$\rho = 8{,}438 \cdot WETDAYS \cdot ADT \cdot \frac{h_c \cdot h_b}{D_{steel} \cdot L_y}$

$a_{\text{field}} = 0.2530\, a_f + 0.1435$

$\Delta = -25.09 \cdot (0.00518 \cdot DAYS90 - WETDAYS) \cdot ADT \cdot \frac{h_c \cdot h_b}{D_{steel} \cdot Ly}$

The q-q plot between observed punchouts and model predicted punchouts are presented in Figure 4-19 and R-squared value of 45 percent represents a somewhat fine fit of model to the field data. Table 4-6 shows statistical analysis result and the null hypothesized of same mean is not rejected at a 95 percent confidence level (t statistic is not bigger than t critical two-tail).

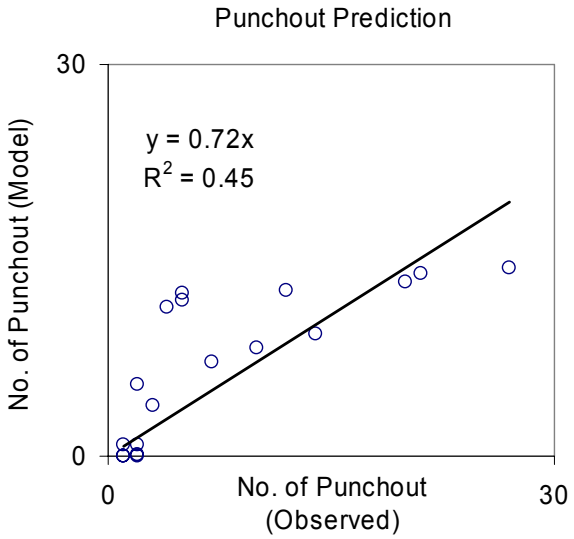

Figure 4-19 Modeled versus Measured Punchout of LTPP data.

Table 4-6 Statistical Analysis for Overall LTPP Punchout Data.

Statistical Quantity	Observed	Model
Mean	7.72	7.00
Variance	63.51	31.59
Observations	18	18
Pearson Correlation	0.77	
Hypothesized Mean Difference	0.0	
df	17	
t Stat	0.59	
P(T<=t) one-tail	0.28	
t Critical one-tail	1.74	
P(T<=t) two-tail	0.56	
t Critical two-tail	2.11	

CHAPTER V

DEVELOPMENT OF SUBBASE DESIGN CONSIDERATIONS

The objective of this chapter is to provide assistance for the economical and sustainable design of the erosion resistant subbase layers for concrete pavement. A decision flowchart provides the guidance for an effective design process of a concrete pavement subbase. Many design factors that affect the performance of the subbase are considered, however, the service history of existing subbases with similar layer properties and environmental conditions should be considered first if such information is available. These guidelines are provided in terms of design recommendations, material specification, and test methods.

SUBBASE DESIGN FLOWCHART

The decision process for the design and subbase material type selection shown in Figure 5-1 is categorized into three areas of consideration or criteria: materials, design, and sustainability. The process begins with the selection of material factors such as type, strength, stiffness, and erodibility requirements. Design factors include friction/bond characteristics, layer thickness, and traffic considerations. Finally, the design engineer considers the sustainability the subbase layer affords the overall pavement design. Load transfer, constructability, and drainability as well as precipitation and joint sealing maintenances should be considered in the design process in order to fully account for erosion damage. Accordingly, following this decision process, the design engineer should evaluate the key factors associated with a given subbase configuration.

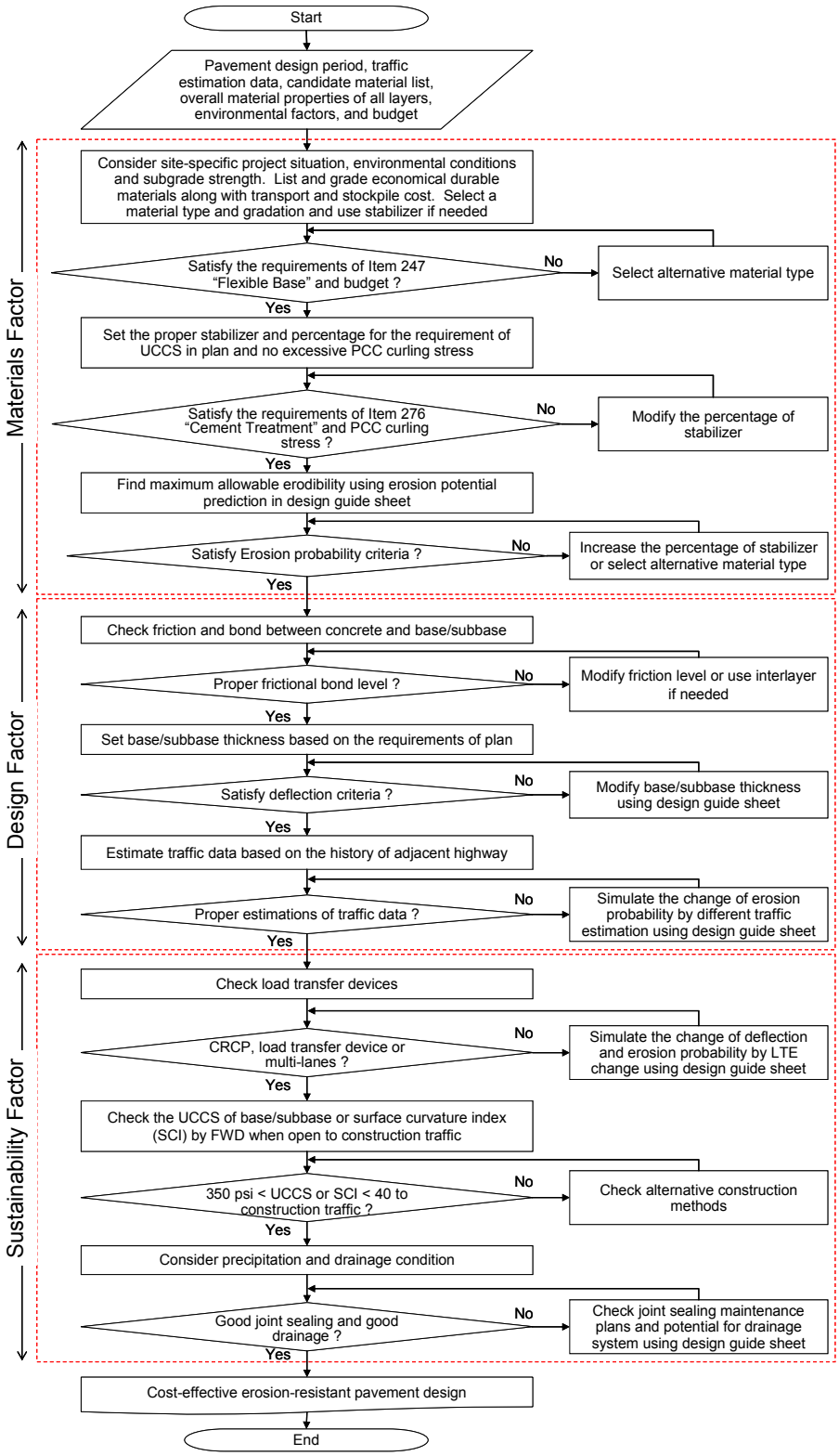

Figure 5-1 Decision Flowchart for Subbase Design of Concrete Pavement.

MATERIAL FACTORS

Subbase design-related decisions should account for many material characteristics and project-related environmental conditions. The longevity of material beneath the slab is an important sustainability-related factor that needs to be addressed in subbase material selection. In this regard, material factors such as material type, stiffness, strength, and erodibility resistance of the subbase and subgrade are important factors. Table 5-1 shows an ordered list of decision factors and their attributes.

Table 5-1 Subbase Design Considerations.

Factor	Item	Criteria Parameter	Test Method
Materials	Type	Minimum requirement, cost	Standard, budget
	Compressive Strength and stiffness	7-day and 28-day compressive strength Elastic modulus	Compressive strength test, Suction test
	Erodibility	Rate of erosion	Hamburg wheel-tracking erosion test
Design	Friction/Bond	Coefficient of friction	Friction test
	Thickness	Deflection	Composite deflection
	Traffic	Volume, load, and axle group	Distribution
Sustainability	Load Transfer	Radius of relative stiffness	Effective k-value FWD
	Constructability	Material functionality, cost	Cost Analysis, Impact Assessment
	Drainability	Moisture susceptibility	Suction test, Durability testing

Material Type

Typically, locally available, economical, and durable materials are used for subbase layer construction to keep transportation costs low. Moreover, recyclable materials are suggested to promote environmental friendly designs; stabilization may be needed to properly assure the agency's requirements. With these suggested features, cement treated base (CTB) using RAP, recycled concrete, or other locally available materials can be feasible candidate alternatives for subbase layers.

The advantage of a CTB is the higher material strength, stiffness, and resistance to erosion whether or not it is fully bonded to the concrete slab. A CTB layer is practically impervious and insensitive to the cyclic damage of freezing and thaw; which improves with time since it gains sufficient strength with age (*22*). However, CTB may have a tendency to reflect cracking through a bonded surface layer; which is one reason why asphaltic interlayer is commonly used with a CRC pavement construction; however, this could be mitigated to some extent through sawcutting (or micro-cracking) the base layer if full bond is a desired design option. Use of a fully bonded CTB may cause irregularities in the cracking pattern which again could be offset by adjustments in the steel percentages in a CRC pavement design. Otherwise, the main consideration in the design of a CTB layer is the need to balance erodibility against layer stiffness and interlayer friction. A consequence of not maintaining this balance is then the need to use an interlayer bond breaker.

RAP has economical and environmental benefits since its use potentially saves material, energy, and disposal costs, as well as conserves natural resources. RAP also typically has good availability for construction since it typically can be obtained, processed, and used onsite. RAP may also provide relatively low friction between the concrete slab and the subbase layer (*22*). The quality of RAP is highly governed by its constituent materials potentially leading to substantial variation in aggregate quality, size, and consistency depending on the source of the original material. Moreover, milling and crushing during processing can cause aggregate degradation and the amount of fines

generated. This variation can cause reduction in subbase stiffness and strength possibly creating low erosion resistance (*23*).

Similar as RAP, the use of recycled concrete may have many economical and environmental advantages such as a lower haul distance, reduced usage of natural aggregates, and lower energy consumption and waste. Previous research has found that recycled concrete (RC) materials cause CTB mixtures to set quicker with slightly higher (about 2 percent) density than mixtures with conventional aggregates as well as higher long-term strength (*24*). Benefits using RC bases could only be realized where sufficient quantities of recycled concrete materials are available near the construction site. RCB may segregate when worked excessively during compaction (*25*).

When a stabilized subbase is planned, sufficient stabilization is necessary to provide the needed erosion resistance as shown in Table 5-2. Typically, the cement percent for CTB should be higher than 4 percent to reduce erosion damage. Otherwise, projected traffic levels can be used to gauge necessary cement contents (as a function of strength). Moreover, the percentage passing the No. 200 (0.075 mm) sieve size in granular materials should not exceed 8 percent by weight.

Table 5-2 Erosion Resistance Requirements.

Environment and Drainage	28-Day Erodibility using Hamburg Wheel-Tracking Device Test, Max. in./million-repetitions	
	Good Drainage	Poor Drainage
Dry Area	6	2
Wet Area	4	1

Compressive Strength and Stiffness

Subbase strengths are typically of low strength since the concrete layer is expected to provide most of the load carrying capacity of the slab. Excessively high strength and stiff subbases are generally avoided to minimize shrinkage cracking in early stages of curing.

A compressive strength of 350 psi is often sufficient to support construction traffic; a 7-day strength range from 400 to 700 psi is recommendable. Even if a high strength subbase is utilized; the subbase strength should not exceed a 7-day compressive strength of 1,000 psi to prevent early-age cracking *(26)*.

A key aspect of long-term concrete pavement performance (particularly those of the unbonded jointed concrete options) is the quality and the nature of the curing effort relative to keeping the set temperature gradient to a minimum during and shortly after construction. The set gradient plays a major part of the magnitude and effect of the resulting curling and warping stresses that often are the cause of early, random cracking that are mainly dictated by the prevailing weather and curing conditions at the time the construction takes place. Tensile stresses and cracking in a concrete pavement often result from temperature and shrinkage effects during the early stages of hydration while the concrete is maturing and developing stiffness. Due to exposure to ambient conditions, a concrete pavement may cool to a minimum temperature as well as shrink due to moisture loss after cycling through a maximum temperature such that tensile stresses can be induced in the concrete slab. Stress development may become significant very soon after placement, perhaps even before the concrete has attained full hydration. Crack development in concrete pavement has been noted to be sensitive to diurnal temperature and wind effects.

The tendency to curl and warp is restrained by the concrete slab weight in which the resulting level of stress development is a function of the stiffness of the underlying subbase layer as reflected in the radius of relative stiffness. When the slab curls and warps in an upward configuration at the corners, tensile stresses are induced in the surface of the mid-slab area. Analysis of stress induced by a linear temperature gradient in a rigid pavement was originally developed by Westergaard *(27)*. The tensile stress pattern due to curling and warping in concrete slab is shown in Figure 5-2. It is related to the effect of the slab support immediately below the slab, particularly when a stabilized base is involved. For a slab of finite dimensions, Bradbury *(28)* suggested an approximate formula to estimate the maximum stress.

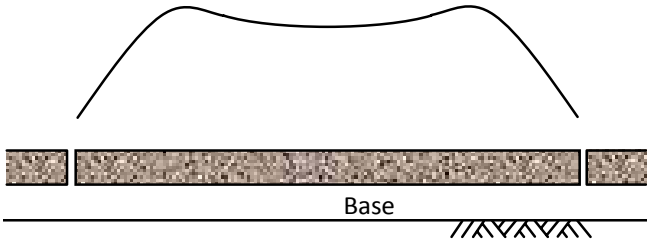

Figure 5-2 Tensile Stress Pattern in Slabs.

The Bradbury coefficient depends on radius relative stiffness of the support, length of the slab, modulus of elasticity of concrete, thickness of the slab, Poisson ratio of concrete, and modulus of subgrade reaction (effective k-value) as indicated in Figure 5-3. The effective k-value depends on the stiffness of the support as dictated by the subgrade k-value and the thickness and stiffness of the subbase layer supporting the concrete slab.

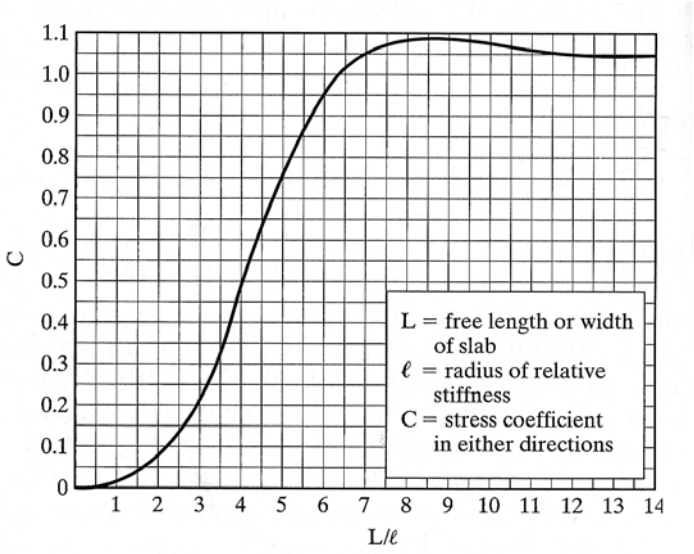

Figure 5-3 Coefficients for Maximum Stress in Curled Slab *(28)*.

When a slab with a finite length (L_x) and a finite width (L_y) is curled (or warped) as subjected to a temperature gradient, stress distributions can be found analytically. For estimating the maximum σ in a finite slab, Bradbury proposed an approximate formula as follows *(27, 28)*:

$$\sigma_x = \frac{E\alpha\Delta t}{2}\left(\frac{C_1 + \nu C_2}{1-\nu^2}\right) \quad \textbf{(5-1)}$$

where:

C = Bradbury coefficient

$$= 1 - \left(\frac{2\cos\lambda\cosh\lambda}{\sin 2\lambda + \sinh 2\lambda}\right)\left[\begin{array}{l}(\tan\lambda + \tanh\lambda)\cos\frac{y}{\sqrt{2}\ell}\cosh\frac{y}{\sqrt{2}\ell} \\ +(\tan\lambda - \tanh\lambda)\sin\frac{y}{\sqrt{2}\ell}\sinh\frac{y}{\sqrt{2}\ell}\end{array}\right] \quad \textbf{(5-2)}$$

and $\lambda = \frac{x}{\sqrt{8}\ell}$. The coefficient C_1 is typically in the longitudinal direction, whereas C_2 is for the perpendicular direction. Coefficient C_1 increases as the ratio L/ℓ increases, having a value of C = 1.0 for $L = 6.7\ell$, reaching a maximum value of 1.084 for $L=8.88\ell$. In summary, the magnitude of the restraint stress is affected by slab dimensions and support stiffness.

Erodibility

Erosion is often the dominant subbase deterioration mechanism resulting in faulting or punchout distress. Certainly, erodibility is related to subbase material type, stiffness, and strength which can be to some extent evaluated on the basis of erosion testing results. Stabilization does decrease erodibility, however the resulting increased stiffness by stabilization could generate other consequences as discussed previously. Proper stabilization level should be determined based on stiffness and erosion analysis for a given material type, design traffic, annual precipitation, and drainage condition.

Table 5-3 shows the general guideline for three erosion resistance levels measured by the HWTD test. The erosion rate criteria list in Table 5-3 is weighed against the rate found from the HWTD test (detailed in Appendix A). The erosion rate may also be confirmed against key design and sustainability factors listed in the decision process for subbase design.

Table 5-3 Subbase Erosion Resistance Criteria in Design Factors.

Erosion Resistance	Mean Erosion Rate Using HWTD, ER (mm/million rep)	Design Recommendation for Subbase under Moderate Drainage Condition
Good	ER < 50	Acceptable
Moderate	50 < ER< 100	Add more stabilizer if frequently saturated condition
Poor	100 < ER	Add more stabilizer or change material type or gradation

DESIGN FACTORS

These factors are related to those most likely to be governed by the design engineer although traffic considerations may override project-related engineering limitations. Nonetheless, the engineer should have some influence over their selection.

Frictional Bond

Interfacial friction between a concrete slab and the subbase is also an important factor for subbase design. Subbases with high friction properties have been found to be problematic relative to the formation of bottom up reflection cracking in JC pavement and poor cracking pattern distribution in CRC pavement. However, if interfacial friction is too low, crack spacing could be too long inducing wide crack widths. Each of these effects could be offset by increased steel percentages in a CRC pavement design. On the other hand, maintaining a medium level of frictional restraint (i.e., using an asphaltic interlayer) is desired to minimize the shear stress between the concrete and the base layer. The use of an asphalt interlayer does reduce excessive subbase friction where a CTB layer is included in the design while protecting against the low erosion potential most CTB materials have. Other bond breaker types (i.e., fabrics) are possible but they may need field evaluations.

Thickness

Subbase thickness and stiffness properties affect the overall composite design thickness of the pavement; its design includes considerations for the projected traffic level as well as the structural capacity needs of pavement system such as deflection criteria, subgrade strength and type, and load transfer of the joints and cracks. The deflection of composite layer could be a criterion for subbase thickness design. If expansive subgrade soils are a concern, measures to mitigate swell potential should be taken.

Subbase stiffness (or modulus) is conveniently expressed in terms of the radius of relative stiffness (ℓ) for design purposes. Higher subbase stiffness can reduce deflection and erosion potential of the subgrade but may increase interfacial friction and curling stress in the concrete slab. If the governing design criteria is acceptable to deflection, lower stiffness would perhaps be preferable in light of reduced interfacial friction and curling stress.

Figure 5-4 is an example of a deflection design chart presented in terms of the composite or effective ℓ - value and overall pavement thickness for a 300 psi/in. composite k-value (relative to a variable slab thickness, subgrade k-value, and subbase thickness and stiffness). The effective ℓ -value increases with a higher effective thickness of concrete pavement, which can be calculated using Equations 5-3 and 5-4 (assuming unbonded layers).

$$h_e = \sqrt[3]{h_c^{\,3} + \frac{E_b}{E_c} h_b^{\,3}} \qquad \textbf{(5-3)}$$

where: h_e = effective thickness of combined slab (in)

h_c = thickness of concrete slab (in)

h_b = thickness of base (in)

E_c = elastic modulus of concrete (psi)

E_b = elastic modulus of base (psi)

$$\ell_e = \sqrt[4]{\frac{Eh_e^{\,3}}{12(1-\nu^2)k}} \qquad \textbf{(5-4)}$$

where: ℓ_e = effective radius of relative stiffness (in)

E = elastic modulus of the PCC layer (psi)

h_e = effective thickness of PCC slab (in)

ν = Poisson's ratio

k = modulus of subgrade reaction

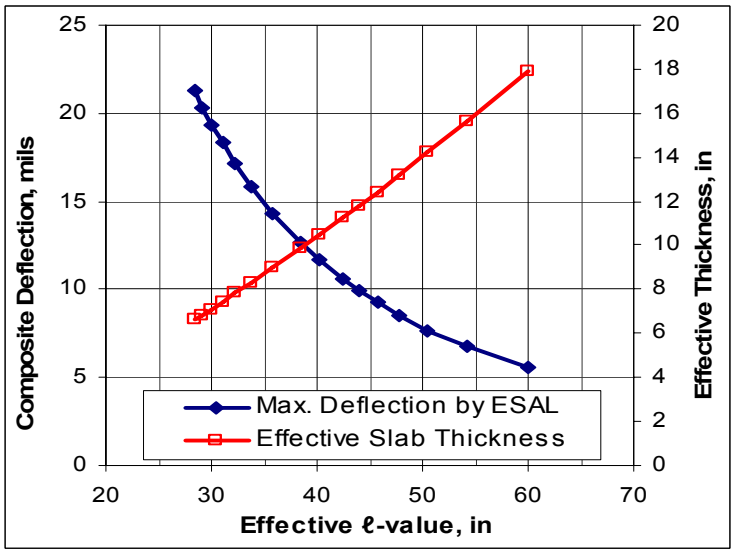

Figure 5-4 Deflection-based Subbase Thickness and Modulus Design Chart.

A thicker and stiffer subbase results in increasing effective slab thickness and the effective ℓ-value causing a lower composite deflection. On the other hand, reducing subbase thickness or the subbase modulus causes a greater composite deflection. Therefore, subbase thickness and modulus can be adjusted to meet design deflection criteria.

Traffic

Traffic is a key factor in pavement design for erosion considerations, and a higher level of traffic requires a more durable subbase system in order to protect the subbase and the subgrade. Traffic in the wheel path interfaces has the largest effect on the development of erosion. Lane distribution factors (LDF) and EER are used to properly account for traffic effects on erosion.

Table 5-4 shows the adjustment of erosion rate by EER. EER converts traffic due to the lateral distribution across the wheel path into the traffic in the wheel path contributing to erosion. A normal distribution is often assumed for the lateral distribution of traffic, and the traffic wandering range would be increased with a wider lane width.

Table 5-4 Erosion Rate Adjustment Factor by Equivalent Erosion Ratio.

Design Lane Width, ft	EER Coefficient
11 or less	0.9
12	0.8
13	0.7
14 or more	0.6

SUSTAINABILITY FACTORS

These factors are key to long term pavement performance and should be determined relative to their role or function in affecting capabilities to conduct long term repair. The inability to make future repair short of total reconstruction is tantamount to non-sustainability.

Load Transfer Efficiency

As the stiffness of the joint or crack decreases, slab deflection increases creating greater frictional stress at the slab interface causing greater distorted damage in the surface material. The accumulation of damaged material creates a greater degree of

susceptibility to pumping action leading to the growth of a void under the slab that induces more deflection and further damage and loss of joint stiffness. This sequence could also accelerate subbase deterioration by interacting effects. However, load transfer devices or PCC shoulder effects could delay subbase damage with less deflection at a joint or crack. Deflection criteria accounts for the effect of LTE on the subbase design indirectly, and Table 5-5 shows the adjustment factor for erosion rate.

Table 5-5 Erosion Rate Adjustment Factor by Load Transfer Systems.

Load Transfer Devices at Transverse Joints or Cracks, or Dowels at Joints	Tied PCC Shoulders, Curb and Gutter, or Greater Than Two Lanes in One Direction	
	Yes	No
Yes	0.7	0.8
No	0.9	1.0

Constructability

The subbase used under concrete pavement needs to have adequate structural capacity to support construction equipment and operations, otherwise the subbase can become damaged and need costly repairs. The current TxDOT requirements for subbases (4 in. ACP or 1 in. ACP over 6 in. cement stabilized base (CSB)) have historically performed well under construction operations. The TxDOT did allow the use of 2 in. ACP over 8 in. LTS in the past on projects in the Fort Worth area; however, TxDOT personnel found that such thin ACP layers were susceptible to damage from construction traffic. In addition, it was found from field coring operations that there appeared to be very little bond between ACP and lime-treated subgrade materials; such low bond can result in damage to thin ACP layers over LTS.

In areas where stabilized subgrade materials are needed to facilitate construction and reduce the effect of expansive soils on pavement roughness, it is recommended to follow the TxDOT document titled, “Guidelines for Modification and Stabilization of Soils and Base for Use in Pavement Structures” (*29*). Stabilized subbases need to have

the proper stabilizer type and content to perform properly and have adequate structural capacity for construction operations. In addition, designers should address areas where significant moisture intrusion into subgrade soils can occur; this is of special concern for construction projects involving curb and gutter sections. Researchers observed isolated areas on one project where it appeared that significant moisture intrusion into the subgrade resulted in construction equipment damaging the subbase.

A falling weight deflectometer (FWD) can be used to assess the structural capacity of subbase. The FWD surface curvature index (SCI) is simply the deflection underneath the FWD load plate (W_1) minus the deflection 12 in. away from the load (W_2), or W_1-W_2. According to the report, if the SCI at a 9,000 lb load level is less than 20 mils, the pavement has a good base; if it is between 20 and 40 mils, the base is marginal; and if it is greater than 40 mils, the base is weak or soft. A minimum of 30 FWD data points along the subbase section of interest should be obtained in order to adequately characterize the section *(30)*.

Drainability

Pumping is a major cause of subbase voiding since eroded fine materials are transported under the slab to and through joints or cracks by water movement under pressure. When the subbase interface is not saturated, pumping action cannot transport or liquefy eroded fines significantly reducing the rate of erosion. The effect of precipitation on the number of wet weather days should be applied to adjust estimates of erosion.

Joint sealing appears to have an important effect on the incidence of interfacial saturation. Well-managed joint sealing could possibly minimize water and incompressible material infiltration into the joint and potential subgrade erosion or spalling of the joint. The longitudinal joint sealing is particularly important since extensive amounts of surface water can enter through the lane/shoulder joints.

In design, the erosion rate should be weighted over dry and wet performance periods based on calibration for local conditions. Table 5-6 shows the adjustment factor of erosion rate according to annual wet days and joint sealing maintenance condition.

Good joint sealing with low precipitation reduces erosion significantly and vice versa. The rate of erosion under dry conditions is approximately 25 percent of the wet condition rate of erosion.

Drainage conditions may also affect the effective number of wet weather days that the interfacial area is saturated. A good drainage system would remove water faster and reduce hydraulic erosion significantly. Therefore, surface drainage measures (along with regular resealing) and ditches should be provided to minimize the infiltration of water to subsurface particularly through the longitudinally oriented joints or cracks.

Table 5-6 Erosion Rate Adjustment Factor Based on Annual Wet Days and Joint Seal Maintenance Condition.

Wet Days (day/year)	Joint Seal Maintenance Condition		
	Good	Moderate	Poor
> 250	0.74	0.82	0.90
200 - 250	0.62	0.68	0.75
150 - 200	0.49	0.55	0.60
100 - 150	0.37	0.41	0.45
50 - 100	0.25	0.27	0.30
< 50	0.12	0.14	0.15

CHAPTER VI

CONCLUSIONS AND RECOMMENDATIONS

CONCLUSIONS

As background, past test methods and models relative to erosion were reviewed. Many erosion tests were developed in the 1970s and 1980s using various testing devices but none of those tests have been easily interpretable relative to field performance. Previous erosion test methods in terms of their utility to characterize the performance of subbase and subgrade materials with respect to erosion resistance are evaluated. The design guides published by TxDOT, AASHTO, NCHRP 1-37 A: MEPDG, and PCA are reviewed for key design aspects of subbase layers such as material selection and layer stiffness.

The proposed test method is a mechanical erosion test using the HWTD that qualifies a subbase under wet conditions relative to the magnitude of the shear stress creating the erosive action, which provides a significant advantage over other approaches in terms of the translation of laboratory derived erosion rates to performance in the field. This test method measures subbase erosion under the contact of a concrete layer even though void development is represented relative to wet conditions; erosion under dry conditions can be estimated from the wet condition test results. Moreover, this approach allows for testing of a core sample from the field as well as laboratory compacted samples in a relatively short period of time while providing a wide range of applicability to all types of subbase or subgrade materials.

Three types of materials (Flex, RC, and RAP) treated by various cement contents (0, 2, 4, 6 percent) were tested and evaluated by different stress levels and number of loads. As expected, more weight loss develops as shear stress and loading number increases; however, the rate of weight loss dropped off to some extent at higher stress levels and loading numbers. RC base materials show the highest erosion rate, and RAP base materials show the least erosion rate as long as the fine-size aggregate fraction is the

same with other materials since the proper amount of asphalt mastic increases shear strength. Up to 2 percent cement for Flex and RAP subbases, however, does not reduce the erosion rate significantly but 4 percent cement reduces erosion remarkably when compared with unstabilized materials.

Many empirical erosion models have been proposed in past research but their application has been limited by the variable ranges included in the database. The proposed mechanistic-empirical model is shown to have application to the new test. The HWTD test method can generate sufficient data in which to determine the model a and ρ parameter values, which are assumed to be applicable for assessing the erosion under both the wet and dry conditions. The weighting of the wet and dry conditions may be a matter of calibration to local performance. Measured and modeled results match well for all material type and treatment ratios. It is important to recognize that even though the proposed erosion model utilizes erosion rates generated under saturated conditions, zero load transfer between adjacent slabs, as well as unbound condition between the concrete slab and the underlying base material, it is capable of translating these results in terms of field performance by representing layer stiffness, deflection, and calibration to local conditions. The calibration coefficients based on field and lab performance can be applied to the erosion model for a maintenance purpose or the design of a new pavement.

The subbase design guidelines for rigid pavements account for many interacting material and slab characteristics and environmental conditions. General material factors such as material type, strength, stiffness, and erodibility; design factors such as thickness, interlayer frictional, and traffic conditions should be considered as well as sustainability issues such as constructability in order to consider the full extent of erosion damage. In design, the erosion rate should be weighted over dry and wet performance periods based on calibration for local conditions and performance to represent such factors as frequency of joint sealing maintenance, changes in drainage conditions, and annual precipitation. When a given subbase material does not satisfy the specific design criteria, an evaluation process following the decision flowchart format is useful to guide the selection of a workable alternative material.

RECOMMENDATIONS FOR FUTURE STUDY

The work described in this study was based on the limited samples using cement stabilization. Further studies considering different type of stabilizers with combinations of various subbase materials and using core samples from the field are needed to understand the erosion characters of the subbase in field conditions. Moreover, erosion model may need further development to match better based on lab test results with field performances through calibration processes. Erosion resistant designs and maintenance strategies also require for better and long-lasting concrete pavement performances.

REFERENCES

1. Van Wijk, A.J. *Rigid Pavement Pumping: (1) Subbase Erosion and (2) Economic Modeling*. Joint Highway Research Project File 5-10, School of Civil Engineering, Purdue University, West Lafayette, Indiana, May 16, 1985.

2. Phu, N.C., and M. Ray. The Erodibility of Concrete Pavement Subbase and Improved Subgrade Materials. *Bulletin de Liaison des Laboratoires des Ponts et Chaussees,* Special Issue 8, France, July 1979, pp. 32-45.

3. de Beer, M. *Aspects of the Erodibility of Lightly Cementitious Materials*. Research Report DPVT 39, Roads and Transport Technology, Council for Scientific and Industrial Research, Pretoria, South Africa.

4. Briaud, J., F. Ting, H. Chen, R. Gudavalli, S. Perugu, and G. Wei. Prediction of Scour Rate in Cohesive Soils at Bridge Piers. *Journal of Geotechnical and Geoenvironmental Engineering*, Vol. 125, No. 4, 1999, pp. 237-246.

5. Wan C., and R. Fell. Investigation of Rate of Erosion of Soils in Embankment. *Journal of Geotechnical and Geoenvironmental Engineering*, Vol. 130, No. 4, 2004, pp. 373-380.

6. Rauhut, J.B., R.L. Lytton, and M.I. Darter. *Pavement Damage Functions for Cost Allocation, Vol. 1, Damage Functions and Load Equivalency Factors*. Report No. FHWA/RD-82/126, Federal Highway Administration, U.S. Department of Transportation, July 1982.

7. Markow, M.J., and B. D. Brademeyer. *EAROMAR Version 2*, *Final Technical Report*. FHWA/RD-82/086, Federal Highway Administration, U.S. Department of Transportation, April 1984.

8. Larralde, J. *Structural Analysis of Ridge Pavements with Pumping*. Ph.D. Dissertation, Purdue University, West Lafayette, Indiana, December 1984.

9. Packard, R.G. *Thickness Design for Concrete Highway and Street Pavements*. Portland Cement Association, Skokie, Illinois, 1984.

10. Jeong, J,. and D. Zollinger. Characterization of Stiffness Parameters in Design of Continuously Reinforced and Jointed Pavements. In *Transportation Research Record: Journal of the Transportation Research Board, No. 1778*, TRB, National Research Council, Washington, D.C., 2001, pp. 54-63.

11. TxDOT. *Pavement Design Guide*. TxDOT Manual, Texas Department of Transportation, November 2008. http://onlinemanuals.txdot.gov/txdotmanuals/pdm/reocmmended_input_design_values.htm. Accessed: October 1, 2009.

12. TxDOT. *Item 276 Cement Treatment (Plant-mixed)*. TxDOT Standard Specifications, Texas Department of Transportation, June 2004. ftp://ftp.dot.state.tx.us/pub/txdot-in.fo/cmd/cserve/specs/.../s276.pdf. Accessed: October 1, 2009.

13. AASHTO. *Guide for Design of Pavement Structures*. American Association of State Highway and Transportation Officials, Washington, D.C., 1986.

14. Huang, Y. H. *Pavement Analysis and Design,* 2nd ed. Pearson Prentice Hall, Upper Saddle River, New Jersey, 2004.

15. NCHRP. *Guide for Mechanistic-Empirical Design of New and Rehabilitated Pavement Structures, Final Report: Part 2. Design Inputs: Chapter 2. Material Characterization*. National Cooperative Highway Research Program, August 2003. http://www.trb.org/mepdg/guide.htm. Accessed: October 1, 2009.

16. NCHRP. *Guide for Mechanistic-Empirical Design of New and Rehabilitated Pavement Structures: Final Report: Part 3. Design Analysis: Chapter 4. Design of New and Reconstructed Rigid Pavements*. National Cooperative Highway Research Program, August 2003. http://www.trb.org/mepdg/guide.htm. Accessed: October 1, 2009.

17. NCHRP. *Guide for Mechanistic-Empirical Design of New and Rehabilitated Pavement Structures: Final Document Appendix JJ: Transverse Joint Faulting Model*. National Cooperative Highway Research Program, August 2003. http://www.trb.org/mepdg/guide.htm. Accessed: October 1, 2008.

18. Zollinger, C.J., D.G. Zollinger, D.N. Little, and A. Godiwalla. Innovative Approach to Pavement Rehabilitation Analysis and Design of Runway (R/W) 15L-33R at

George Bush Intercontinental Airport (IAH) in Houston, TX. *Proceedings, 8th International Conference on Concrete Pavements*, Vol. 3, Colorado Springs, Colorado, August 15-18, 2005, pp.1101-1119.

19. Ioannides, A. M. Dimensional Analysis in NDT Rigid Pavement Evaluation. *Journal of Transportation Engineering,* Vol. 116, No. 1, July 1990, pp. 23–36.

20. Webster, S. L., R. H. Grau, and T. P. Williams. *Description and Application of the Dual Mass Dynamic Cone Penetrometer*. Instruction Report GL-93-3, Department of Army, Waterways Experiment Station, Corps Engineers, Vicksburg, Mississippi, 1992, pp. 50.

21. Phu, N.C., and M. Ray. The Hydaulics of Pumping of Concrete Pavements. *Bulletin de Liaison des Laboratoires des Ponts et Chaussees*, Special Issue 8, France, July 1979, pp. 15-31.

22. PCA. *Pavement – Soil Cement*. Portland Cement Association, Skokie, Illinois, 2008. http://www.cement.org/pavements/pv_sc.asp. Accessed: October 1, 2008.

23. *Reclaimed Asphalt Pavement-User Guideline-Asphalt Concrete*. Turner-Fairbank Highway Research Center, McLean, Virginia. http://www.tfhrc.gov/hnr20/recycle/waste/rap131.htm. Accessed: October 1, 2008.

24. Lim, S., D. Kestner, D.G. Zollinger, and D.W. Fowler. *Characterization of Crushed Concrete Materials for Paving and Non-paving Applications*. Report 4954-1. Texas Transportation Institute, Texas A&M University System, College Station, Texas, January 2003.

25. USDOT-FHA. *Summary of Texas Recycled Concrete Aggregate Review*. United States Department of Transportation—Federal Highway Administration, July 18, 2006. http://www.fhwa.dot.gov/pavement/recycling/rcatx.cfm. Accessed: October 1, 2008.

26. Hall, J.W., J. Mallela, and K.L. Smith. *Report IPRF-01-G-002-021(G) Stabilized and Drainable Base for Rigid Pavement: A Design and Construction Guide*. JP010P, American Concrete Pavement Association, Skokie, Illinois, October 2005.

27. Westergaard, H.M. Analysis of Stresses in Concrete Pavements Due to Variations of Temperature. *Proc*., *Highway Research Board*, Vol. 6, Washington, D.C., pp. 201-215, 1926.

28. Bradbury, R.D. *Reinforced Concrete Pavement*. Wire Reinforcement Institute, Washington, D.C., 1938.

29. TxDOT. *Guidelines for Modification and Stabilization of Soils and Base for Use in Pavement Structures*. Texas Department of Transportation, September 2005. ftp://ftp.dot.state.tx.us/pub/txdot-in.fo/cmd/tech/stabilization.pdf. Accessed: October 1, 2009.

30. Scullion, T. *Incorporating a Structural Strength Index into the Texas Pavement Evaluation System*. TTI Research Report 409-3F. Texas Transportation Institute, Texas A&M University System, College Station, Texas, April 1988.

31. Hall, K.T., M.I. Darter, T.E. Hoerner, and L. Khazanovich. *LTPP DATA ANALYSIS Phase I: Validation of Guidelines for k-Value Selection and Concrete Pavement Performance Prediction*. Research Report No. FHWA-RD-96-198, ERES Consultants, Inc., Champaign, Illinois, January 1997.

32. ACI Committee 325, *Guide for Design of Jointed Concrete Pavements for Streets and Local Roads*. ACI Committee Report 325. 12R-02, American Concrete Institute, Farmington Hills, Michigan, 2002.

APPENDIX A

EROSION TEST PROCEDURE USING HAMBURG WHEEL-TRACKING DEVICE

1. SCOPE

1.1 Use this test method to determine the erosion susceptibility of subbase or subgrade materials due to mechanical and hydraulic shear on the layer interface generated by concrete slab movement under an applied moving wheel load. The configuration of the test device is the same as the one used for "Tex-242-F, Hamburg Wheel-Tracking Test" except the shape of polyethylene mold. This test method measures the erosion depth versus number of passes.

1.2 The values given in parentheses (if provided) are not standard and may not be exact mathematical conversions. Use each system of units separately. Combining values from the two systems may result in nonconformance with the standard.

2. APPARATUS

2.1 *Wheel-Tracking Device,* an electrically powered device capable of moving a steel wheel with a diameter of 8 in. (203.6 mm) and width of 1.85 in. (47 mm) over a test specimen.

2.1.1 The load applied by the wheel is 158 ± 5 lb. (705 ± 22 N).

2.1.2 The wheel must reciprocate over the test specimen, with the position varying sinusoidally over time.

2.1.3 The wheel must be capable of making 60 ± 2 passes across the test specimen per minute.

2.1.4 The maximum speed of the wheel must be approximately 1.1 ft/s (0.305 m/s) and will be reached at the midpoint of the slab.

2.2 *Temperature Control System,* a water bath capable of controlling the test temperature within ± 4 °F (2 °C) over a range of 77 to 158 °F (25 to 70 °C).

2.2.1 This water bath must have a mechanical circulating system to stabilize temperature within the specimen tank.

2.3 *Erosion Depth Measurement System,* a Linear Variable Differential Transducer (LVDT) device capable of measuring the erosion depth induced by the steel wheel within 0.0004 in. (0.01 mm), over a minimum range of 0.8 in. (20 mm).

2.3.1 The system, should be mounted, to measure the erosion depth at the midpoint of the wheels path on the slab.

2.3.2 Take erosion depth measurements at least every 100 passes of the wheel.

2.3.3 This system must be capable of measuring the erosion depth without stopping the wheel. Reference this measurement to the number of wheel passes.

2.3.4 Fully automated data acquisition and test control system (computer included).

2.4 *Wheel Pass Counter,* a non-contacting solenoid that counts each wheel pass over the test specimen.

2.4.1 Couple the signal from this counter to the erosion depth measurement, allowing the erosion depth to be expressed as a fraction of the wheel passes.

2.5 *Specimen Mounting System,* a stainless steel tray that can be mounted rigidly to the machine in the water bath.

2.5.1 This mounting must restrict shifting of the specimen during testing.

2.5.2 The system must suspend the specimen, allowing free circulation of the water bath on all sides.

2.5.3 The mounting system must provide a minimum of 0.79 in. (2 cm) of free circulating water on all sides of the sample.

3. MATERIALS

3.1 *Two high-density polyethylene molds,* shaped according to Figure A-1, to secure circular, cylindrical test specimens.

3.2 *Two vibration absorbing neoprene pads*, 0.375 in. (9.5 mm) thick and 6 in. (152.5 mm) diameter, to simulate subgrade layers which support and prevent the compressive fracture of test specimens.

3.3 *Two jointed concrete capping blocks*, shaped according to Figure A-2, to simulate the vertical movement of PCC slab under the wheel load on test specimens.

3.4 *Two rubber pads*, 0.125 in. thick (3.2 mm), 2.5 in. (63.5 mm) wide, and 6 in. (152.5 mm) length, to simulate tire contact and prevent the damage of concrete block surface by metal wheel edges during the test.

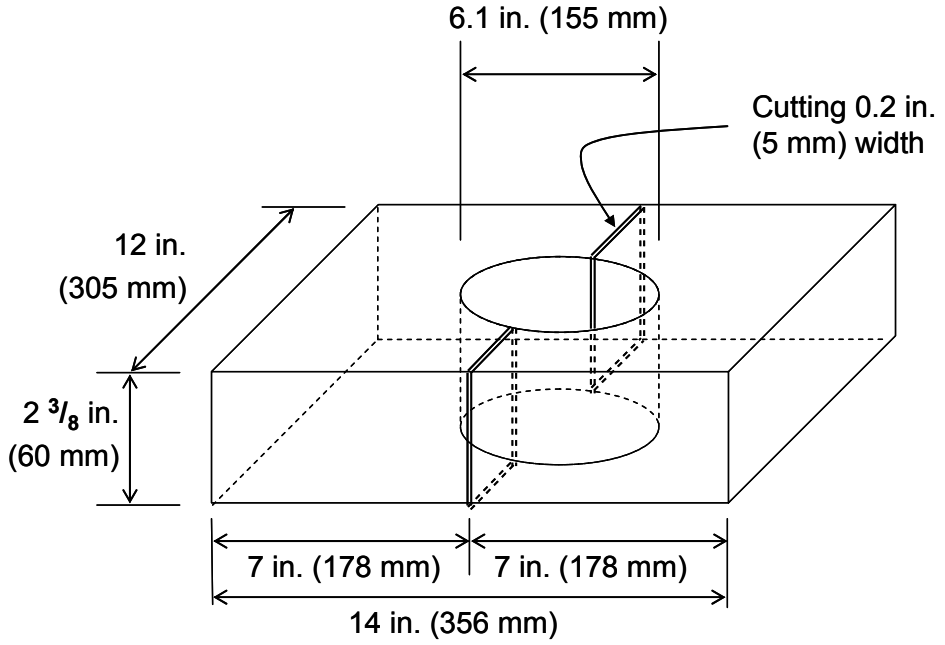

Figure A-1 Configuration of High-density Polyethylene Molds.

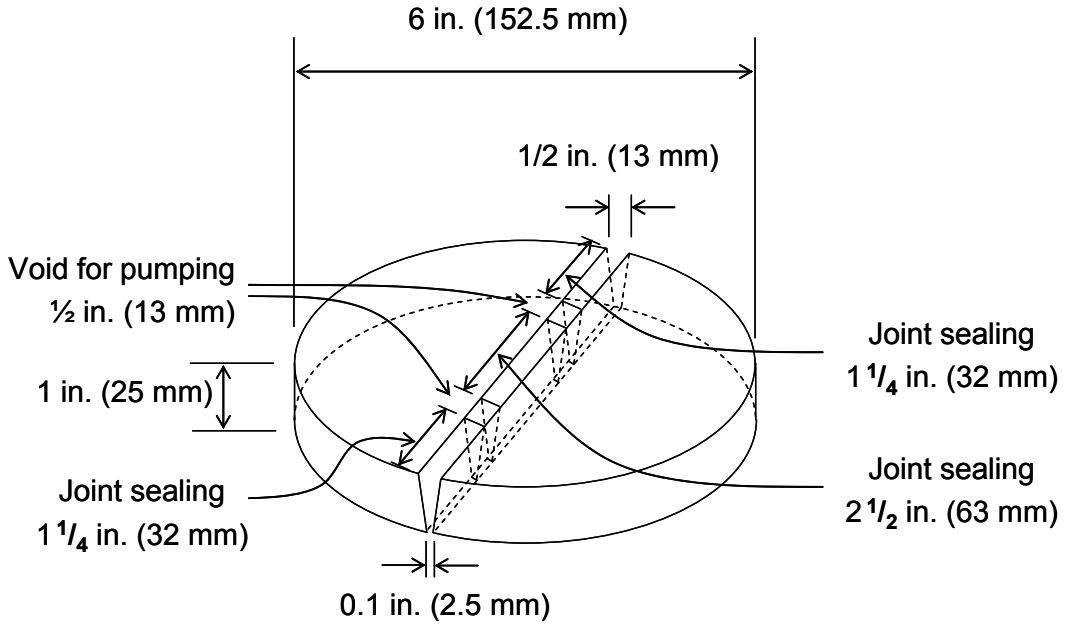

Figure A-2 Configuration of Jointed Concrete Capping Blocks.

4. **SPECIMEN**

4.1 *Laboratory Molded Specimen*—Prepare specimens in accordance with Tex-101-E, Tex-110-E, Tex-113-E, and Tex-120-E. Specimen diameter must be 6 in. (152.5 mm), and specimen height must be 1 in. (25 mm).

4.1.1 Maximum aggregate size should be 0.4 in. (10 mm) and use the gradation under 0.4 in. (10 mm) to make specimens.

4.1.2 2.5 lb (1,100 g) of soil per sample is recommended and when a 6 in. (152.4 mm) height compaction mold is used, place a 5 in. (127 mm) thick disk in the mold to make a 1 in. (25.4 mm) thick sample.

4.1.3 Optimum moisture content for the compaction of specimens should be modified by the cement content rate according to Tex-120-E.

4.1.4 Specimens cured during 28 days in a moisture chamber are recommended to evaluate long-term erosion susceptibility.

Note 1 - When a test result is required in a short period, specimens cured during 7 days in a moisture chamber could be used instead with an adjustment factor which defined by previous tests using the same material types.

4.1.5 Density of test specimens must be 93 ± 1%.

Note 2 - Weights for specimens prepared in the laboratory typically vary between 2 and 2.5 lb (900 and 1100 g) to achieve density due to different aggregate sources and mix types.

4.1.6 Use the bottom of the cured specimen as the top for erosion test. Seal other side (top while compacting) and side using plastic tapes after surface water elimination.

4.2 *Core Specimen*—Specimen diameter must be 6 in. (150 mm) and need to be cut with care as 1 in. (25 mm) height.

4.2.1 Use the dense and smooth cut surface of specimen as top and seal bottom and side using plastic tape after surface water elimination.

4.2.2 There is not a specific density requirement for core specimens.

5. PROCEDURE

5.1 Use two cylindrically molded specimens in accordance with Section 4.

5.2 Measure the sample weight.

5.3 Place a half of high-density polyethylene molds into the mounting tray.

5.4 Place the vibration absorbing neoprene pads, specimens, jointed concrete capping blocks, and rubber pad (bond on to concrete blocks) in order into the molds.

5.5 Set the joints perpendicular to wheel path.

5.6 Place the other half of high-density polyethylene molds and secure into the mounting tray.

5.7 Fasten the mounting trays into the empty water bath.

5.8 Start the software, supplied with the machine, and enter the required test information into the computer (60 passes per minute and 5,000 or 10,000 load repetition).

5.9 Fill the water bath until the water temperature is at the desired test temperature (test temperature should be 77 ± 2 °F (25±1°C) for all specimens), and monitor the temperature of the water on the computer screen.

5.9.1 Saturate the test specimen in the water for an additional 30 minutes once reaching the desired water temperature.

5.10 Start the test after the test specimens have been in the water for 30 minutes at the desired test temperature. The testing device automatically stops the test when the device applies the number of desired passes or when reaching the maximum allowable erosion depth, 0.5 in. (13 mm).

6. REPORT

6.1 For each specimen, report the following items:

- the stabilizer content,
- the erosion depth versus number of passes at all 11 sensing locations,
- maximum erosion rate at the joint location,
- average erosion rate from the erosions of all 11 locations,
- weight of tested specimen after 24 hours oven dry, and
- gradation of tested specimen.

6.2 Erosion rate is the slope of linear regression line of test data.

APPENDIX B

EXAMPLE OF DESIGN PROCESS BY THE DECISION FLOWCHART AND THE DESIGN GUIDE SHEET

The base/subbase design guide sheet in Figure B-1 can be a good assistance to decide design parameters based on traffic level and environmental factors. Input and output factors used in the design guide sheet are explained from Table B-1 to Table B-5.

BASE/SUBBASE DESIGN GUIDE SHEET

Input Design Factors

Traffic

Design period (yr)	ADT (two ways)	Percentage of Trucks (%)	Truck factor	Directional distribution factor	Lane Distribution Factor	Annual growth rate (%)	Vehicle speed (mph)
30	50,000	15	1.7	0.5	0.7	1	70

PCC layer

PCC slab thickness (in)	Lane width (ft)	Joint or crack spacing (ft)	PCC modulus (psi)	PCC Poisson's ratio	PCC unit weight (pcf)	Compressive strength (psi)	Tensile strength (psi)
10	12	15	4,000,000	0.15	160	6,000	500

CoTE of PCC (in/in/°F)	PCC set temperature (°F)	Max. PCC top temperature (°F)	Min. PCC top temperature (°F)	PCC bottom temperature (°F)	Transverse load transfer devices	Longitudinal load transfer	Joint seal maintenance cycle
0.000004	75	105	60	80	Yes	Multi-lane	5-7yr (goo

Base layer

Base material type	Base thickness (in)	Base modulus (psi)	Base Poisson's ratio	Base unit weight (pcf)	Base UCCS (psi)	Base friction coefficient	Base erodibility
AC	1	350,000	0.3	140	2,000	7.5	10

Subbase layer

Subbase material type	Subbase thickness (in)	Subbase modulus (psi)	Subbase Poisson's ratio	Subbase unit weight (pcf)	Subbase UCCS (psi)	Subbase friction coefficient	Subbase erodibility
CTB-Limes	6	2,000,000	0.2	135	1,500	9	30

Subgrade layer

Subgrade material type	Subgrade k-value (psi/in)	Subgrade modulus (psi)	Subgrade Poisson's ratio	Subgrade unit weight (pcf)	Subgrade UCCS (psi)	Subgrade friction coefficient	Subgrade erodibility
Sandy soil	100	6,000	0.35	130	20	1.1	1000

Environmental factors and others

Wet days per year (day)	Max. ambient temperature (°F)	Min. ambient temperature (°F)	Ambient relative humidity (%)	Equivalent damage ratio	Drainage condition	Constructability	Cost analysis
120	100	55	50	0.7	Good	Good	Good

Output Design Factors

Total ESAL in design lane	Effective ESAL in design lane	Max. deflection by loading (mils)	Effective thickness (in)	Effective k-value (psi/in)	Max. curling stress (psi)	Early cracking potential (%)	Subbase erosion after design life (%)
54,000,000	12,427,397	1.7	16.7	300	326	35	70

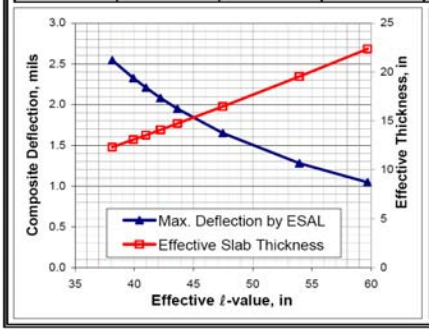

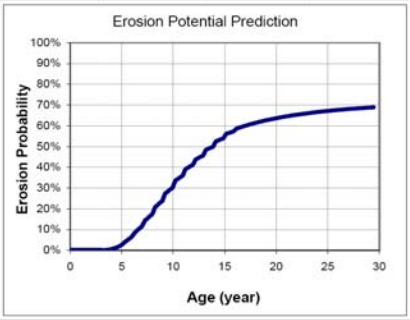

Figure B-1 Design Guide Sheet for Base/Subbase Design of Concrete Pavement.

Table B-1 Input and Output Factors of Design Guide Sheet - Traffic.

<table>
<tr><th>Term</th><th>Description</th></tr>
<tr><td>Design period, Y</td><td>Years for traffic and erosion analysis which need to be decided reasonably to achieve economical layer thickness and material type</td></tr>
<tr><td>ADT (two way)</td><td>Average daily traffic in two directions at the start of the design period</td></tr>
<tr><td>Percentage of trucks, T</td><td>Percentage of trucks in the ADT</td></tr>
<tr><td>Truck factor, T_f</td><td>Truck factor can be calculated by following equation (14):
$$T_f = \left(\sum_{i=1}^{m} p_i F_i \right) A$$
where, p_i is the percentage of total repetitions for the ith load group, F_i is the equivalent axle load factor (EALF) for the ith load group, m is the number of load groups, and A is the average number of axles per truck</td></tr>
<tr><td>Directional distribution factor, D</td><td>Ratio of ADT in design direction usually assumed to be 0.5 unless the traffic in two directions is different</td></tr>
<tr><td>Lane distribution factor, L</td><td>Ratio of ADT in design lane which varies with the volume of traffic and the number of lanes. AASHTO guide recommended following values (13):
<table>
<tr><th>No. of lanes in each direction</th><th>Percentage of 18-kip ESAL in design lane</th><th>Typical lane distribution factor</th></tr>
<tr><td>1</td><td>100</td><td>1.0</td></tr>
<tr><td>2</td><td>80 - 100</td><td>0.9</td></tr>
<tr><td>3</td><td>60 - 80</td><td>0.7</td></tr>
<tr><td>4</td><td>50 - 75</td><td>0.6</td></tr>
</table></td></tr>
<tr><td>Annual growth rate, r</td><td>Growth factor, G can be calculated by following equation recommended by AASHTO guide (13):
$$\mathrm{G} = \frac{(1+r)^Y - 1}{r \cdot Y}$$</td></tr>
<tr><td>Vehicle speed</td><td>Design vehicle speed in mph</td></tr>
</table>

Table B-2 Input Factors of Design Guide Sheet - PCC Layer.

Term	Description
PCC slab thickness	Design PCC layer thickness in inch
Lane width	Design PCC layer width in feet
Joint or crack spacing	Joint spacing of a JC pavement in feet or mean crack spacing of a CRC pavement in feet
PCC modulus	Elastic modulus of PCC. Default value is 4,000,000 psi
PCC Poisson's ratio	Poisson's ratio of PCC. Default value is 0.15
PCC unit weight	Unit weight of PCC. Default value is 160 pcf
Compressive strength	Compressive strength of PCC obtained from unconfined compressive strength test. Default value is 6,000 psi
Tensile strength	Tensile strength of PCC obtained from indirect tensile strength test. Default value is 500 psi
Coefficient of thermal expansion (CoTE) of PCC	Coefficient of thermal expansion of PCC mainly governed by coarse aggregate type. Default value is 4×10^{-6} /°F for the PCC using limestone aggregate. CoTE for the PCC using gravel is 6×10^{-6} /°F
PCC set temperature	Temperature of PCC during setting stage after paving. PCC will have zero volume change and stress at the set temperature. Volumetric change will occurs by the gap between the set temperature and the current temperature of PCC which occur the curling and shrinkage stresses
Max. PCC top temperature	Maximum temperature on top of PCC during the curing period (earlier than 28 days) which can induce the early cracking by curling
Min. PCC top temperature	Minimum temperature on top of PCC during the curing period which can induce the early cracking by shrinkage
PCC bottom temperature	Average temperature on bottom of PCC during the curing period
Transverse load transfer devices	Transverse load transfer devices such as reinforcing steel, dowel bar, and sleeper slab
Longitudinal load transfer	Longitudinal load transfer system such as multi-lane, tied PCC shoulder, and curb and gutter
Joint seal maintenance cycle	Plan of joint seal maintenance cycle which affect to the erosion and pumping of sub-layer by the amount of water intrusion through the joint. CRCP also needs the longitudinal joint seal maintenance

Table B-3 Input Factors of Design Guide Sheet - Base, Subbase, and Subgrade.

<table>
<tr><th>Term</th><th>Description</th></tr>
<tr><td>Material type</td><td>Base: Select one among AC, bond-break layer, and No base
Subbase: Select one among untreated (flex) base, AC, and CTB-aggregate types (limestone, gravel, RC, and RAP), and No subbase
Subgrade: Input any soil type directly</td></tr>
<tr><td>Thickness</td><td>Design layer thickness in inch. TxDOT design guide suggests using the one of two types of base layer combinations: 1) 4 in. of AC pavement or asphalt stabilized base or 2) a minimum 1 in. AC bond breaker over 6 in. of a cement stabilized base</td></tr>
<tr><td>Modulus</td><td>Elastic modulus of each layer obtained from the resilient modulus test. Without test results, following values are recommended by Hall et al. (31)
<table>
<tr><th>Base Type</th><th>Modulus of Elasticity (psi)</th></tr>
<tr><td>Fine-grained soils</td><td>3,000 - 40,000</td></tr>
<tr><td>Sand</td><td>10,000 - 25,000</td></tr>
<tr><td>Aggregate</td><td>15,000 - 45,000</td></tr>
<tr><td>Lime-stabilized clay</td><td>20,000 - 70,000</td></tr>
<tr><td>Asphalt-treated base</td><td>300,000 - 600,000</td></tr>
<tr><td>Cement-treated base</td><td>1000 × (500+compressive strength)</td></tr>
<tr><td>Lean concrete base</td><td>1000 × (500+compressive strength)</td></tr>
</table></td></tr>
<tr><td>Poisson’s ratio</td><td>Poisson’s ratio of each layer. Following typical values are recommended for design by Huang (14)
<table>
<tr><th>Material</th><th>Range</th><th>Typical</th></tr>
<tr><td>Hot mix asphalt</td><td>0.30 - 0.40</td><td>0.35</td></tr>
<tr><td>Portland cement concrete</td><td>0.15 - 0.20</td><td>0.15</td></tr>
<tr><td>Untreated granular materials</td><td>0.30 - 0.40</td><td>0.35</td></tr>
<tr><td>Cement-treated granular materials</td><td>0.10 - 0.20</td><td>0.15</td></tr>
<tr><td>Cement-treated fine-grained soils</td><td>0.15 - 0.35</td><td>0.25</td></tr>
<tr><td>Lime-stabilized materials</td><td>0.10 - 0.25</td><td>0.20</td></tr>
<tr><td>Lime-flyash mixtures</td><td>0.10 - 0.15</td><td>0.15</td></tr>
<tr><td>Loose sand or silty sand</td><td>0.20 - 0.40</td><td>0.30</td></tr>
<tr><td>Dense sand</td><td>0.30 - 0.45</td><td>0.35</td></tr>
<tr><td>Fine-grained soils</td><td>0.30 - 0.50</td><td>0.40</td></tr>
<tr><td>Saturated soft clays</td><td>0.40 - 0.50</td><td>0.45</td></tr>
</table></td></tr>
<tr><td>Unit weight</td><td>Unit weight of each layer in pcf</td></tr>
</table>

Table B–3 (Continued).

<table>
<tr><th>Term</th><th>Description</th></tr>
<tr><td>UCCS</td><td>Compressive strength of each layer obtained from the unconfined compressive strength test. Approximate UCCS for subgrade are suggested as following by ACI (32):
<table>
<tr><th>Classification</th><th>Approximate UCCS, psi</th></tr>
<tr><td>Stiff, fine-grained</td><td>33</td></tr>
<tr><td>Medium, fine-grained</td><td>23</td></tr>
<tr><td>Soft, fine-grained</td><td>13</td></tr>
<tr><td>Very soft, fine-grained</td><td>6</td></tr>
</table></td></tr>
<tr><td>Friction coefficient</td><td>Friction coefficient of each layer. AASHTO guide recommended following values (13):
<table>
<tr><th rowspan="2">Subbase/Base type</th><th colspan="3">Friction Coefficient</th></tr>
<tr><th>Low</th><th>Mean</th><th>High</th></tr>
<tr><td>Fine grained soil</td><td>0.5</td><td>1.1</td><td>2</td></tr>
<tr><td>Sand</td><td>0.5</td><td>0.8</td><td>1</td></tr>
<tr><td>Aggregate</td><td>0.5</td><td>2.5</td><td>4</td></tr>
<tr><td>Lime-stabilized clay</td><td>3</td><td>4.1</td><td>5.3</td></tr>
<tr><td>ATB</td><td>2.5</td><td>7.5</td><td>15</td></tr>
<tr><td>CTB</td><td>3.5</td><td>8.9</td><td>13</td></tr>
<tr><td>Soil cement</td><td>6</td><td>7.9</td><td>23</td></tr>
<tr><td>Lean Concrete Base (LCB)</td><td>3</td><td>8.5</td><td>20</td></tr>
<tr><td>LCB not cured</td><td colspan="3">> 36 (higher than LCB cured)</td></tr>
</table></td></tr>
<tr><td>Erodibility</td><td>Erodibility of stabilized materials from the erosion test using Hamburg wheel-tracking device. Follow values are recommended for design purpose:
<table>
<tr><th rowspan="2">Percent of Stabilizer and Aggregate Type</th><th colspan="4">Erodibility using HWTD Test, mm/million-repetitions</th></tr>
<tr><th colspan="2">Natural Gravel Base (Limestone and Soil)</th><th>Reclamed Asphalt + Soil (1:2)</th><th>100% Recycled Concrete</th></tr>
<tr><td>Stabilizer type</td><td>Asphalt</td><td>Cement</td><td>Cement</td><td>Cement</td></tr>
<tr><td>0</td><td>150</td><td>150</td><td>200</td><td>250</td></tr>
<tr><td>2</td><td>50</td><td>100</td><td>150</td><td>200</td></tr>
<tr><td>4</td><td>20</td><td>30</td><td>50</td><td>80</td></tr>
<tr><td>6</td><td>10</td><td>20</td><td>40</td><td>50</td></tr>
</table></td></tr>
</table>

Table B-4 Input Factors of Design Guide Sheet - Environmental Factors and Others.

<table>
<tr><th>Term</th><th>Description</th></tr>
<tr><td>Wet days per year</td><td>Number of days which precipitation were greater than 0.01 in. (0.25 mm) during the year. Data can be retrieved from LTPP data as the field name of “INTENSE_PRECIP_DAYS_YR” from the table of “CLM_VWS_PRECIP_ANNUAL”</td></tr>
<tr><td>Max. ambient temperature</td><td>Highest air temperature during the curing period (earlier than 28 days) which can induce the early cracking by curling</td></tr>
<tr><td>Min. ambient temperature</td><td>Lowest air temperature during the curing period which can induce the early cracking by curling and shrinkage</td></tr>
<tr><td>Ambient relative humidity</td><td>Relative humidity of ambient during the curing period which affect to shrinkage and warping behaviors</td></tr>
<tr><td>Equivalent damage ratio</td><td>Ratio converts lateral distribution across the wheel path into the traffic in the wheel path. A normal distribution is often assumed for the lateral distribution of traffic, and the traffic wandering range would be increased with wider lane width. Default is 0.7</td></tr>
<tr><td>Drainage condition</td><td>Drainage condition also needs to be counted since a better drainage would remove water faster and reduce hydraulic erosion significantly. AASHTO guide suggested the general definitions corresponding to different drainage levels from the pavement structure by free water removing time (13):
<table>
<tr><th>Quality of Drainage</th><th>Water Removed Within</th></tr>
<tr><td>Excellent</td><td>2 hours</td></tr>
<tr><td>Good</td><td>1 day</td></tr>
<tr><td>Fair</td><td>1 week</td></tr>
<tr><td>Poor</td><td>1 month</td></tr>
<tr><td>Very poor</td><td>(water will not drain)</td></tr>
</table></td></tr>
<tr><td>Constructability</td><td>The subbase used under concrete pavement needs to have adequate structural capacity to support construction equipment and operations. Otherwise, stabilized subbas is required with the proper stabilizer type and content to perform properly and have adequate structural capacity for construction operations</td></tr>
<tr><td>Cost analysis</td><td>Material cost, construction expenditure, and construction time should be considered with the performance requirements to select a most economical design</td></tr>
</table>

Table B-5 Output Factors of Design Guide Sheet.

Term	Description
Total ESAL in design lane	Total equivalent single axle load during design period, ESAL can be calculated by following equation (*14*): $\text{ESAL} = Y \cdot 365 \cdot \text{ADT} \cdot T \cdot T_f \cdot D \cdot L \cdot G$
Effective ESAL in design lane	Equivalent number of ESAL under the most critical condition for erosion (sublayers are saturated and all loading pass over wheel path only) matching with HWTD erosion test condition. It can be expressed simply as following equation: $\text{Effective ESAL} = \text{Wet days}/365 \times \text{EDR} \times \text{ESAL}$
Max. deflection by loading	Maximum deflection by an 18-kip loading on the design pavement system
Effective thickness	Composite thickness of PCC, base, and subbase layers to calculate the deflection by loading. It can be calculated using following equation: $h_e = \sqrt[3]{h_c^{\,3} + \frac{E_b}{E_c} h_b^{\,3}}$ where, h_e is the effective thickness of combined slab, h_c is the thickness of concrete slab, h_b is the thickness of base, E_c is the elastic modulus of concrete, and E_b is elastic modulus of base
Effective k-value	Composite k-value of a single sublayer converted from multi-layers (base, subbase, and subgrade) to calculate the deflection and stress of PCC by curling. It can be calculated by matching the curling deflection of the equivalent single layer with the curling deflection of the multi-layered system (tabulated by FEM program analysis)
Max. curling stress	Maximum tensile stress on PCC by curling. Curling occurs by the temperature difference between the top surface and bottom surface of PCC
Early cracking potential	When the curling stress is higher than PCC tensile strength (this normally happens during the curing period), PCC would have a high chance of early cracking
Erosion after design life	Erosion of sublayers would develop continuously during service period at the joint or crack locations. When the ultimate erosion depth is higher than design criteria, try more stabilizer or change material type to decrease erosion rate and erosion depth accordingly

STEP 1: Input general design factors into the design guide sheet

Pavement design period, traffic estimation data, candidate material list, overall material properties of all layers, environmental factors, and budget. An example of base/subbase design process is explained as follow.

STEP 2: Select base/subbase material type

Consider site-specific project situation, environmental conditions and subgrade strength. List and grade economical durable materials along with transport and stockpile cost. Select a material type and gradation and use stabilizer if needed. Check the requirements of Item 247 "Flexible Base" and budget. If requirements are not satisfied, use alternative material type. In the example, a 6 in. cement treated (4 percent cement) limestone aggregate subbase and 1 in. AC base are used.

STEP 3: Decide base/subbase stabilization based on strength and stiffness

Set the proper stabilizer and percentage for the requirement of 7-day and 28-day unconfined compressive strength (UCCS) in plan. Check the strength requirements of Item 276 "Cement Treatment" and 28-day UCCS in plan and apply more percentage of stabilizer if strength is lower than requirement for 7-day UCCS. Check the early cracking potential by curling and shrinkage stress of PCC in the design guide sheet and reduce the percentage of stabilizer (or change material type if 7-day UCCS requirement is conflict) when the potential is higher than 70 percent (recommendation but no requirement). In the example, strength of base and subbase are satisfied with the requirement of Item 276 "Cement Treatment" and 28-day UCCS.

STEP 4: Modify base/subbase stabilization or material type based on erosion

Find proper stabilizer and percentage by the maximum allowable erodibility using erosion potential in the design guide sheet. Check the erosion probability in the design guide sheet and apply more percentage of stabilizer or change material type (if early cracking potential is too high) when erosion probability of current design is higher than

90 percent at the end of design period (recommendation but no requirement). Figure B-2 shows a change of erosion probability along with subbase material type and stabilization level change.

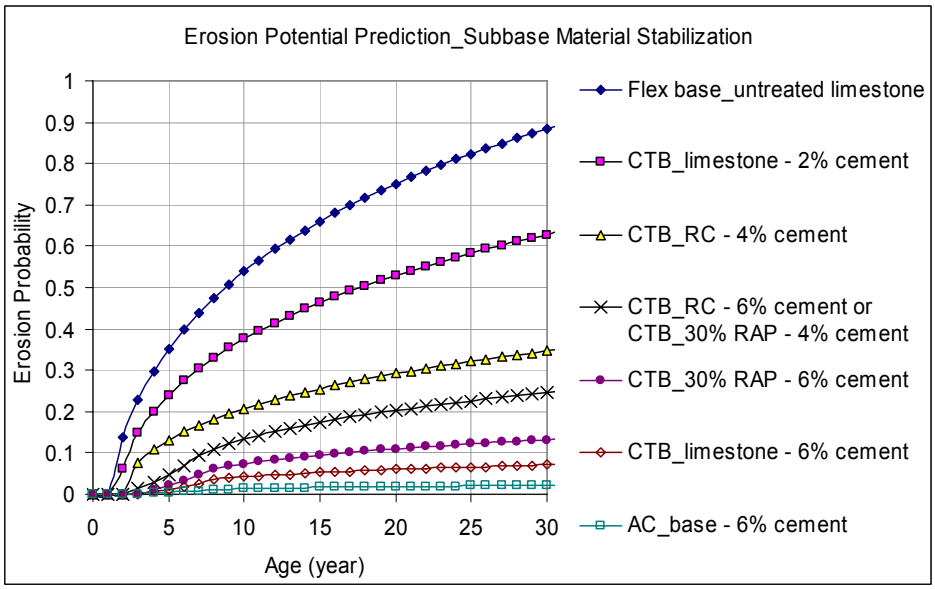

Figure B-2 Erosion Potential versus Material Type and Stabilization.

STEP 5: Modify base/subbase stabilization or material type based on friction

Check friction and bond between concrete and base/subbase by friction test. Modify friction level by the change of stabilization and material type or consider using interlayer. In the example, 1 in. AC layer is working as bond breaker and provides good moderate friction and bond level. When CTB is employed directly under the PCC slab, friction level and bond condition need to be checked carefully.

STEP 6: Set base/subbase thickness based on the requirements of plan

Examine various base/subbase thicknesses using the design guide sheet and evaluate composite deflections along with the change of effective thickness. If composite deflection is higher than design criteria, increase layer thickness. Figure B-3 shows a change of composite deflection (corner deflection with no LTE) and effective thickness

along with subbase thickness change when effective subgrade k-value is 300 psi/in. Deflection is not sensitive to subbase thickness compare with PCC slab thickness.

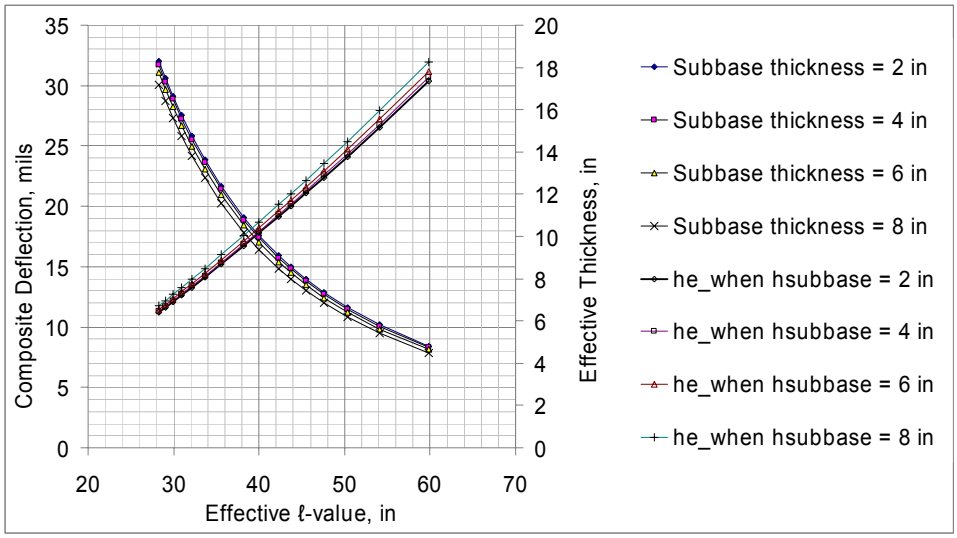

Figure B-3 Composite Deflection and Effective Thickness versus Subbase Thickness.

STEP 7: Estimate traffic data based on the history of adjacent highway

Simulate the change of erosion probability by different traffic estimation as changing traffic input factors in the design guide sheet. If erosion probability is higher than 90 percent at the end of design period (recommended value but no requirement), modification of material properties or drainage condition is recommended. Figure B-4 shows changes of erosion probability when the percentage of truck and annual growth rate change (when percentage of truck is 40 percent).

STEP 8: Check load transfer devices

Simulate the change of deflection and erosion probability by LTE changes using the design guide sheet since LTE decreases as time goes by the degradation of load transfer device. This is not directly related with base/subbase design but erosion is related with PCC slab deflection by load transfer devices. Figure B-5 shows changes of composite deflection and erosion probability along with the load transfer device situations.

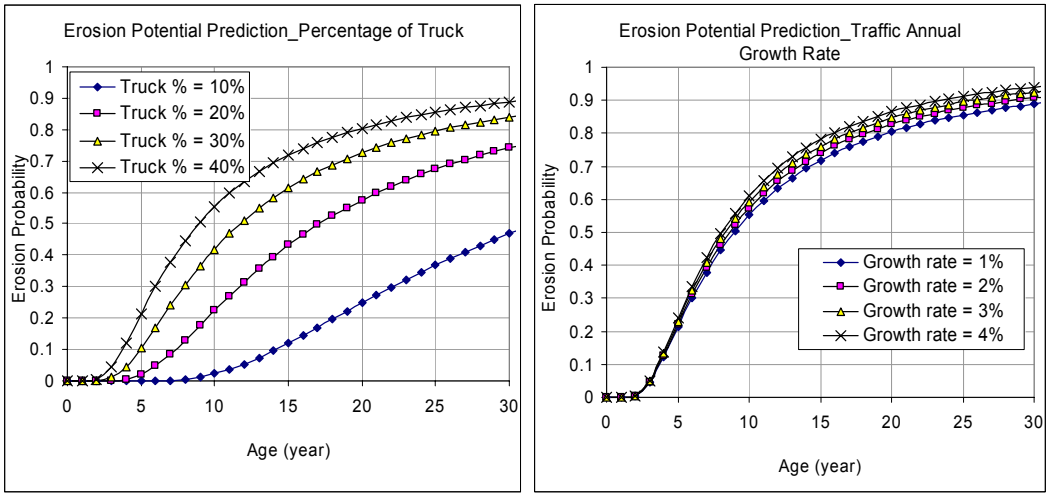

Figure B-4 Erosion Potential versus Traffic Factors.

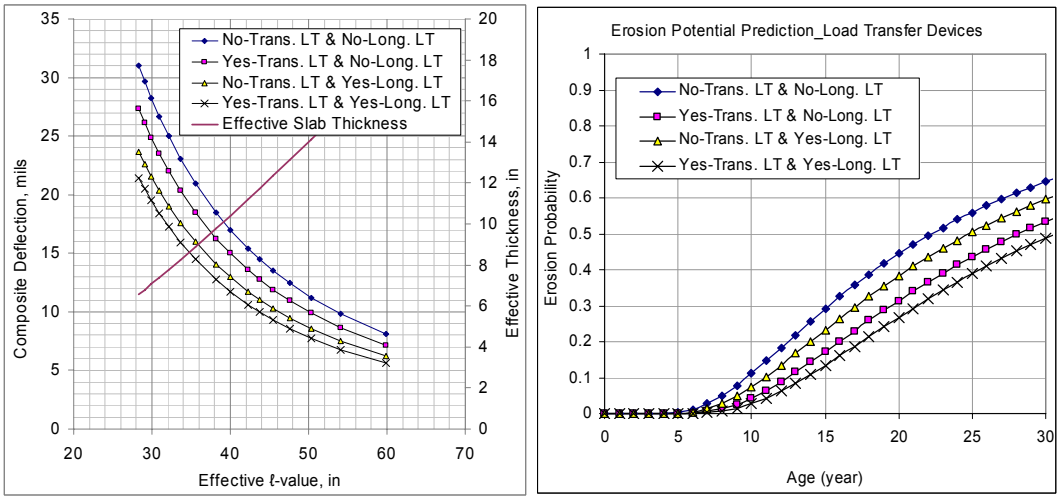

Figure B-5 Erosion Potential versus Load Transfer Devices.

STEP 9: Check the UCCS of subbase or SCI by FWD when open to construction traffic

If the UCCS of base/subbase is insufficient to heavy construction traffic even the deflection and erosion requirements under PCC layer are satisfied, careful consideration of alternative construction method is recommended.

STEP 10: Consider precipitation and drainage condition

Check joint sealing maintenance plans and potential for the employment of drainage system related with erosion potential using the design guide sheet. It affects to base/subbase material type and stabilization since good joint sealing and good drainage reduce erosion potential significantly and less percentage of stabilization need to be applied. Figure B-6 shows changes of erosion probability by the different drainage conditions and joint seal maintenance cycles (no base and 30 % RAP subbase are used).

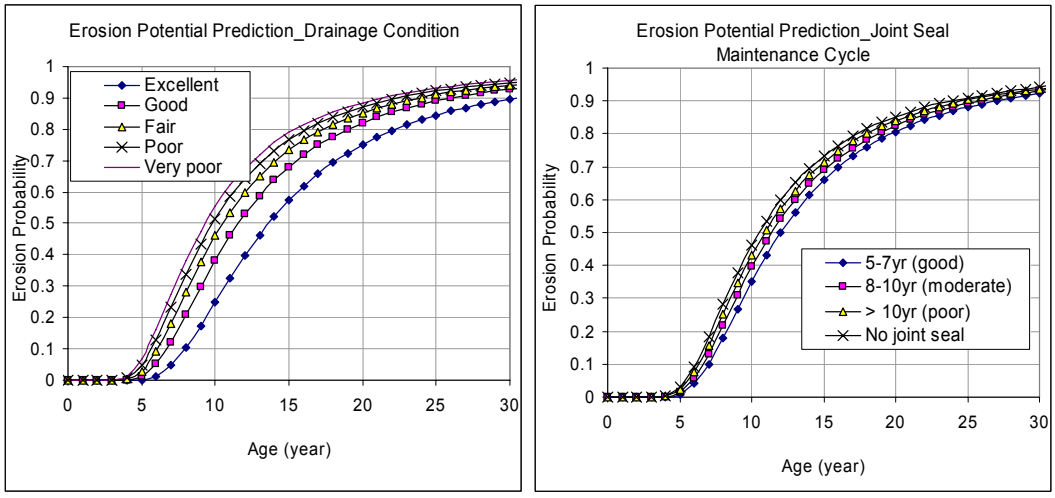

Figure B-6 Erosion Potential versus Drainage and Joint Seal Conditions.

STEP 11: Results cost-effective erosion-resistant pavement design

Design process is described step by step for each design factors. However, comprehensive considerations of all design factors are required to achieve the cost-effective base/subbase long-term good performance design.

VITA

Name:	Youn Su Jung
Address:	Zachry Department of Civil Engineering Texas A&M University College Station, Texas 77843-3136
Email Address:	yesjung@gmail.com
Education:	B.S., Civil Engineering, Pusan National University, 1998 M.S., Civil Engineering (Geotechnical Engineering), Pusan National University, 2001 M.E., Civil Engineering (Transportation Engineering), Texas A&M University, 2005 Ph.D., Civil Engineering (Materials Engineering), Texas A&M University, 2010